MODELING THE CONTRIBUTIONS OF LEFT VENTRICULAR GEOMETRY, AFTERLOAD, AND FIBER ORIENTATION ON THE PROGRESSION OF HEART FAILURE WITH PRESERVED EJECTION FRACTION

by

Sujan Dewanjee

Supervisor: Dr. Sheikh Mohammad Shavik

A thesis submitted in partial fulfillment of the requirements for the degree of

MASTER OF SCIENCE IN MECHANICAL ENGINEERING

Department of Mechanical Engineering

BANGLADESH UNIVERSITY OF ENGINEERING AND TECHNOLOGY

Dhaka, Bangladesh

December 2020

MODELING THE CONTRIBUTIONS OF LEFT VENTRICULAR GEOMETRY, AFTERLOAD, AND FIBER ORIENTATION ON THE PROGRESSION OF HEART FAILURE WITH PRESERVED EJECTION FRACTION

by

Sujan Dewanjee

Supervisor: Dr. Sheikh Mohammad Shavik

A thesis submitted in partial fulfillment of the requirements for the degree of

MASTER OF SCIENCE IN MECHANICAL ENGINEERING

Department of Mechanical Engineering

BANGLADESH UNIVERSITY OF ENGINEERING AND TECHNOLOGY

Dhaka, Bangladesh

December 2020

The thesis titled "**MODELING THE CONTRIBUTIONS OF LEFT VENTRICULAR GEOMETRY, AFTERLOAD, AND FIBER ORIENTATION ON THE PROGRESSION OF HEART FAILURE WITH PRESERVED EJECTION FRACTION**" submitted by **Sujan Dewanjee**, Roll No.: **0417102002**, Session: **April, 2017**, has been accepted as satisfactory in partial fulfillment of the requirement for the degree of MASTER OF SCIENCE IN MECHANICAL ENGINEERING on December 23, 2020.

BOARD OF EXAMINERS

Dr. Sheikh Mohammad Shavik
Assistant Professor
Department of Mechanical Engineering,
BUET, Dhaka- 1000

Chairman (Supervisor)

Dr. Shaikh Reaz Ahmed
Professor and Head
Department of Mechanical Engineering,
BUET, Dhaka- 1000

Member (Ex- officio)

Dr. A. B. M. Toufique Hasan
Professor
Department of Mechanical Engineering,
BUET, Dhaka- 1000

Member

Dr. Mohammad Abdul Motalab
Professor
Department of Mechanical Engineering,
BUET, Dhaka- 1000

Member

Dr. Muhammad Tarik Arafat
Associate Professor
Department of Biomedical Engineering,
BUET, Dhaka- 1000

Member
(External)

CANDIDATE'S DECLARATION

It is hereby declared that this thesis or any part of it has not been submitted elsewhere for the award of any degree or diploma.

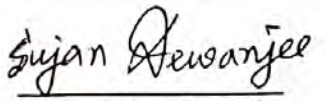

Sujan Dewanjee
Author

DEDICATION

Dedicated to My Parents and Brother

TABLE OF CONTENTS

LIST OF FIGURES

LIST OF TABLES

ACKNOWLEDGEMENT

I would like to express my deepest gratitude and indebtedness to my supervisor Dr. Sheikh Mohammad Shavik, Assistant Professor, Department of Mechanical Engineering, BUET for his kind supervision, constant guidance, encouragement, support, and thoughtful discussion throughout the entire research. Without his guidance, it was impossible to complete the thesis work.

I am also grateful to the Department of Mechanical Engineering, BUET, for giving me the opportunity to use the "Postgraduate Computer Lab" for the research.

I would like to acknowledge the contribution of Dr. Lik Chuan Lee, Associate Professor, Department of Mechanical Engineering, Michigan State University, for providing clinical data and giving permission to use these data for successful completion of this thesis.

I wish to thank my parents, brother, relatives, colleagues, friends and well-wishers for their help and mental support during the research.

Finally, I wish to thank almighty for everything in my entire life.

Author

ABBREVIATION

HF	: Heart Failure
EF	: Ejection Fraction
HFrEF	: Heart Failure with reduced Ejection Fraction
HFpEF	: Heart Failure with preserved Ejection Fraction
ED	: End Diastole
ES	: End Systole
LV	: Left Ventricle
LA	: Left Atrium
RV	: Right Ventricle
RA	: Right Atrium
SL	: Semilunar Valve
HTN	: Hypertension
DD	: Diastolic Dysfunction
AV	: Atrioventricular Valve
SV	: Stroke Volume
MR	: Magnetic Resonance
ECG	: Electrocardiography
DBP	: Diastolic Blood Pressure
SBP	: Systolic Blood Pressure
ESPVR	: End-Systolic Pressure-Volume Relationship
EDPVR	: End-Diastolic Pressure-Volume Relationship
TPR	: Total Peripheral Resistance
Ees	: End Systolic Elastance
Pes	: End Systolic Pressure
STE	: Speckle Tracking Echocardiography

ABSTRACT

Heart Failure with preserved ejection fraction (HFpEF) has emerged as a prevalent heart disease which has high risk of short-term and long-term mortality rate. HFpEF has been associated with a progressively impaired interaction between the left ventricle (LV) and the systemic arteries. The progression of HFpEF along with the key factors which contributes to this process, is an area of active research. Since the structural and functional changes of Left Ventricle (LV) governs the progression of HFpEF, computational models have emerged as a robust tool to study the features of HFpEF as well as to develop effective treatment plan in recent years. FE model of LV would help to assess the contributions of the key factors to the progression of HFpEF. In the present study a coupled LV FE-lumped parameter circulatory modeling framework has been developed and calibrated with the measurements acquired from a normal subject and a HFpEF patient. The models for normal and HFpEF cases reproduced the clinical datasets within acceptable limits though the longitudinal strain was found nearly equal for both the cases, which can be a consequence of higher ejection fraction found in the HFpEF case. After that, the HFpEF model parameters such as, geometry (thickness 1 – 1.9 cm), preload (LV end diastolic volume 144.6 – 194.9 ml), afterload (110000 - 192500 Pa ms ml^{-1}), and transmural myofiber orientation (fiber angle -50^o/50^o to -70^o/70^o), were varied to physiologically reproduce the effects of these parameters on progression of HFpEF due to remodeling, diastolic dysfunction, hypertension, hypertrophy etc. which are the causes and effects of HFpEF progression. The model predicts features of HFpEF progression except increased circumferential strain as LV wall thickness is increased, which is found in HFpEF patient. Reduced preload replicated the prominent feature of HFpEF progression that is, decrease in longitudinal strain. So increased LV wall thickness with reduced preload can be a possible path of HFpEF progression. Increasing afterload predicts decrease in both circumferential and longitudinal strains, but the associated systolic pressure shows unphysiological increment. Change in fiber angle has negligible effect on LV functioning, but has a considerable effect on strains. It has been found that, though isolated variation of these parameters shows contribution towards progression of HFpEF, but it is likely that more than one mechanism has to be combined to reproduce all the pathophysiological features found during the progression of HFpEF.

CHAPTER 1

INTRODUCTION

The most common cause of death globally is Cardiovascular diseases, which accounts for 30% of global deaths [1]. More than 75% of these are because of coronary artery disease and stroke [1]. Smoking, being overweight, little exercise, high cholesterol, high blood pressure, and poorly controlled diabetes are the common factors which develops Cardiovascular diseases. These cardiovascular diseases frequently do not have symptoms or may cause chest pain or shortness of breath. Diagnosis of heart disease is often done by the taking of a medical history, listening to the heart-sounds with a stethoscope, ECG, and ultrasound etc. Ejection fraction which is the percentage of the volume of blood ejected from the left ventricle with each heartbeat divided by the volume of blood when the left ventricle is maximally filled, is being used as the indicator of Heart Failure (HF) clinically as, it is the most important clinical parameter that is used to detect HF.

Heart failure with preserved ejection fraction (HFpEF) is a form of heart failure. In HFpEF, the ejection fraction is normal, which greater than 50% [2]. The ejection fraction is usually measured by echocardiography or cardiac catheterization. Roughly half of people with heart failure have HFpEF, while the other half have a reduction in ejection fraction, which is called heart failure with reduced ejection fraction (HFrEF).

Hypertension, diabetes, hyperlipidemia, smoking, and obstructive sleep apnea are the major risk factors for HFpEF [3]. In most cases HFpEF is marked by abnormal diastolic function. Usually in HFpEF there is an increase in the stiffness of the left ventricle. This in turn causes a decrease in left ventricular relaxation during diastole and resultant increased pressure and/or impaired filling [4]. HFpEF has been also found to be associated with the increased risk of atrial fibrillation and pulmonary hypertension.

Over the years, computer heart models with realistic description of cardiac geometry and muscle architecture have advanced significantly [5-9]. Computer model prompts the researcher to investigate the root cause of heart diseases which cannot even be thought to be studied in clinical setting. There are some unresolved issues and aspects

that need improvements despite these significant advancements. The goal of this study is to investigate one of those issues by understanding the underlying mechanics in heart failure with preserved ejection fraction (HFpEF).

This thesis focuses on the progression of HFpEF, due to the remodeling of Left Ventricular (LV) geometrical and structural parameters and change in afterload via computer simulation of the Finite Element Model of LV. Due to complex mechanisms of systemic and cardiac adaptation that vary over time, particularly with aging, HFpEF is usually progressive [10-11]. This highly prevalent, heterogeneous clinical syndrome grows by change in left ventricular (LV) size and structure in elderly who subjects with hypertension (HTN), LV diastolic dysfunction (DD) etc. These have prominent role in the pathophysiology of heart failure with preserved ejection fraction (HFpEF) [12]. This causes substantial morbidity and mortality and has no effective treatment. The current study will quantify the effects of changes in heart function due to undergoing changes in parameters like geometry, afterload, myo-fiber orientation in HFpEF diagnosed heart, and will relate these changes to clinical characteristics and risk of incident HF. This is a step towards developing strategies to prevent HF of HFpEF patient.

This chapter discusses about basic anatomy and functioning of heart and the different viewpoints regarding progression of HFpEF, challenges as well as reliability concerns for impeding HFpEF progression.

1.1 Human Heart Anatomy in Brief

A muscular organ that pumps blood through the systemic and pulmonary vascular systems is known as heart. The basic task of the heart and vasculature is to sustain an adequate supply of oxygen and nutrients to all the tissues for all operating conditions of human body. The normal adult human heart is partitioned into four muscular chambers, two atria and two ventricles. (Figure 1.1). The left heart is comprised of the left atrium and left ventricle. It drives blood from the pulmonary veins to the aorta. The human left ventricle has an axisymmetric, truncated ellipsoid shape, that has

approximately 1 cm wall thickness [13]. The right heart comprises of right atrium and right ventricle that pumps blood from the vena cava to the pulmonary arteries. The left ventricle is more powerful than the right ventricle. Right ventricle has a crescent-shape and a thinner wall. Myofibers, which are arranged in a highly organized way, construct the heart wall. The local myofiber orientation alters along the transmural direction from the inner (endocardium) to the outer (epicardium) wall and is mostly circumferential at the mid-wall [13]. The tricuspid valve in the right heart and the mitral valve in the left heart isolate the atria from their corresponding ventricle. The valves are arranged in a manner to make sure one-way flow through the heart and forbids backward flow during the contraction of the ventricles. By preventing blood from flowing from the artery back into the ventricle the aortic and pulmonary valve separate each ventricle from its arterial connection and ensure unidirectional flow. The cardiovascular system works in a closed loop. The average human heart is a little larger than the size of average human fist and weighs between 200 to 425 grams. On an average heart beats 100,000 times, pumping about 2,000 gallons (7,571 liters) of blood each day [13]. The average of time of a single heartbeat is around 864 milliseconds. The heart, blood vessels (arteries, capillaries, and veins) and blood all together, construct the circulatory system.

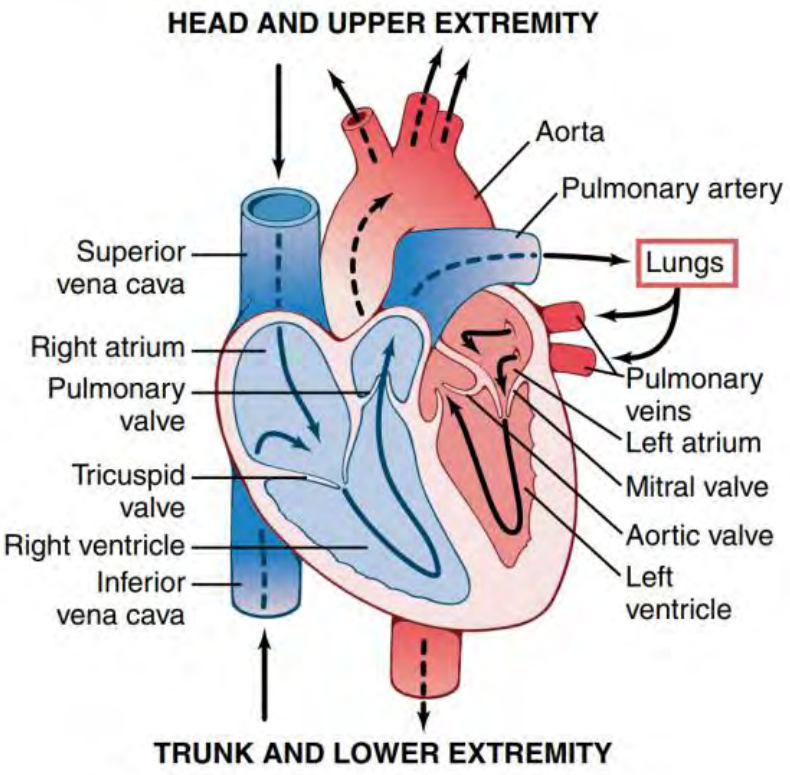

Figure 1. 1: Simplified structure of the human heart, and direction of blood flow through the heart chambers and heart valves. [13]

1.2 Circulatory System: Systemic and Pulmonary Circulation

The cardiovascular system supplies oxygen and nutrients to the tissues and carries away waste materials that is to be eliminated by organs such as lungs, liver, and kidneys. The pulmonary and systemic circulations help in accomplishing this role. The pulmonary circulation is a low resistance, high capacitance bed, and the systemic circulation, in comparison, is a relatively high resistance vascular bed. As shown in Figure 1.2, the deoxygenated blood from the superior vena cava (from upper extremities, head, and chest wall), inferior vena cava (trunk, abdominal organs, and lower extremities) and the coronary sinuses (from myocardium) goes to the Right Atrium (RA). The RA is filled with deoxygenated blood, increasing pressure in the atrial chamber. As the atrial pressure exceeds the pressure in the RV, the tricuspid valve opens permitting this blood to enter the RV. As a result of this filling, and as the

RV starts to contract, the pressure in the RV builds up pushing the tricuspid valve to close and the pulmonary valve to open, thereby ejecting the blood into the pulmonary arteries and lung. Oxygenated blood from the lungs goes to the LA via the pulmonary veins and as a result, pressure in LA builds up and when it exceeds that of the LV, the mitral valve opens, permitting the blood to enter the LV. When the blood fills the LV, and as the LV starts to contract, the increase of the LV chamber pressure forces the mitral valve to close and aortic valve to open, thus ejecting blood into the aorta, that is to be distributed throughout the body.

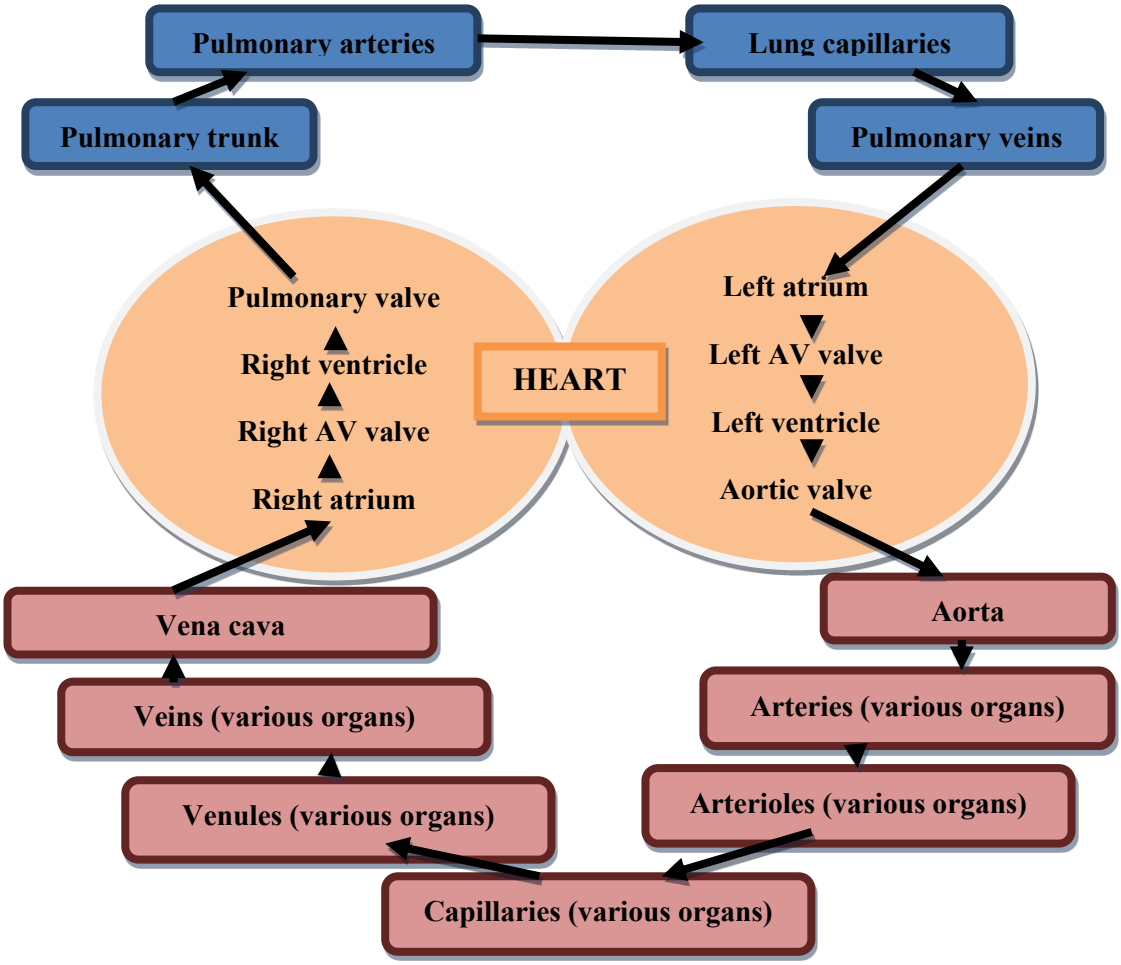

Figure 1. 2: Circulatory pathway of the cardiovascular system during systemic and pulmonary circulation [14].

1.3 Cardiac Cycle

The cardiac cycle consists of contraction and relaxation of both atria and ventricles (Figure 1.3). The heart does not contract or expand as a single unit. The cardiac cycle consists of cyclic structural and functional changes which the heart experiences every 0.8 s on average to maintain the blood flow through the body. The cycle begins with an atrial systole. The atrial systole helps to, but is not essential for, ventricular filling, but it does become an important factor in a diseased heart. During this phase time, the atrioventricular (AV) valves are open, and the ventricles are relaxing. The semilunar valves (SL) (i.e., pulmonary valve and aortic valve) are closed, which stops re-entry of blood from the pulmonary artery or the aorta. The isovolumetric ventricular contraction (start of ventricular systole while the SL valves are closed) starts after the atrial systole, during which the ventricular volume remains constant. The isovolumetric ventricular contraction is preceded by the disperse of the electric impulse from the AV node to the rest of the ventricular myocardium. When the ventricular pressure becomes larger than the atrial pressure, the AV valves close, corresponding to the first heart sound, with the mitral valve closing fractionally before the tricuspid valve. The semilunar (SL) valves open as the pressure in the ventricles exceeds that of the pressure in the aorta and the pulmonary artery, which results rapid ventricular ejection. This results in a reduction in the ventricular volume because most of the ventricular blood (stroke volume) is ejected during this phase. The atria also begin to fill during this phase. At the end of the ventricular contraction the ejection of blood from the ventricles is slower as the ventricular pressure starts to drop. This is followed by isovolumetric ventricular relaxation characterized by closure of the aortic and pulmonic valves. The closure of the semilunar valves relates to the second heart sound. The AV valves are closed, and the ventricular volume stays constant. The pressure in the ventricles is decreased rapidly. While the ventricular pressure becomes less than the atrial pressure, the AV valves open indicating the end of the isovolumetric phase of ventricular relaxation and the onset of rapid ventricular filling. At the start of this phase of ventricular relaxation, there is passive filling of the ventricles with the blood from the atria, that is rapid. The rapid flow of blood from the atria into ventricles causes the third heart sound, that is normal in children but in adults is associated with

disease. Reduced ventricular filling sometimes referred to as diastasis, that is the longest period of the cardiac cycle, follows the rapid filling. Most of the myocardium gets its blood supply during this phase of the cardiac cycle.

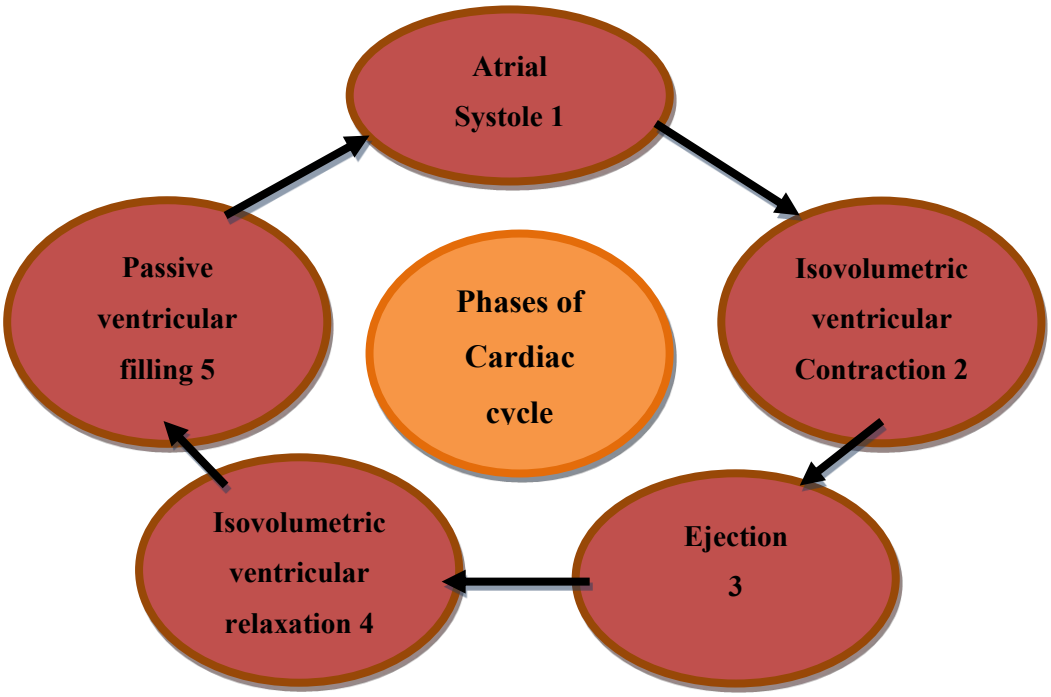

Figure 1. 3: Brief presentation of the phases of cardiac cycle during systemic and pulmonary circulation [14].

1.4 Left Ventricular Pressure-Volume Relationship

Systole, and diastole are the two major phases of cardiac cycle. In systole the ventricular muscles convert from its totally relaxed state to the point of maximal mechanical activation or force. During diastole, the muscle relaxes from the end-systolic (maximally activated) state back towards its resting state. The ventricular wall contracts and relaxes in each cardiac cycle. Correspondingly, during a cardiac cycle the mechanical properties of the ventricle are time-varying. The time-varying mechanical properties are linked to the pressure-volume relationship of the ventricle over the cardiac cycle (Figure 1.4 a), which is a suitable way to interpret the ventricular function. The PV points go around the loop in a counterclockwise direction as time proceeds in cardiac cycle.

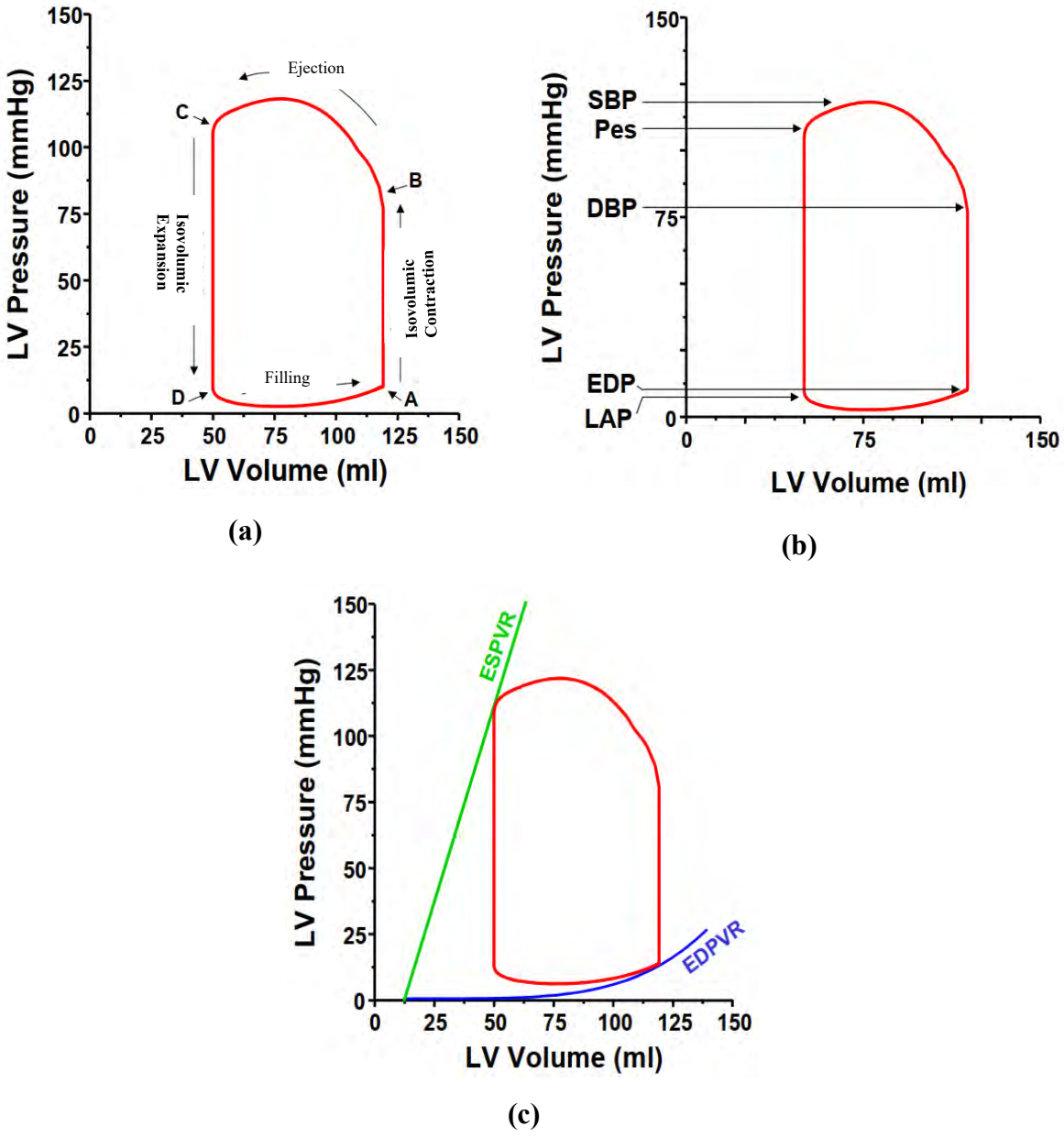

Figure 1. 4: (a) A typical pressure – volume (PV) loop, (b) PV loop with identifiable physiological parameters, and (c) PV loop with ESPVR and EDPVR [15].

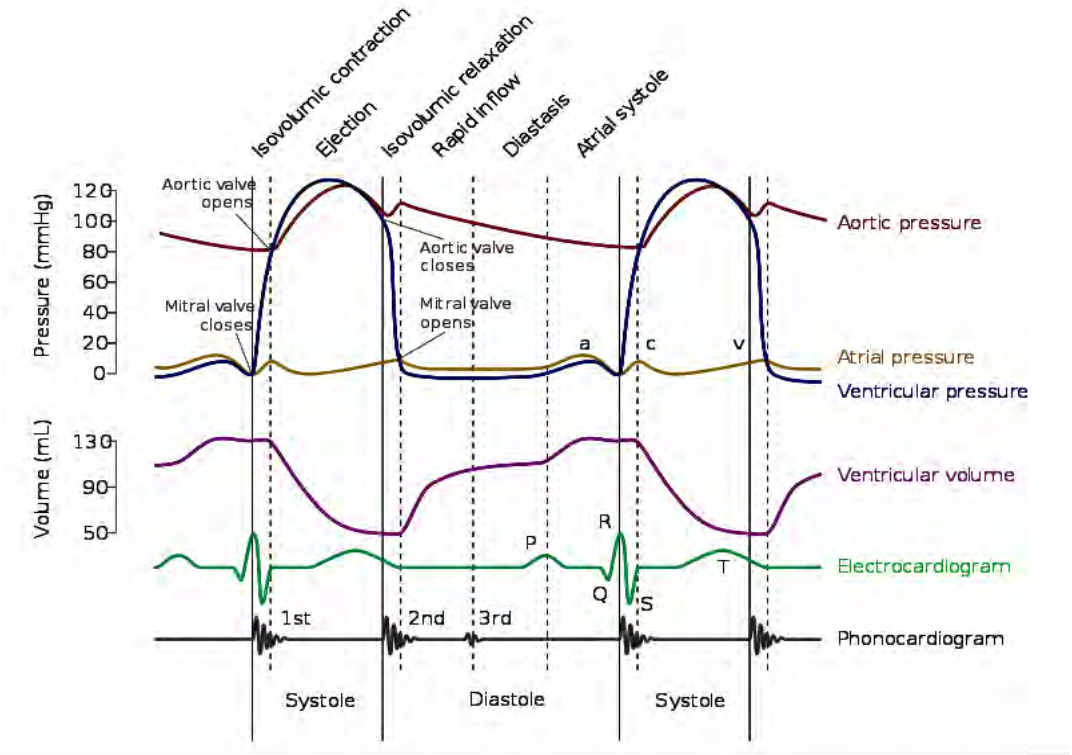

Figure 1. 5: Wiggers diagram showing aortic, left atrial, left ventricular pressure; left ventricular volume; electrocardiogram; phonocardiogram with respect to heart cycle time [13].

Point A indicates the end of diastole or, start of the systole. Using this point as a reference, pressure rises but volume remains the same in the first part of the cycle which is known as the isovolumic contraction phase, where the ventricle contracts with both valves remaining closed. Ultimately ventricular pressure grows above the aortic pressure, the aortic valve opens (B), ejection begins, and volume starts to shrink during the ejection phase. After the ventricle gets to its maximum activated state (C, upper left corner of PV loop), the ventricular pressure drops below aortic pressure, following which the aortic valve closes and isovolumic relaxation initiates. Finally, filling starts when the mitral valve opens (D, bottom left corner) and terminates when the valve closes (A) and the cycle repeats. Several parameters and variables of physiologic importance can be taken from analysis of the PV loop (Figure 1.4 b). Specifically, the maximum volume of the cardiac cycle is described as the end-diastolic volume (EDV), which can be determined from point A (Figure 1.4 a). The minimum volume known

as the end-systolic volume (ESV) can be retrieved from point D**,** that is the ventricular volume at the end of the ejection phase. The difference between EDV and ESV determines the amount of blood ejected during the cardiac cycle and is referred as the stroke volume (SV). Near the top right of the loop, the point at which the ventricle begins to eject (the point at which ventricular pressure just exceeds aortic pressure and volume starts to decrease) can be identified. This pressure therefore reflects the pressure existing in the aorta at the start of ejection and is called the diastolic blood pressure (DBP). Aortic and ventricular pressures are essentially equal during the ejection phase. Therefore, the point of greatest pressure on the loop also signifies the greatest pressure in the aorta which is called the systolic blood pressure (SBP). The end-systolic pressure (Pes) is recognized as the pressure of the left upper corner of the loop. The pressure of the point at the bottom right corner (point D in Figure 1.4 a) of the loop is the pressure in the ventricle at the end of the cardiac cycle and is labeled as the end-diastolic pressure (EDP). Ventricular filling appears along the end-diastolic pressure-volume relationship (EDPVR), which is also called passive filling curve for the ventricle. The curvature of this line is decided by the mechanical properties of the muscle as well as the structural and geometrical features of the ventricle (e.g., wall thickness). The maximal pressure that can be built by the ventricle, is defined by the end-systolic pressure-volume relationship (ESPVR). An example of a PV loop is shown (Figure 1.4 c), that is bounded by the ESPVR and EDPVR. The upper left-hand corner (end-systolic point) of each loop appears on the ESPVR, while the bottom right part of the loop appears on the EDPVR. The slope of the ESPVR is recognized as the end-systolic elastance, *Ees*. It is a measure of the ventricular contractility. Wiggers diagram (Figure 1.5) shows aortic, left atrical, left ventricular pressure; left ventricular volume; electrocardiogram; phonocardiogram with respect to heart cycle time [13].

1.5 Contractility, Preload and Afterload

Contractility, preload, and afterload are three important ideas that are related to the ventricular function. Contractility implies to the intrinsic strength of the ventricle or cardiac muscle. It represents the intrinsic ability of the cardiac muscle to produce force that is not dependent on external loads or stretch. Myocardial contractility arises from the excitation-contraction coupling, the sequence of events that lead to myocardial contraction stimulated by electrical depolarization of the cells. Myocardial contractility can be changed by modifying one or combination of events (for instance, number of myofilaments available to participate in the contraction process, the amount of calcium released, etc.) related to the excitation-contraction coupling process. The end systolic elastance *Ees* is an indicator of contractility as it varies with the ventricular contractility (Figure 1.6 a) but is not influenced by the changes in the arterial system (afterload and preload). Preload is recognized as the hemodynamic load or stretch on the myocardial wall at the end of diastole but just before contraction begins. Ventricular preload can be anticipated by measuring 1) EDP, 2) EDV, 3) wall stress at end-diastole and 4) end-diastolic sarcomere length. In the clinical setting, EDP probably offers the most meaningful measure of preload in the ventricle and it is assessed by measuring the pulmonary capillary wedge pressure (PCWP) using a catheter which is placed through the right ventricle into the pulmonary artery. A change in preload controls the SV and pressure but end systolic elastance *Ees* stays same (Figure 1.6 b). Afterload is the hydraulic load enforced on the ventricle during ejection. This load is normally imposed on the heart by the arterial system. There are several measures of afterload, which are used in different settings. These are 1) aortic pressure, 2) total peripheral resistance (TPR), 3) arterial impedance and 4) myocardial peak wall stress. The change in afterload also affects the SV and pressure of the ventricle, but the Ees remains unchanged (Figure 1.6 c).

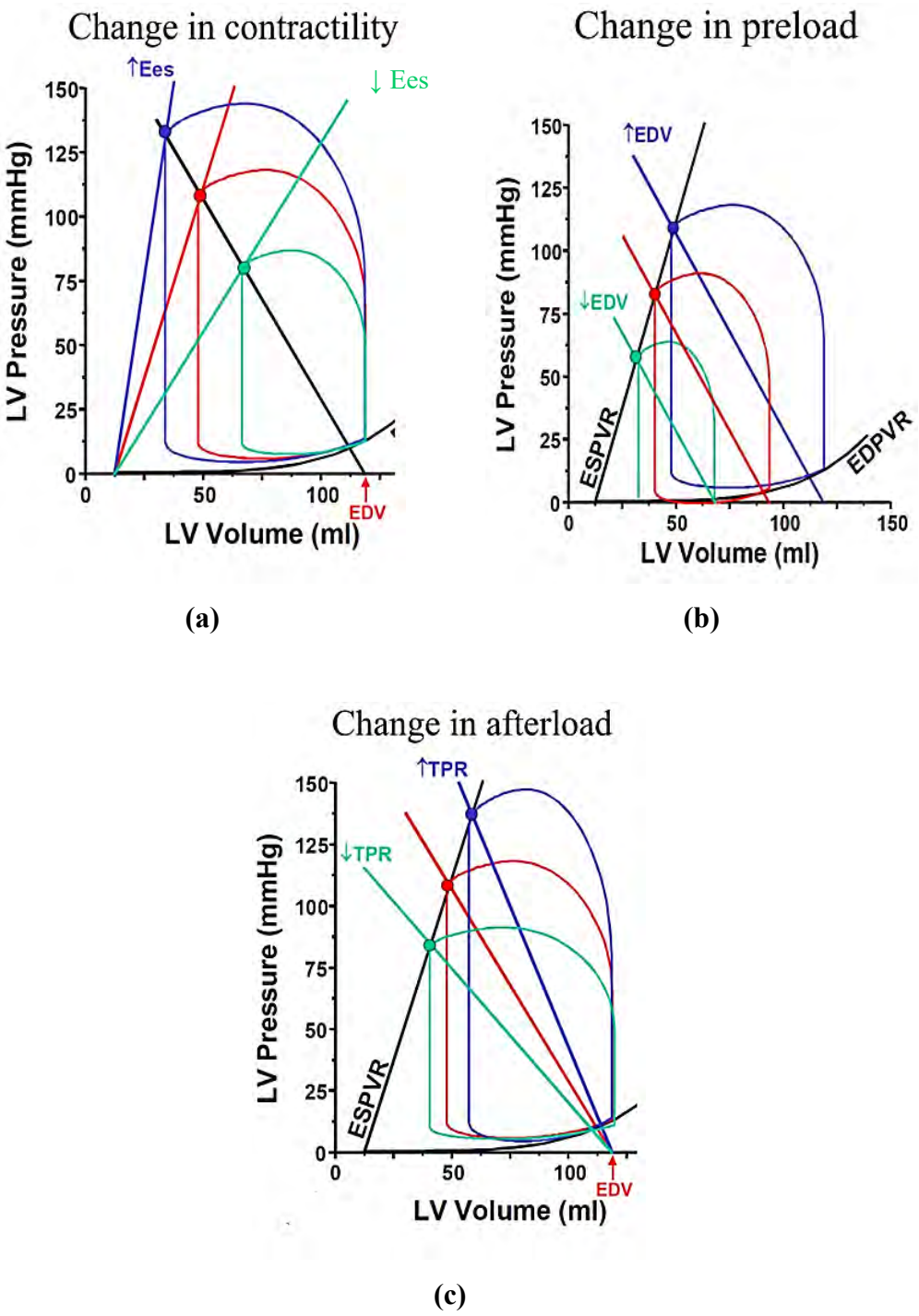

Figure 1. 6: Effect of change in (a) contractility, (b) preload, and (c) afterload on PV loop over single cardiac cycle [15].

1.6 Heart Failure

Heart failure (HF) is an impaired condition when the heart cannot pump sufficiently to maintain blood flow to satisfy the body's requirements. Common causes of heart failure include coronary artery disease, including a previous myocardial infarction (heart attack), high blood pressure (hypertension), atrial fibrillation, valvular heart disease, excess alcohol use, infection, and cardiomyopathy of an unknown cause [13]. Shortness of breath, excessive tiredness, and leg swelling are the common symptoms and signs of heart failure. Limited ability to exercise is also a frequent feature. Usually, heart failure occurs due to alteration of either the structure or the function of the heart. Heart failure is not the similar as heart attack (in which part of the heart muscle dies) or cardiac arrest (in which blood flow stops completely). The severity of the heart failure is graded by the seriousness of symptoms with exercise. The diagnosis is normally based on the symptoms, physical findings, and echocardiography. Blood tests, electrocardiography (ECG or, EKG), chest radiography, Magnetic resonance (MR) imaging and Computed Tomography (CT) scans may be effective to determine the underlying cause [13]. Treatment depends on the seriousness and cause of the disease. In people with chronic stable mild heart failure, treatment commonly consists of lifestyle adjustments such as stopping smoking, physical exercise, and dietary changes, as well as medications. In those with heart failure due to left ventricular dysfunction, patients need to be under drug treatments with constant consultation with the clinicians. Sometimes, depending on the cause, an embedded device such as a pacemaker or an implantable cardiac defibrillator may be suggested. In some moderate or serious cases, cardiac resynchronization therapy or cardiac contractility modulation may be of benefit. A ventricular assist device (for the left, right, or both ventricles), or occasionally a heart transplant may be advised in those with severe disease that persists despite all other procedures. Heart failure is a common, costly, and potentially fatal situation. Around 2% of adults have heart failure and among those over the age of 65, this increases to 6–10%. Rates are expected to increase. The probability of death is about 35% the first year after diagnosis, while by the second year the risk of death is less than 10% for those who stay alive [1].

Failed heart may have a reduced force of contraction due to overburdening of the ventricle. Increased filling of the ventricle results in increased contraction force in a normal heart, and thus a rise in cardiac output. In heart failure, this mechanism fails, as the ventricle is loaded with blood to the point where heart muscle contraction comes to be less efficient.

One historical method of categorizing heart failure is by the side of the heart affected (right heart failure versus left heart failure). Right heart failure was thought to compromise blood flow to the lungs comparing with left heart failure compromising blood flow to the aorta and therefore to the brain and the rest of the body's systemic circulation. However, integrated presentations are common and left heart failure is a usual cause of right heart failure.

More accurate classification of heart failure type is rendered by measuring ejection fraction, or the proportion of blood pumped out of the heart during a solo contraction. The ejection fraction is the fractional amount of the end-diastolic volume (EDV) that is ejected with each beat; that is, it is stroke volume (SV) divided by end-diastolic volume (EDV).

$$\mathrm{EF}(\%) = \frac{\mathrm{SV}}{\mathrm{EDV}} \mathrm{X}100\%$$

Where the stroke volume is given by, $\mathrm{SV} = \mathrm{EDV} - \mathrm{ESV}$

EF is inherently a relative measurement, as is any percentage, fraction, or ratio, whereas the stroke volume, end-diastolic volume or end-systolic volume are absolute quantities. The normal range of EF is between 50 and 70% [2].

There are two types of Heart Failure, they are:

1) Heart failure due to reduced ejection fraction (HFrEF): HFrEF is defined when ejection fraction less than 40% [2].

2) Heart failure with preserved ejection fraction (HFpEF): HFpEF occurs when the left ventricle contracts normally during systole, but does not relax normally during diastole, as the ventricle is stiff and, which impairs filling.

Acute or chronic heart failure is also a category of heart failure. The acute decompensated heart failure can result in acute respiratory difficulty, that is worsening of chronic heart failure symptoms. Chronic heart failure is a long-term disorder, and it is usually kept stable by the treatment of symptoms. Due to enhanced cardiac demand high-output heart failure can occur, that results in increased left ventricular diastolic pressure that can develop into pulmonary congestion.

Several terms are intimately related to heart failure and may be the cause of heart failure but, these should not be confused with HF. Cardiac arrest and asystole describe to situations in which no cardiac output occurs at all. These result in sudden death without urgent treatment. Myocardial infarction ("Heart attack") [16] refers to heart muscle damage due to inadequate blood supply, usually because of a clogged coronary artery. Cardiomyopathy refers explicitly to problems within the heart muscle, and these problems can result in heart failure. Ischemic cardiomyopathy suggests that the cause of muscle damage is coronary artery disease. The dilated cardiomyopathy implies that the muscle damage has resulted in expansion of the heart. On the other hand, Hypertrophic cardiomyopathy includes enlargement and thickening of the heart muscle [17].

1.7 Heart Failure with Preserved Ejection Fraction (HFpEF)

The volume of blood pumped by the heart depends on two aspects:

(a) The contraction of the cardiac muscle, how well the heart squeezes
(b) The filling of the cardiac chambers, how well the heart relaxes and fills with blood

Heart failure is categorized based on which of these two functions is abnormal [13]. If the heart muscle is too weak, then the condition is recognized as heart failure with a reduced ejection fraction (HFrEF).

If the heart pumps as usual but is too stiff to fill properly, the condition is known as heart failure with preserved ejection fraction (HFpEF) and if EF is less than 50% [2] then it is called HFrEF.

1.7.1 Factors which Cause HFpEF

It has been found from current research that HFpEF occurs when chronic medical conditions harm the heart and the other organ systems of the body [18]. The following medical circumstances can contribute to HFpEF:

- Obesity
- Hypertension (high blood pressure)
- Diabetes mellitus
- Chronic kidney disease
- Atrial fibrillation
- Coronary artery disease
- Chronic obstructive pulmonary disease (COPD)
- Obstructive sleep apnea
- Anemia

Though it is not always true, patients with HFpEF often have one or more of the above conditions. These conditions are assumed to gradually change the structure and function of the heart over time. These changes stiffen the heart and then making it more difficult for it to fill properly. Insufficient filling of the heart restricts the amount of blood pumped with each beat during exercise (or even at rest). At this point the patient starts to show symptoms.

1.7.2 The Most Common Symptoms of HFpEF

The followings are the common symptoms of HFpEF,

- Shortness of breath with exertion or at rest
- Decreased exercise tolerance
- Chest discomfort
- Swelling in the lower extremities
- Fatigue
- Shortness of breath lying flat

The buildup of blood/fluid in the lungs, veins, and tissues of the body can be the source of the symptoms of HFpEF. As the heart is not filling sufficiently fluid backs up into these areas. The buildup of fluid in the lungs can cause shortness of breath while fluid in the legs causes swelling. These symptoms can also originate from the heart not being able to pump enough blood during exercise, or high workload. This can lead to decrease in an individual's exercise capacity and fatigue.

1.8 Progression of HFpEF

Heart failure (HF) disproportionately affects the elderly who predominantly develop HF with preserved left ventricular (LV) ejection fraction (HFpEF), for which no efficacious therapies exist. HFpEF has emerged as a prevalent heart disease which has high risk of short-term and long-term mortality rate recently. Though the ejection fraction, the systolic function might become impaired in HFpEF patients [19 - 21] which is not well understood so far. On the other hand, HFpEF has been associated with a progressively impaired interaction between the left ventricle (LV) and the systemic arteries [22, 23]. Recent data flashes important role of LV diastolic dysfunction, ventricular remodeling, hypertension, myocyte stiffness, hypertrophy, fibrosis etc. on the progression of HFpEF [24]. Very few human data exist from broader samples linking the factors affecting progression of HFpEF. The knowledge for the natural history of clinical progression from the pre-clinical diastolic dysfunction (PDD) until the final clinical stages is considerably limited. The subclinical progression of PDD to the clinical phenotype of HFpEF and the further clinical progression to some more complex clinical models with multi-organ engagement, similar to heart failure with reduced ejection fraction (HFrEF), continue to be poorly recognized. Prospective studies are needed to explain the natural history of clinical progression in patients with HFpEF and to identify the exact left ventricular remodeling, other related physiological variation in the mechanism that underlies this progression. The relevant clinical trials are suboptimal in their design, and the treatment to a great degree is empiric [25]. The pathophysiology of HFpEF is likely to be multifactorial [26, 27]. The number of patients with HFpEF is increasing, partly that is related to the diastolic left ventricular (LV) dysfunction due to aging and to

contributing other comorbidities. The comorbidities have a noticeable effect on the diastolic LV function and on the appearance of the clinical characteristics of heart failure (HF) syndrome, in both phenotypes of HFrEF and HFpEF [25]. Probably the identification of the left ventricular remodeling and other physiological mechanism that underlie the HFpEF, would help to identify the natural history and progression of the syndrome.

1.9 Finite Element Analysis of Human Heart

The goal of computational modeling of heart is to advance mechanistic insight, inspired diagnosis, and innovative therapies for cardiovascular disease by combining imaging sciences, mathematical modeling, informatics, and cardiovascular biology. Advances in medical imaging facilitate acquisition of the structure of vessels and the whole heart with high resolution has greatly enhanced the potential of developing realistic three-dimensional (3D) computational models in recent years. Then the 3D model of heart is solved using efficient FEM (Finite Element Method) solver to replicate the physiology more accurately [28]. Moreover, the increase in the amount of clinical data has improved the field of cardiovascular informatics. The 3D computational models of cardiac anatomy and function combined with clinical data can be used to create advanced patient-specific models which can boost the understanding of cardiovascular diseases. Computational simulations can cost-efficiently prototype the mechanics and the biology of important components of the cardiovascular system. For example, a mathematical model can be developed to simulate the electrophysiological behavior of the myocardium once heart anatomy and structure of the heart is well-defined in 3D. Moreover, electromechanical heart models can mimic the overall organ function to structures from molecular level [29]. Pathological changes, that cause structural and functional cardiac remodeling, may affect the cardiac electromechanical performance [30]. Methods, aiming to simulate both types of remodeling were developed by researchers. Cardiovascular modeling has matured and is progressing towards personalized medicine. The study of cardiac flow is separated into cardiac and vascular hemodynamics. The former includes blood flow in heart chambers, while the latter confers blood transport to/from these chambers via

cardiac vessels. As simplified models can be readily employed in large vessels, the more sophisticated computational modeling focuses on the circulation of smaller arteries by incorporating mathematical lumped-parameter models to simulate the heart cycle [31]. As boundary conditions play a significant role in computational hemodynamics their proper establishing is important for the validity of the computational models. Therefore, lumped-parameter models can serve computational studies of larger vessels hemodynamics to tune the boundary conditions of the exterior arteries. Computational modeling has been recognized by manufacturers and regulatory officials as an economical, yet reliable tool to improve the device design with optimized efficacy. On the other hand, virtual intervention/surgery planning is a promising future step for computational models, wherein device type, sizing, and procedural guidelines might potentially be optimized in complicated clinical cases [32]. Computational models of heart still face several challenges that need to be addressed for the introduction of customized computational medicine into clinics. The Cardiovascular pathogenesis is accompanied by several other co-morbidities, such as diabetes and pulmonary edema, that is initiated and accompanied by several risk factors including smoking, obesity, and other negative life habits. More realistic prognoses and diagnoses would only be obtained if these confusing factors are also included. Over past few years the uses of FEM techniques to model different compartments of heart has been greatly strengthened to recreate hemodynamic behavior of human physiology considering the coupled peripheral mechanisms and closed loop circulation of blood [33-35]. Though these models are successful to predict pathophysiology of Heart failure to a certain extent, but using such modeling framework with the capability of simulating the physiological, hemodynamic, and functional indices found in HFpEF is relatively new in cardiovascular research society.

1.10 Objectives of the Study

Finite element model of the LV with realistic geometry and microstructures is coupled to a closed-loop lumped parameter circulatory model to simulate the cardiac cycle in a normal subject as well as a HFpEF patient. The geometry of LV is created based on the Magnetic Resonance (MR) images acquired from the normal subject and the HFpEF patient. The models are calibrated with the clinical measurements observed in the normal subject and the HFpEF patient.

The specific aims of this study are:

1. To develop a lumped-finite element modeling framework of the systemic circulation that uses 3D FE models of the LV of normal subject and HFpEF patient.
2. To calibrate the model with the clinical measurements of left ventricular volume and pressure waveforms acquired from the normal subject and the HFpEF patient.
3. To quantify the longitudinal and circumferential strain and stress distributions in LV for both cases.
4. To use the calibrated HFpEF model to quantify the contributions of some key factors, such as the LV geometry, afterload, and LV fiber orientation on the progression of HFpEF.

CHAPTER 2

LITERATURE REVIEW

One of the major causes of the death globally is Heart disease. Computational models are being used increasingly to better understand the mechanics of the normal and diseased heart. Over the years Finite element (FE) modeling of the heart having realistic geometry and architectural assembly of cardiac muscle descriptor has advanced significantly. Coupling between electrophysiology and mechanics [36-38] and long-term remodeling of the heart [39-42] have been achieved using such models. Though animal and clinical studies were most used to understand the mechanisms and effects of novel treatments and diseases in the past, computer models are increasingly used to explain the pathophysiology of heart diseases and mechanisms of treatments such as cardiac resynchronization therapy and surgical ventricular restoration [43-45]. Computational models can be used to supplement the animal and clinical studies because of their versatility and low cost. In animal studies often only a limited number of parameters can be manipulated without affecting the others. It makes the process very difficult to distinguish between the contributions of different factors that may affect the pathophysiology of heart diseases. Nevertheless, computer heart models that are validated based on physiological principles are reproducible and has the flexibility to investigate the isolated effects [46, 47] of each parameter without the confounding effects of others. There are some issues still unresolved and facets that need improvements. Additionally, accurate heart models will prompt the researchers to address important unanswered questions about human heart diseases that is not possible through experimentation. Using these models, patient specific medication plan can be developed swiftly in case of urgency, which is time consuming via traditional treatment process.

According to the literature, FE models of the heart were developed either separately [45, 48-50] or an electrical analog of the circulatory system was coupled to the FE model in open [42, 51-54] or closed loop manners [34, 35]. The coupled electrical analog was developed using a simplified representation of the heart's peripheral system, which is based on a time-varying elastance function. Though outlet boundary

conditions the FE ventricular model is generally coupled to a Windkessel model [35] to simulate the ejection of blood in an open-loop circulatory modeling framework. In this process the ends are restricted using physiological conditions. By increasing and constraining the ventricular cavity volume the isovolumic phases and expansion are simulated. So that the four distinct cardiac phases form a closed pressure volume loop to simulate actual heart functioning, the free parameters in the modeling framework are adjusted for both methods. Closed loop circulatory modeling framework is believably more physical since the total blood volume is naturally conserved in the cardiovascular system. In electrical analog (or lumped parameter) and finite element LV coupled model, the ventricular-arterial interactions and the peripheral cardiovascular system is described [55, 56], using highly idealized electrical circuit elements such as resistor, capacitor, and voltage generator. From the beginning of the mathematical modeling of cardiovascular system, one of the major challenges was to model cardiac fiber contraction. Initially only passive contraction [57] model, which is the imposed contraction of cardiac muscle due to its surrounding mechanical conditions, was used. But this does not accurately model cardiac functioning. Accurate description of ventricular active contraction behavior is particularly important in ensuring that the model predictions are consistent with well-established physiological principles at the whole heart level. Active contraction is driven by complicated process which includes calcium ions association-dissociation, number of actin sites available to react with myosin, classical kinetics, differential equation etc. A number of constitutive relations [58-60] for active fiber stress in cardiac muscle was proposed. These relations give some tuning parameters to fit experimental data from the literature. This description of active contraction is still developing and an active research area.

Approximately one-half of all chronic heart failure (HF) patients are associated with Heart failure with preserved ejection fraction (HFpEF). The occurrence of HFpEF is increasing at a rate of about 1% per year, [2,61, 62] with mortality rates comparable to HF with reduced ejection fraction (HFrEF) [63, 64]. Patients diagnosed with HFpEF are older and most of them have hypertension [2]. Though new therapies are being proposed [65-69] and discovered, but there is still no proven treatment option currently

exists for HFpEF patients [26, 70]. Many pathological features are present which impairs LV filling [71] such as, cardiomyocyte stiffening, [72] concentric hypertrophy [73], slow LV relaxation, [72] etc. Diastolic dysfunction, which was previously referred to as diastolic HF [62, 74], was initially believed to be the only mechanism underlying HFpEF. Recent studies have suggested that myocardial contractility in HFpEF patients may also be impaired. So, the original notion that systolic function is preserved, as EF is preserved in this syndrome [75-78] is also under question. It has been found that LV ejection fraction (EF) and end-systolic elastance (E_{es}) are normal or increased in HFpEF. This suggests the preservation or increment of global ventricular contractility [22, 79]. Contradictorily, HFpEF diagnosed hearts exhibit decreased global longitudinal strain, which in turn suggests that myocardial contractility is decreased. Only using clinical or experimental studies, these prominent conflicting observations are difficult to resolve. HFpEF patients also shows increased LV mass, increased vascular resistance (afterload), altered LV geometry. These has individual and coupled effect on longitudinal strain, which in turn confuse the link between myocardial contractility and longitudinal strain. But computational modeling framework inherently solve this problem by isolating the factors affecting LV function and progression in HFpEF patients. So, it is possible to separate the individual roles and contributions of these factors over preclinical and subclinical stages of HFpEF. However, there are only some studies that have explored the use of computational modeling to understand ventricular mechanics in HFpEF [80-84]. As understanding the mechanisms for progression of HFpEF provides the opportunity, to target these mechanisms in therapeutic or preventive strategies, the transition among stages of HFpEF is an area of intense research [85]. The traditional understanding of HFpEF progression is focused on structural left ventricular remodeling, left ventricular hypertrophy, hypertension, left ventricular diastolic dysfunction, left atrial dilatation, macrovascular stiffening, left ventricular fibrosis, etc. which involve both central and peripheral factors [86-87]. But until now, very few studies have been conducted to understand the mechanisms underlying the pathophysiology of HFpEF [10, 88]. Recent computational study investigated effect of increased myocardial stiffness [89] on HFpEF progression. So, to the best of our knowledge, the effects of LV geometry,

fiber orientation and after load on HFpEF progression have not received much attention so far which is the primary goal of this study.

CHAPTER 3

MODELING THE LEFT VENTRICLE AND CIRCULATORY SYSTEM

This chapter discusses the details about the systemic circulatory model, the finite element model of left ventricle and their coupling.

3.1 Modeling the Systemic Circulatory System

The systemic circulatory system was modeled using a Finite element model of the LV and coupling it with other compartments of the systemic circulation using a closed-loop lumped parameter circulatory model.

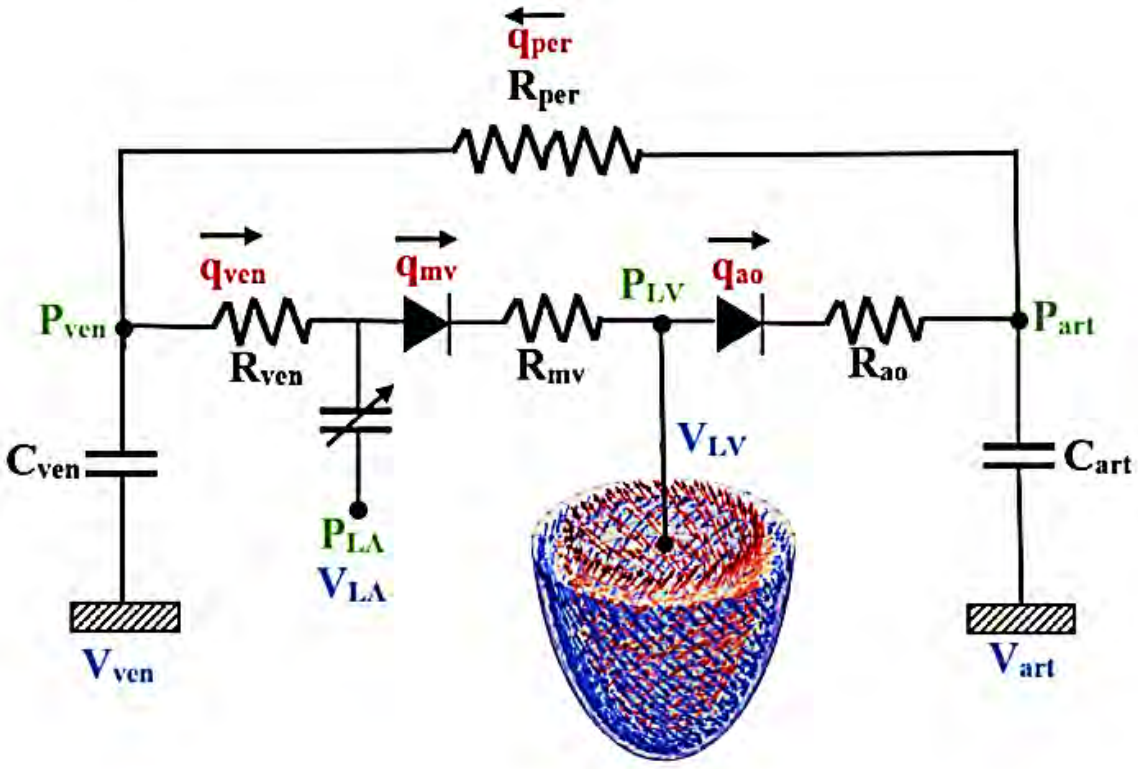

Figure 3. 1: Schematic diagram of the modeling framework showing the LV FE model and other compartments of the systemic circulation which were modeled using their electrical analog [34].

Electrical analogs (Figure 3.1) were used to model other components of the circulatory system, namely, the left atrium (LA), the systemic arteries and the veins. As the total mass of blood in the circulatory system has to be conserved, the rate of volume change in each storage compartment of the circulatory system must be related to the net change of inflow and outflow rates by the following equations [34],

$$\frac{dV_{LA}(t)}{dt} = q_{ven}(t) - q_{mv}(t); \quad (1)$$

$$\frac{dV_{LV}(t)}{dt} = q_{mv}(t) - q_{ao}(t); \quad (2)$$

$$\frac{dV_{art}(t)}{dt} = q_{ao}(t) - q_{per}(t); \quad (3)$$

$$\frac{dV_{ven}(t)}{dt} = q_{per(t)} - q_{ven}(t); \quad (4)$$

Where,

V_{LA}, V_{LV}, V_{art} and V_{ven} are volumes of left atrium, left ventricle, systemic arteries, and systemic veins respectively, where the subscript *LA, LV, art* and *ven* denotes the left atrium, left ventricle, systemic arteries, and systemic veins, respectively. q_{ven}, q_{mv}, q_{ao} and q_{per} are flow rates at systemic veins, mitral valve, aorta, and peripheral system respectively (Figure 3.1).

The flowrate depends on the pressure gradient and resistance to flow as described by the following equations at each segment [34],

$$q_{ao}(t) = \begin{cases} \dfrac{P_{LV,cav}(t) - P_{art}(t)}{R_{ao}}, & when, P_{LV,cav}(t) \geq P_{art}(t) \\ 0, & when, P_{LV,cav}(t) < P_{art}(t) \end{cases}; \quad (5)$$

$$q_{per}(t) = \frac{P_{art}(t) - P_{ven}(t)}{R_{per}}; \quad (6)$$

$$q_{ven}(t) = \frac{P_{ven}(t) - P_{LA}(t)}{R_{ven}}; \quad (7)$$

$$q_{mv}(t) = \begin{cases} \frac{P_{LA}(t) - P_{LV,cav}(t)}{R_{mv}}, & when, P_{LA(t)} \geq P_{LV,cav}(t) \\ 0, & when, P_{LA(t)} < P_{LV,cav}(t) \end{cases}; \quad (8)$$

Where, R_{ao} and R_{mv} are the aortic valve and mitral valve resistances. The peripheral and venous vessel resistance of the systemic circulation are denoted by R_{per} and R_{ven} respectively. The pressure in each storage compartment can be obtained as a function of its volume by incorporating the compliance of each vessel. The following pressure volume relationships were used in the model for the veins and the aorta [34],

$$P_{ven}(t) = \frac{V_{ven}(t) - V_{ven}(0)}{C_{ven}}; \quad (9)$$

$$P_{art}(t) = \frac{V_{art}(t) - V_{art}(0)}{C_{art}}; \quad (10)$$

Where,

$V_{ven}(0)$ and $V_{art}(0)$ are resting volume of the veins and aorta, respectively.

C_{ven} and C_{art} is the total compliance of the venous system and aorta, respectively.

Pressure in the left atrium $P_{LA}(t)$ was calculated from a function of its volume $V_{LA}(t)$ by the following equations that describe its contraction which uses a time-varying elastance function $e(t)$ [34]**:**

$$P_{LA}(t) = e(t)P_{es,LA}(V_{LA}(t)) + (1 - e(t))P_{ed,LA}(V_{LA}(t)); \quad (11)$$

Where,

$$P_{es,LA}(V_{LA}(t)) = E_{es,LA}(V_{LA}(t) - V_{0,LA}); \quad (11\ a)$$

$$P_{ed,LA}(V_{LA}(t)) = A_{LA}(e^{B_{LA}(V_{LA}(t)-V_{0,LA})} - 1); \quad (11\text{ b})$$

$$e(t) = \begin{cases} \frac{1}{2}(\sin[(\frac{\pi}{t_{\max}})t - \frac{\pi}{2}] + 1); & 0 < t \le \frac{3}{2}t_{\max} \\ \frac{1}{2}e^{-(t-\frac{3}{2}t_{\max})/\tau}; & t > \frac{3}{2}t_{\max} \end{cases}; \quad (11\text{ c})$$

In Equations (11 a) & (11 b), $E_{es,LA}$ is the end-systolic elastance of the left atrium, $V_{0,LA}$ is the volume axis intercept of the end-systolic pressure volume relationship (ESPVR) of LA, and both A_{LA} and B_{LA} are parameters of the end-diastolic pressure volume relationship (EDPVR) of the left atrium. Here, the driving function $e(t)$ is given in Equation (11 c) in which t_{max} is the point of highest chamber elastance of the LA, and τ is the time constant of relaxation of the LA. The values of $E_{es,LA}$, $V_{0,LA}$, A_{LA}, B_{LA}, t_{max}, and τ are listed in Table 3.1. Pressure in the Left Ventricle depends on its corresponding volume through non-closed form functions,

$$P_{LV,cav}(t) = f^{LV}(V_{LV}(t)); \quad (12)$$

The functional relationships between pressure and volume of the LV has been achieved using the FE method described in the next section.

Table 3. 1: Time varying elastance model parameters for left atrium [31].

Parameters	**Units**	**Values (Normal and HFpEF baseline)**
End-systolic elastance, $E_{es,LA}$	Pa/ml	60
Scaling factor for EDPVR, A_{LA}	Pa	58.67
Time constant of relaxation, τ	ms	25
Exponent for EDPVR, B_{LA}	ml^{-1}	0.05
Time to end-systole, t_{max}	ms	120
Volume axis intercept, $V_{0,LA}$	ml	10

Table 3. 2: Parameters of the closed loop lumped parameter circulatory model [31].

Parameters	Units	Values (Normal baseline)	Values (HFpEF baseline)
Peripheral resistance, R_{per}	Pa ms ml^{-1}	150000	110000
Mitral valve resistance, R_{mv}	Pa ms ml^{-1}	500	500
Aortic valve resistance, R_{ao}	Pa ms ml^{-1}	1600	500
Venous resistance, R_{ven}	Pa ms ml^{-1}	2,000	2,000
Resting volume for vein, $V_{ven,0}$	ml	3430	2900
Venous compliance, C_{ven}	ml Pa	0.3	0.3
Aortic compliance, C_{ao}	ml Pa	0.007	0.01
Resting volume for aorta, $V_{art,0}$	ml	670	740

3.2 Formulation of the Left Ventricular Finite Element model

The left ventricle was modeled using the finite element method. The weak form associated with the left ventricular finite element model was derived based on the minimization of the following Lagrangian functional [90, 91],

$$\begin{aligned}\mathcal{L}_{LV}(\boldsymbol{u_{LV}}, p_{LV}, P_{LV,cav}, \boldsymbol{c_{1,LV}}, \boldsymbol{c_{2,LV}}) = \\ \int_{\Omega_{0,LV}} W_{LV}(\boldsymbol{u_{LV}})dV - \int_{\Omega_{0,LV}} p_{LV}(J_{LV}-1)dV - \\ P_{LV,cav}(V_{LV,cav}(\boldsymbol{u_{LV}})-V_{LV}) - \boldsymbol{c_{1,LV}}\int_{\Omega_{0,LV}} \boldsymbol{u_{LV}}dV - \\ \boldsymbol{c_{2,LV}}\int_{\Omega_{0,LV}} \boldsymbol{X_{LV}}\times\boldsymbol{u_{LV}}dV;\end{aligned} \tag{13}$$

In the above equation, $\boldsymbol{u_{LV}}$ is the displacement field, $P_{LV,cav}$ is the Lagrange multiplier to constrain the cavity volume $V_{LV,cav}(\boldsymbol{u_{LV}})$ to a prescribed value V_{LV} [90], p_{LV} is a Lagrange multiplier to impose incompressibility of the tissue (i.e., Jacobian of the deformation gradient tensor $J_{LV} = 1$), and both $\boldsymbol{c_{1,LV}}$ and $\boldsymbol{c_{2,LV}}$ are Lagrange multipliers to constrain rigid body translation (i.e., zero mean translation) and rotation (i.e., zero mean rotation) [91]. The functional relationship between the cavity volumes of the LV to its displacement fields is provided by

$$V_{LV,cav}(\boldsymbol{u_{LV}}) = \int_{\Omega_{inner}} dV = -\frac{1}{3}\int_{\Gamma_{inner}} \boldsymbol{x_{LV}} \cdot \boldsymbol{n_{LV}} da \; ; \tag{14}$$

Where, Ω_{inner} is the volume enclosed by the Γ_{inner} surface and the basal surface at $z = 0$, and $\boldsymbol{n_{LV}}$ is the outward unit normal vector.

Taking the first variation of the functional in Equation (13) leads to the following expression:

$$\begin{aligned}
&\delta\mathcal{L}_{LV}(\boldsymbol{u_{LV}}, p_{LV}, P_{LV,cav}, \boldsymbol{c_{1,LV}}, \boldsymbol{c_{2,LV}}) = \\
&\int_{\Omega_{0,LV}} (\boldsymbol{P_{LV}} - p_{LV}\boldsymbol{F_K^{-T}}) : \nabla \delta \boldsymbol{u_{LV}} dV - \int_{\Omega_{0,LV}} \delta p_{LV}(J_{LV} - 1) dV \; - \\
&P_{LV,cav} \int_{\Omega,LV} cof(\boldsymbol{F_{LV}}) : \nabla \delta \boldsymbol{u_{LV}} dV - \delta P_{LV,cav}(V_{LV,cav}(\boldsymbol{u_{LV}}) - V_{LV}) - \\
&\delta \boldsymbol{c_{1,LV}} \int_{\Omega_{0,LV}} \boldsymbol{u_{LV}} dV \; - \; \delta \boldsymbol{c_{2,LV}} \int_{\Omega_{0,LV}} \boldsymbol{X_{LV}} \times \boldsymbol{u_{LV}} dV \; - \\
&\boldsymbol{c_{1,LV}} \int_{\Omega_{0,LV}} \delta \boldsymbol{u_{LV}} dV \; - \; \boldsymbol{c_{2,LV}} \int_{\Omega_{0,LV}} \boldsymbol{X_{LV}} \times \delta \boldsymbol{u_{LV}} dV \; ;
\end{aligned} \tag{15}$$

In Equation (15), $\boldsymbol{P_{LV}}$ is the first Piola Kirchhoff stress tensor, $\boldsymbol{F_{LV}}$ is the deformation gradient tensor, $\delta\boldsymbol{u_{LV}}$, δp_{LV}, $\delta P_{LV,cav}$, $\delta\boldsymbol{c_{1,LV}}$, $\delta\boldsymbol{c_{2,LV}}$ are the variation of the displacement field, Lagrange multipliers for enforcing incompressibility and volume constraint, zero mean translation and rotation, respectively. The Euler-Lagrange problem then

becomes finding $\boldsymbol{u_{LV}} \in H^1(\Omega_{0,LV})$, $p_{LV} \in L^2(\Omega_{0,LV})$, $P_{LV,cav} \in \mathbb{R}$, $\boldsymbol{c_{1,LV}} \in \mathbb{R}^3$, $\boldsymbol{c_{2,LV}} \in \mathbb{R}^3$ that satisfies

$$\delta \mathcal{L}_{LV}(\boldsymbol{u_{LV}}, p_{LV}, P_{LV,cav}, \boldsymbol{c_{1,LV}}, \boldsymbol{c_{2,LV}}) = 0; \tag{16}$$

Boundary Condition, $u_Z = 0$ (for constraining the basal deformation to be in-plane).

An explicit time integration scheme was used to solve the ODEs in Equations (1), (2), (3), (4). Specifically, compartment volumes (V_{LA}, V_{LV}, V_{art}, V_{ven}) at each timestep t_i was calculated from their respective values and the segmental flow rates (q_{ven}, q_{mv}, q_{ao}, q_{per}) at previous timestep t_{i-1} in Equation (1)-(4). Then the computed compartment volumes at t_i were used to update the corresponding pressures (P_{LA}, $P_{LV,cav}$, P_{art}, P_{ven}). Pressures in the left atrium (P_{LA}), aorta (P_{art}) and veins (P_{ven}) were calculated from Equations (11), (10) and (9) respectively. On the other hand, pressures in the LV ($P_{LV,cav}$) was calculated from the FE solutions of Equation (16) with the volume (V_{LV}) at timestep t_i as input. Here $P_{LV,cav}$ is scalar Lagrange multiplier in the FE formulation for constraining the cavity volumes to the prescribed values (V_{LV}). The computed pressures at timestep t_i were then utilized to update the segmental flow rates in Equations (5), (6), (7), (8) that will be used to calculate the compartment volumes at timestep t_{i+1} in the next iteration. The steady-state pressure-volume loop was established by running the simulation over several cardiac cycles, each with a cycle time of 773 ms (equivalent to 78 bpm) for normal subject and 900 ms (equivalent to 67 bpm) for the HFpEF case. All the parameter values used in the circulatory model are listed in Table 3.2. The initial conditions are tabulated in Table 3.3. The modeling framework was implemented using FEniCS [92], which is an open-source platform for solving PDEs. The simulation flow diagram for obtaining steady state solution using the described model is shown below:

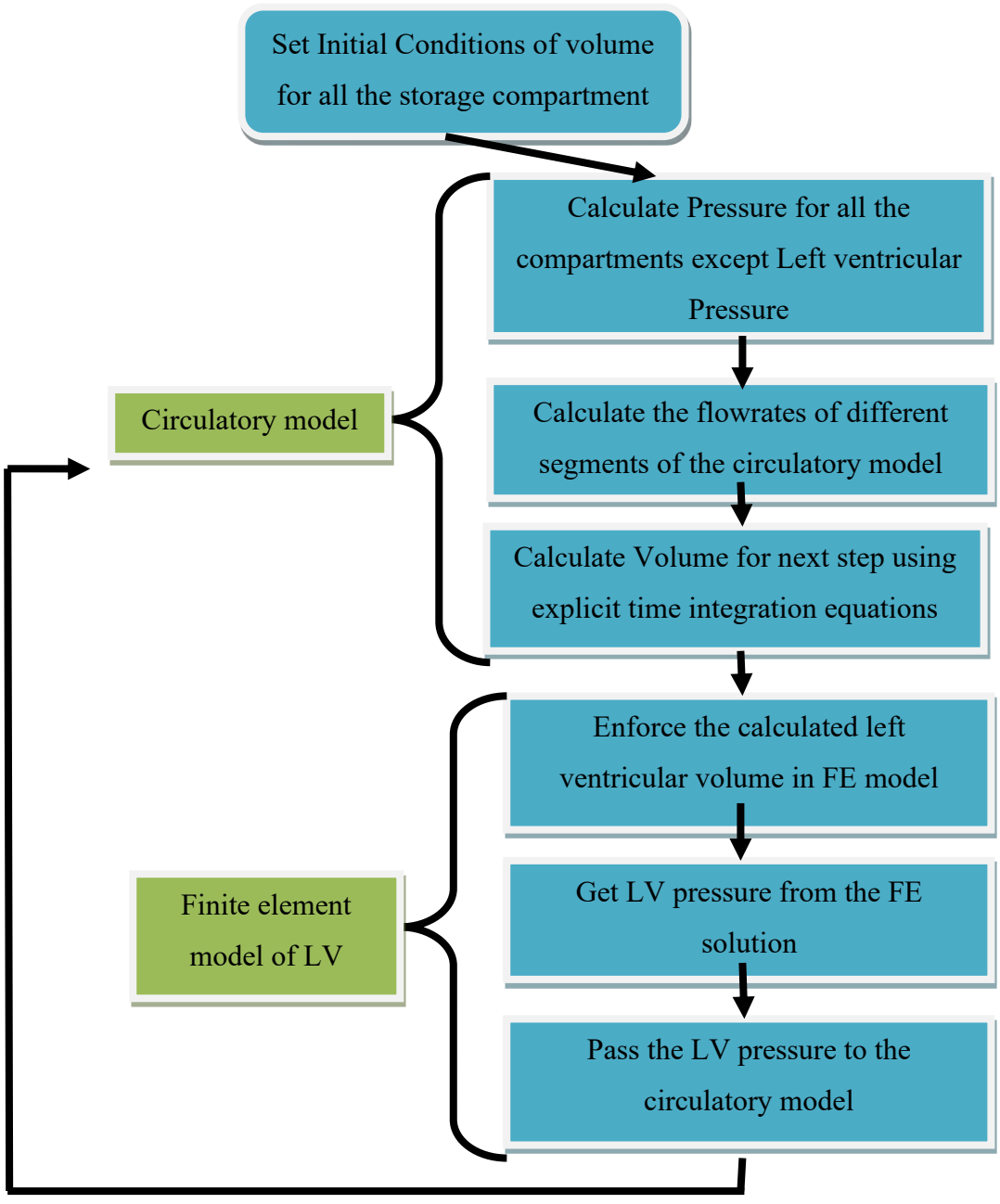

Figure 3. 2: Simulation flow diagram for obtaining the steady state solution using the coupled LV FE lumped parameter systemic circulatory model.

Table 3. 3: Parameters supplied as the initial conditions for the compartmental volumes and pressures.

Parameters	Units	Values
P_{art}	mmHg	0
P_{ven}	mmHg	0
P_{LA}	mmHg	0
$P_{LV,cav}$	mmHg	0
V_{ven}	ml	3700
V_{art}	ml	740
V_{LA}	ml	12

3.3 LV Geometry, Meshing and Microstructure of the LV

Clinical data (Pressure, Volume for a single cardiac cycle) and MR images of left ventricle had been acquired from a normal subject and a patient who was diagnosed with HFpEF in National Heart Center (NHC), Singapore. LV endocardium surfaces were constructed (Figure 3.3) based on the acquired MR images of Normal patient and for HFpEF case. Using the reconstructed LV endocardium surfaces, the 3D LV geometry was created using a half prolate ellipsoid shape. The LV volume was constructed to match the minimum pressure condition which is a position in between ESV and EDV, but near to EDV, as acquired from the clinical data. The geometrical parameters of the LV models are shown in Table 3.4. Here the wall thickness of LV has been adjusted using previous studies [10, 24].

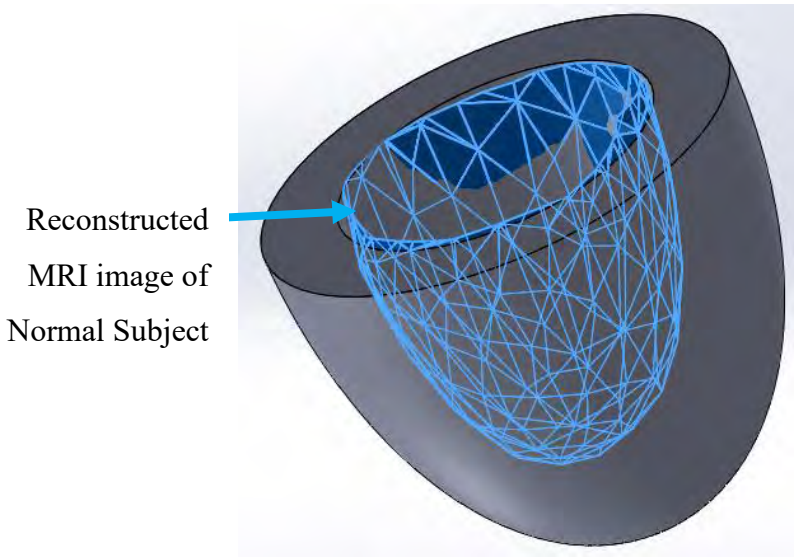

(a)

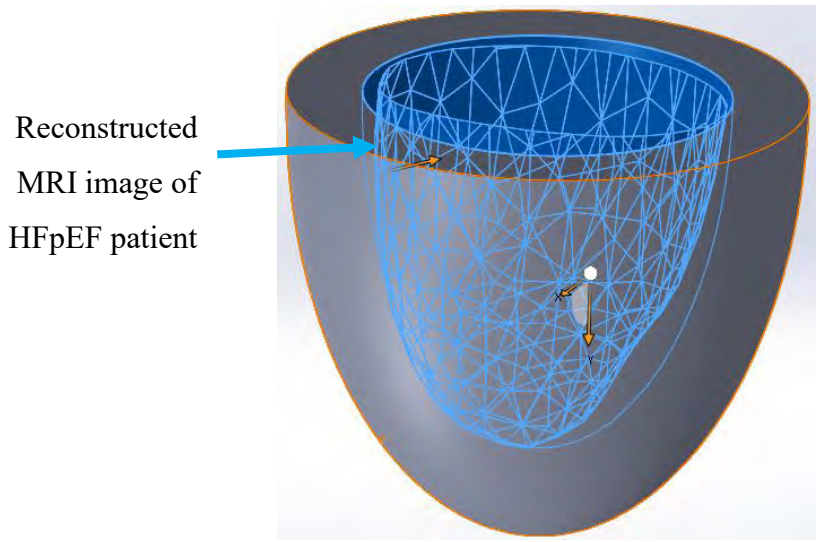

(b)

Figure 3. 3: Half prolate ellipsoid geometrical models of LV, constructed based on the acquired MRI images of (a) normal subject and (b) HFpEF patient.

Table 3. 4: Geometrical Parameters of LV for Normal and HFpEF baseline model.

	Normal		HFpEF baseline	
	Model (unloaded)	Clinical (at minimum pressure)	Model (unloaded)	Clinical (at minimum pressure)
Cavity Diameter (cm) (at basal plane)	4.63	4.72	5.5	5.31
Length (cm)	4.82	4.86	5.49	5.49
Wall thickness(cm)	1.13	_	1.45	_

The LV geometry was discretized (Figure 3.4) with 1150 - 1450 quadratic tetrahedral elements which was determined using grid independence test (Section 3.6). So, there were 10 nodes for each quadratic element, and each has 3 Degrees of freedom (DOF) in three cartesian co-ordinate directions. So, each quadratic element has total 30 DOF. The microstructure of Heart is fibrous. The myocardial fiber of left ventricle is arranged helically across its length (Figure 3.5). The helix angle associated with the myofiber direction was varied with a linear transmural variation from 60° at the endocardium to -60° at the epicardium in the LV for both normal and HFpEF cases based on previous experimental measurements [93, 94] (Figure 3.6).

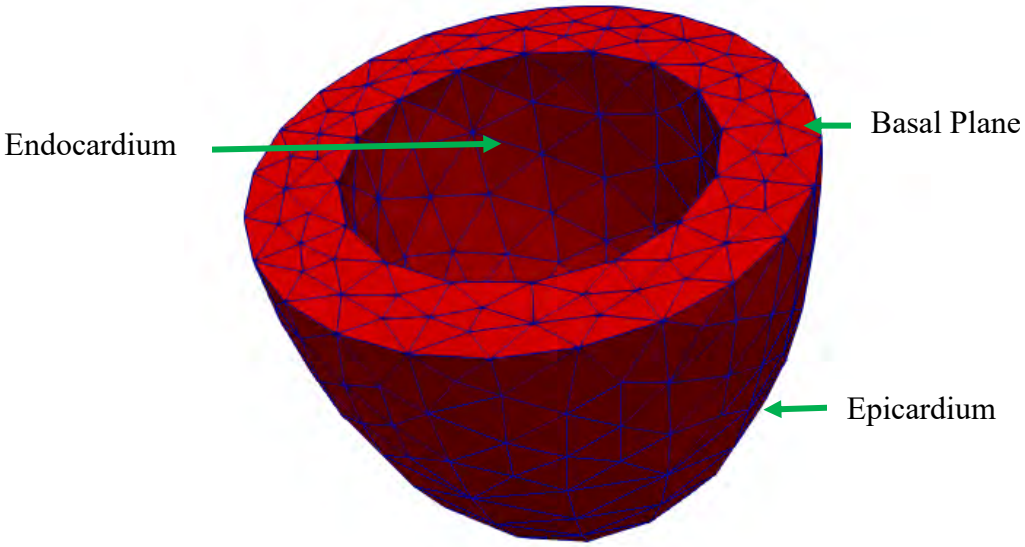

Figure 3. 4: LV geometry defined using a half prolate ellipsoid and discretized with quadratic tetrahedral elements

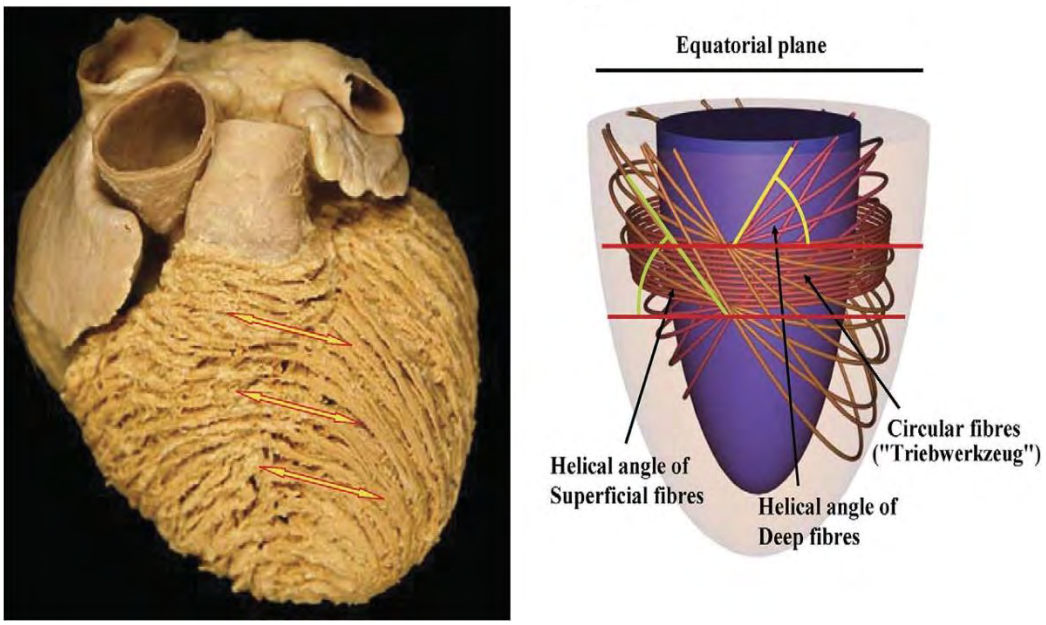

Figure 3. 5: Linear transmural variation of helix angle associated with the myofiber direction from endocardium to the epicardium shown in a (a) real heart image and (b) computational model [94].

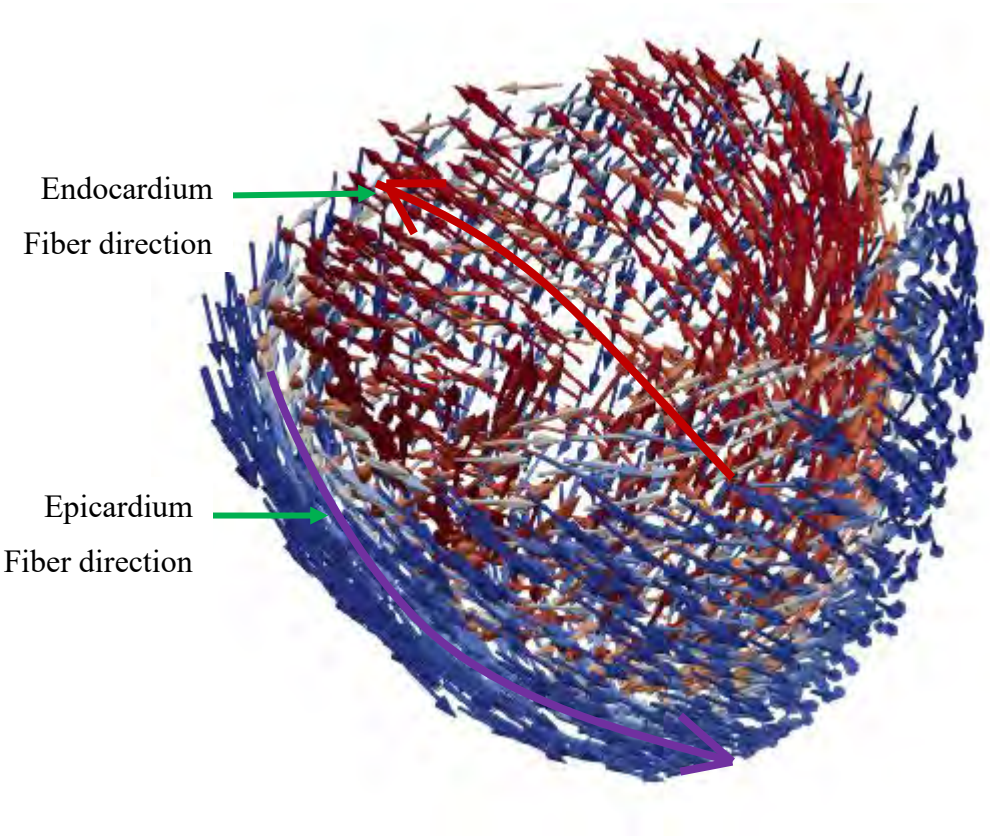

Figure 3. 6: Variation of the helix angle associated with the myofiber direction from the LV endocardium to the epicardium used in the FE model

3.4 Constitutive Law of the LV

An active stress formulation was utilized to describe the LV's mechanical behavior in the cardiac cycle. In this formulation, the stress tensor P_{LV} can be disintegrated additively into a passive component $P_{LV,p}$ and an active component $P_{LV,a}$ (i.e., $P_{LV} = P_{LV,a} + P_{LV,p}$). The active stress $P_{LV,a}$ applied along the local fiber orientation [58].

The passive stress tensor was defined by

$$P_{LV,p} = \frac{dW_{LV}}{dF_{LV}} \tag{17}$$

Where, W_{LV} is a strain energy function of a Fung-type hyperelastic material and $\boldsymbol{F_{LV}}$ is the deformation tensor gradient for Left ventricle. [58].

$$W_{LV} = \frac{1}{2}C(e^{Q} - 1); \tag{18}$$

Where,

$$\begin{aligned} Q = b_{ff}\boldsymbol{E_{ff}^2} + b_{XX}(\boldsymbol{E_{ss}^2} + \boldsymbol{E_{nn}^2} + \boldsymbol{E_{sn}^2} + \boldsymbol{E_{ns}^2}) + \\ b_{fX}(\boldsymbol{E_{fn}^2} + \boldsymbol{E_{nf}^2} + \boldsymbol{E_{fs}^2} + \boldsymbol{E_{sf}^2}); \end{aligned} \tag{19}$$

Here, C is a material parameter (unit is Pa) that can be varied to change the stiffness of the material (resembles Young's modulus). The values of material parameters b_{ff}, b_{xx} and b_{fx} can be modified to change the stiffness along the direction of myofibers and the plane perpendicular to the myofibers to get polar anisotropic response. The values of material parameters b_{ff}, b_{xx} and b_{fx} that are used in this model are based on the previously published studies [57, 59]. The parameter C has been adjusted to match the measured end-diastolic pressure (EDP) of the normal and HFpEF cases.

In Equation (19), $\boldsymbol{E_{ij}}$ with $(i, j) \in (f, s, n)$ are components of the Green-Lagrange strain tensor $\boldsymbol{E_{LV}}$ with f, s, n denoting the myocardial fiber, sheet, and sheet normal directions, respectively (Figure 3.7).

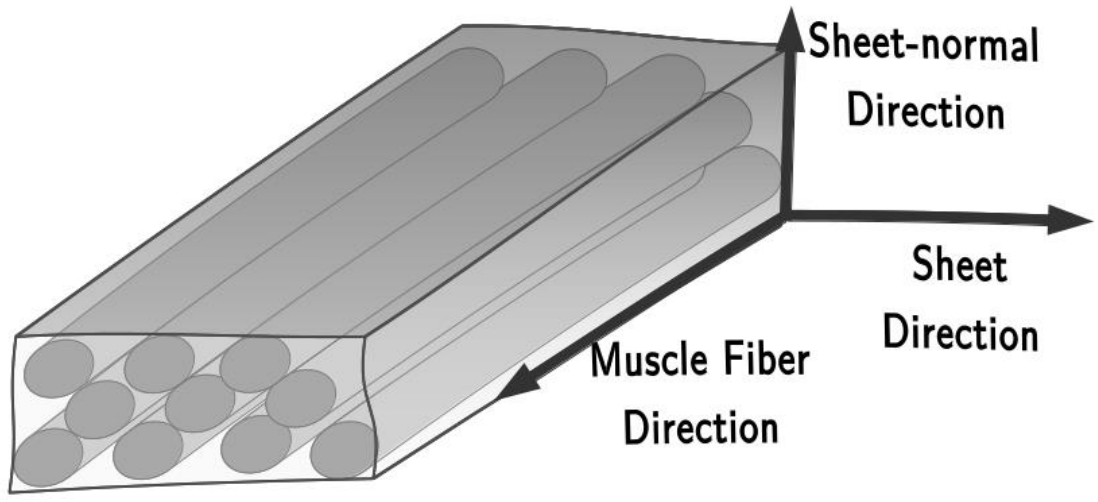

Figure 3. 7: Myocardial fiber direction f, sheet direction s and sheet normal direction n.

The active stress $\boldsymbol{P_{LV,a}}$ was computed along the local fiber direction using a previously developed active contraction model [59, 95].

$$\boldsymbol{P_{LV,a}} = T_{\max}\frac{C_{a0}^2}{C_{a0}^2 + EC_{a50}^2} C_t \ \boldsymbol{e_f} \otimes \boldsymbol{e_{f0}}; \tag{20}$$

In the above equation, $\boldsymbol{e_f}$ and $\boldsymbol{e_{f0}}$ are, respectively, the local vectors characterizing the muscle fiber direction in the current and reference configurations, T_{max} is the isometric tension attained at the longest sarcomere length and C_{a0} denotes the peak intracellular calcium concentration. The length dependent calcium sensitivity EC_{a50} and the variable C_t are given by,

$$EC_{a50} = \frac{(C_{a0})_{\max}}{\sqrt{\exp(B(l - l_0)) - 1}}; \tag{21}$$

$$C_t = w_1 + w_2 + w_3; \tag{22}$$

In Equation (21), B is a constant, $(C_{a0})_{max}$ is the maximum peak intracellular calcium concentration and l_0 is the sarcomere length at which no active tension develops. The variables w_1, w_2, w_3 in Equation (22) is given by

$$w_1 = \frac{1}{2}[\sin(\frac{\pi t}{t_0} - \frac{\pi}{2}) + 1], \text{ when } t < t_{trans0}; \tag{22 a}$$

$$w_2 = 0.9\exp(-\frac{t - t_{trans}}{t_r}), \text{ when } t \geq t_{trans}; \tag{22 b}$$

$$w_3 = y_0 + \frac{0.9 - y_0}{t_{trans} - t_{trans0}}(t - t_{trans0}); \text{ when } t_{trans0} \leq t < t_{trans}, \tag{22 c}$$

$$\text{where } \ y_0 = \frac{1}{2}[\sin(\frac{\pi . t_{trans0}}{t_0} - \frac{\pi}{2}) + 1],$$

In the above equation, t_0 is the time taken to reach peak tension and t_r is the duration of relaxation of Left ventricle. Time t_{trans0} and t_{trans} are used to specify the transition time for the different functional relations. In between t_{trans0} and t_{trans} the relation is linear. Before t_{trans0} the relation is sinusoidal and after t_{trans} the relation is exponential decay.

The sarcomere length l can be calculated from the myofiber stretch λ_{LV} by

$$\lambda_{LV} = \sqrt{\boldsymbol{e}_{f0} \cdot \boldsymbol{C}_{LV} \boldsymbol{e}_{f0}}; \tag{23}$$

$$l = \lambda_{LV} l_r; \tag{24}$$

In Equation (23), $\boldsymbol{C}_{LV} = \boldsymbol{F}_{LV}^{T} \boldsymbol{F}_{LV};$ is the right Cauchy Green deformation tensor and l_r is the relaxed sarcomere length. Parameter values related to the LV constitutive model are tabulated in Table 3.5.

Table 3. 5: Constitutive model parameters for the Left Ventricle. [57, 59]

	Parameters	**Description**	**Values (Normal baseline)**	**Values (HFpEF baseline)**
Passive material model	C	material parameter, kPa	0.05	0.05
	b_{ff}	material parameter	29	29
	b_{xx}	material parameter	26.6	26.6
	b_{fx}	material parameter	16	16
Active contraction model	T_{max}	isometric tension under maximal activation, kPa	400	170
	C_{a0}	peak intracellular calcium concentration, μM	4.35	4.35
	$(C_{a0})_{max}$	maximum peak intracellular calcium concentration, μM	4.35	4.35
	B	governs shape of peak isometric tension-sarcomere length relation, μm^{-1}	4.75	4.75
	l_0	sarcomere length at which no active tension develops, μm	1.58	1.58
	t_r	Left ventricular relaxation time constant, ms	35	60
	t_0	time to peak tension, ms	350	330
	t_{trans}	time constant, ms	350	350
	t_{trans0}	time constant, ms	340	340
	l_r	relaxed sarcomere length, μm	1.85	1.85

3.5 Calculation of Myocardial Strain

Regional three-dimensional strains in the longitudinal and circumferential, and directions were computed using end-diastole as the reference configuration. Specifically, the myofiber stretch in these directions were expressed as:

$$\lambda_i = \sqrt{\boldsymbol{e_i} . \boldsymbol{C_{LV}} \boldsymbol{e_i}}; \tag{25}$$

where, $\boldsymbol{C_{LV}} = \boldsymbol{F_{LV}}^T \boldsymbol{F_{LV}}$; is the right Cauchy-Green deformation tensor, and $\boldsymbol{e_i}$ with $i \in$ (l, c) are the unit vectors in the longitudinal l and circumferential c directions, respectively. The radial direction $\boldsymbol{e_r}$ is described to be normal to the LV wall. The circumferential direction $\boldsymbol{e_c}$ is described to be orthogonal to $\boldsymbol{e_r}$ and the apex-base direction. Finally, the longitudinal direction, $\boldsymbol{e_l}$ is described to be orthogonal to both $\boldsymbol{e_r}$ and $\boldsymbol{e_c}$. Therefore, this longitudinal direction is tangential to the LV cavity wall surface. Euler-Almansi strains were calculated using the following definitions [34]:

$$\varepsilon_i = \frac{1}{2}(1 - \frac{1}{\lambda_i^2}); \tag{26}$$

The spatially averaged strain has been computed for each time step by,

$$\varepsilon_{i,avg} = \frac{1}{V}\int_{\Omega_{0,LV}} e_i dV; \tag{27}$$

3.6 Grid Independence Test

To establish consistency in the finite element results with the variation of element numbers, grid independence study was conducted. Simulation study has been done for element size ranging from 240 - 1870 quadratic tetrahedral elements. After 800 element numbers, the results do not change significantly with the number of elements. PV loop, LV volume and pressure waveforms for normal LV model are shown in Figure 3.8 for the variations of number of quadratic tetrahedral elements of the LV model. As change in pressure is more prominent than volume, we see that the maximum difference between the pressure values for 1150 elements and 1870 elements is only ~1.91%. But running the model with 1870 elements significantly increase the simulation time. Therefore, to efficiently simulate the cases with respect to simulation time, 1150 - 1450 elements was chosen for the numerical simulation of the different cases in this study. From this discussion we can conclude that the results presented in this study are mesh independent.

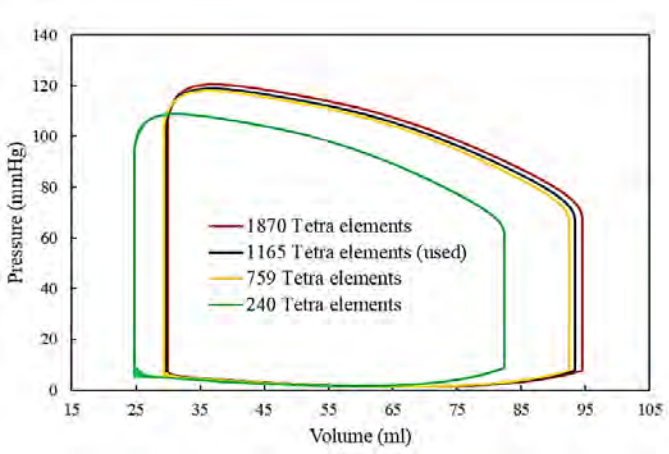

(a)

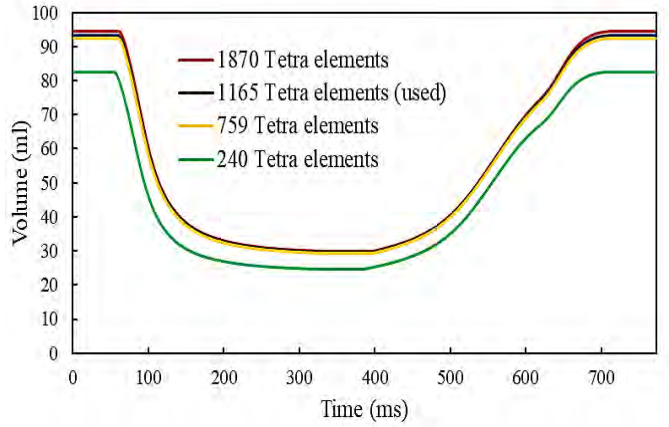

(b)

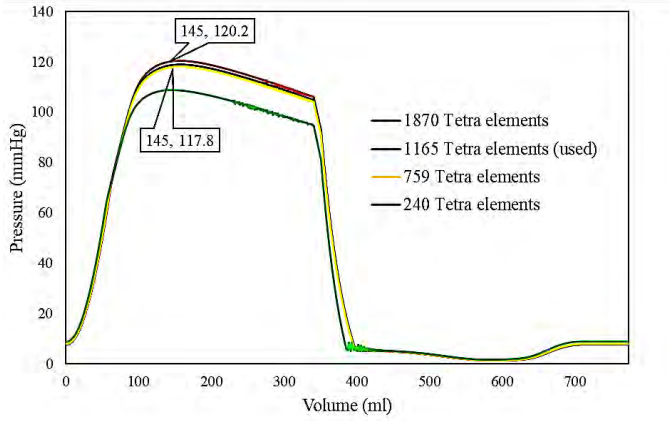

(c)

Figure 3. 8: Comparison of steady-state LV (a) PV loop, (b) volume waveforms, (c) pressure waveforms for normal case for different number of quadratic tetrahedral elements.

CHAPTER 4

RESULTS AND DISCUSSION

The model has been calibrated with the clinical data of one normal subject and one HFpEF patient acquired from National Heart Center (NHC), Singapore. With these two models it has been verified that model can successfully predict the subject specific or patient specific characteristics. Later, the calibrated HFpEF model has been used to study some of the possible paths of progression by varying relevant parameters. The model parameters that correspond to the geometry, afterload and fiber orientation were changed for different cases. The results (hemodynamics and overall mechanical behaviors) obtained from these HFpEF models with isolated change in geometry or, afterload or, fiber direction was compared with the baseline HFpEF model (calibrated with patient data).

4.1 Comparison between Simulation and Clinical Measurements for the Normal Subject

The PV loops, volume and pressure waveforms of the LV for the normal subject predicted by the model were closely matched with the measured data as shown in the Figure 4.1. The measured EDV (94 ml) and ESV (26.9 ml) were reasonably matched with the model (94 ml EDV and 29.4 ml ESV). As a result, the EF was 68.7% for the model which is close to the measured EF of 71.3% (which is within the normal range > 55%). Pressure waveforms of the LV (Figure 4.1) in the baseline case were also showed good match with the measurements. The simulated aortic pressure waveform is within the normal range with an aortic pulse pressure of 48 mmHg (systolic: 125 mmHg, diastolic: 77 mmHg). R-squared values of the scatter plots of simulated vs. measured volume and pressure are 0.937 and 0.945 respectively, which confirms a good fit. The parameters matched for normal subject are tabulated in Table 4.1.

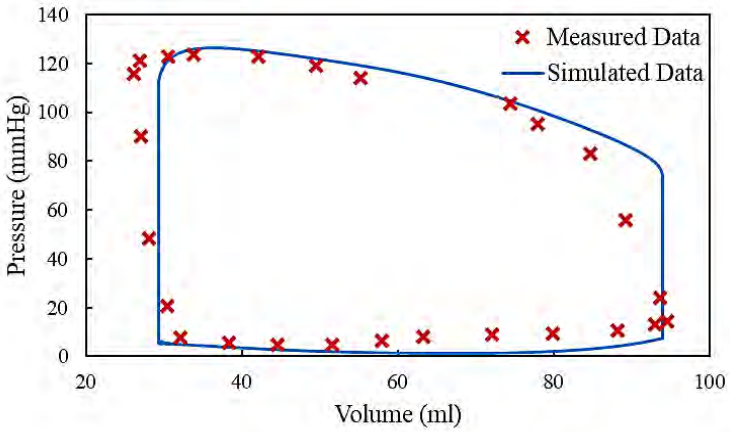

(a)

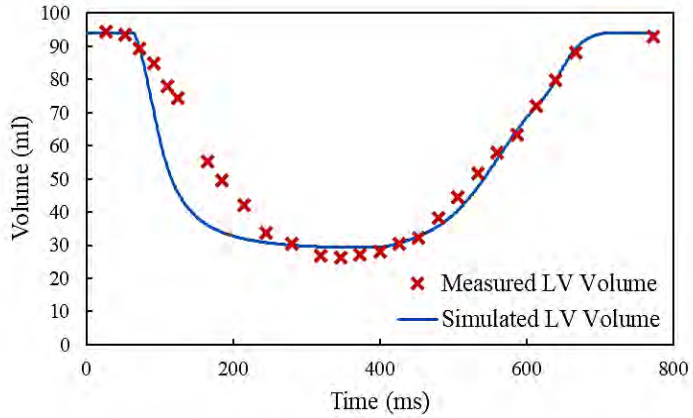

(b)

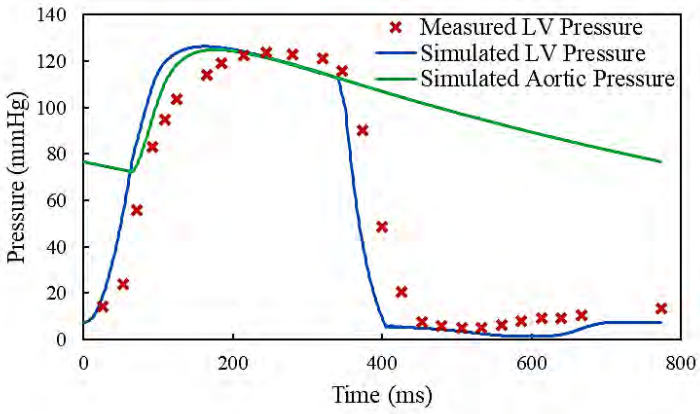

(c)

Figure 4. 1: Comparison between the model prediction and measurements for LV (a) PV loop, (b) volume waveforms and (c) pressure waveforms for the normal subject.

Table 4. 1: Parameters matched with clinical data for normal subject.

Parameter matched	Measured value	Model value	Error (%)
EDV (ml)	94	94	0
ESV (ml)	26.9	29.4	9.2
EF (%)	71.3	68.7	3.6
ESP (mmHg)	125	125	0

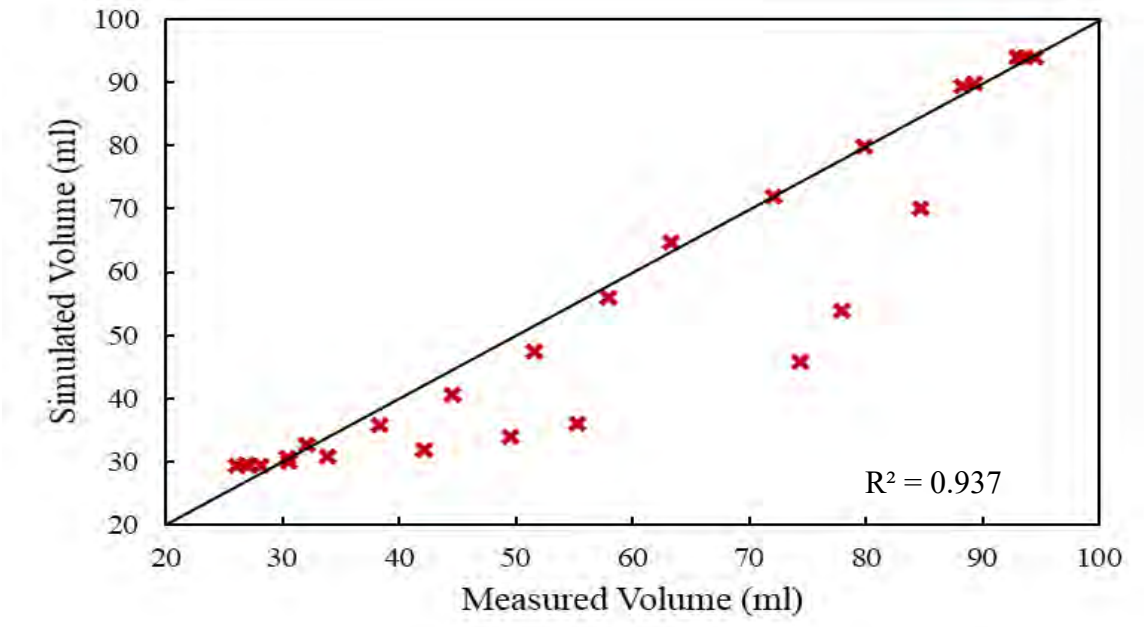

Figure 4. 2: Scatter plot of simulated (y-axis) LV Volume from the model and measured (x-axis) LV Volume from the clinical data for normal case. The R-squared or co-efficient of determination value is 0.937.

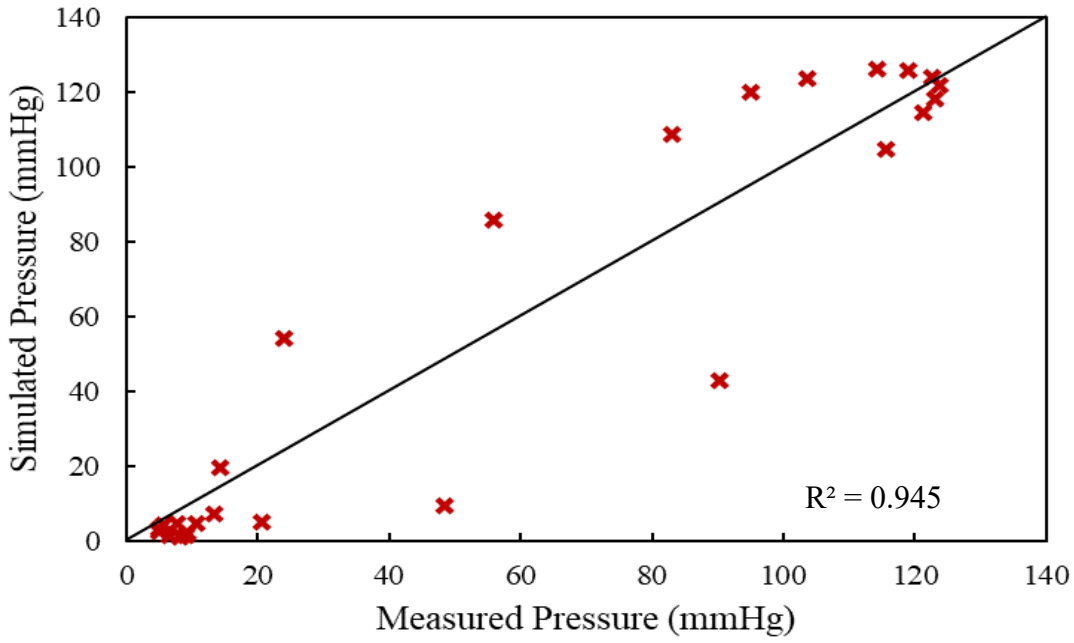

Figure 4. 3: Scatter plot of simulated (y-axis) LV Pressure from the model and measured (x-axis) LV Pressure from the clinical data for normal case. The R-squared or co-efficient of determination value is 0.945.

4.2 Comparison between Simulation and Clinical Measurements for the HFpEF Patient

Similar to the normal case, the PV loops, volume and pressure waveforms of the LV for the baseline HFpEF case as predicted by the model were reasonably matched with the measurements as shown in the Figure 4.4. 163.7 ml (measured 167.7 ml) EDV and 60 ml (measured 58.3 ml) ESV was found from the HFpEF model. So, Model prediction of the LV ejection fraction (EF) was 63.3% (clinical EF = 65.2%), which is within the normal range in humans. Aorta pressure waveforms shows that the HFpEF patient has a hypertensive systolic pressure of 137.8 mmHg (> 130 mmHg) (Figure 4.4). The aortic pulse pressure is around 52.4 mmHg (systolic: 137.8 mmHg, diastolic: 85.4 mmHg). R-squared values of the scatter plots of simulated vs. measured volume and pressure are greater than 0.964 and 0.982 respectively, which confirms a good fit. The parameters matched for HFpEF case are tabulated in Table 4.2.

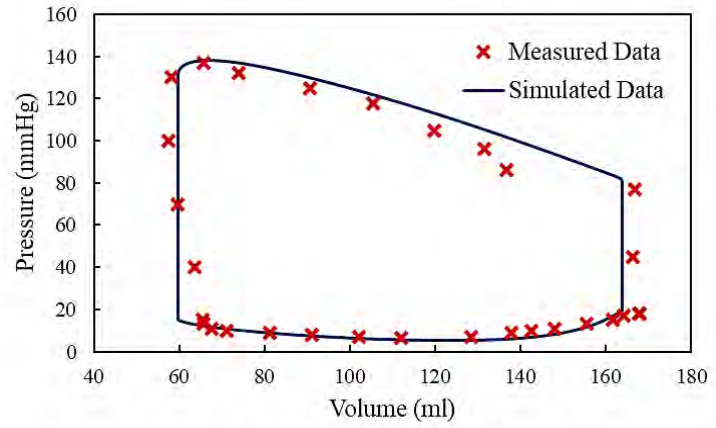

(a)

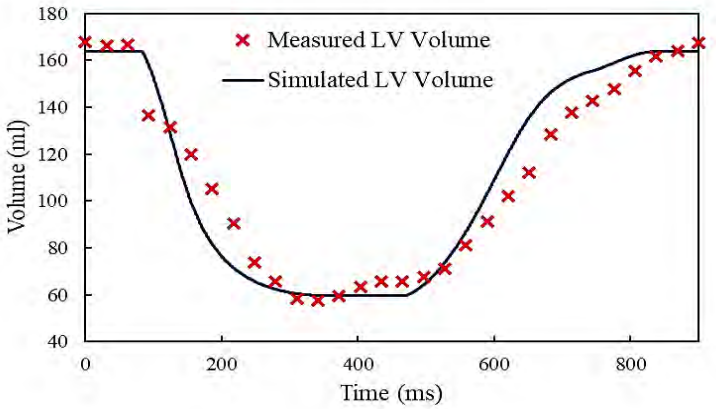

(b)

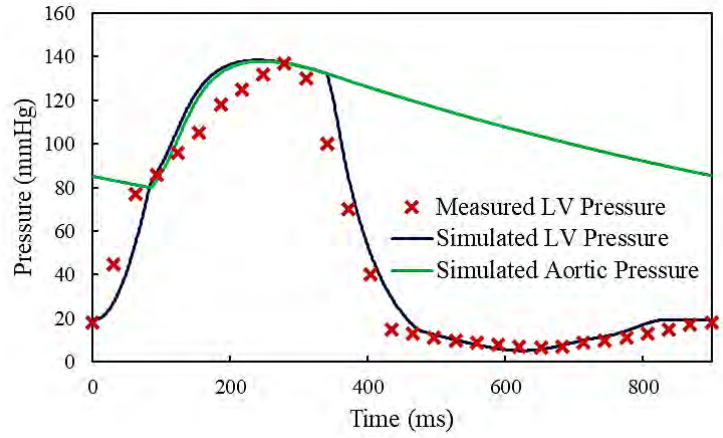

(c)

Figure 4. 4: Comparison between the model prediction and measurements for LV (a) PV loop, (b) volume waveforms and (c) pressure waveforms for the HFpEF patient.

Table 4. 2: Parameters matched with clinical data for HFpEF case.

Parameter matched	Measured value	Model value	Error (%)
EDV (ml)	167.7	163.7	2.3
ESV (ml)	58.3	60	2.9
EF (%)	65.2	63.3	2.9
ESP (mmHg)	137	137.8	0.58

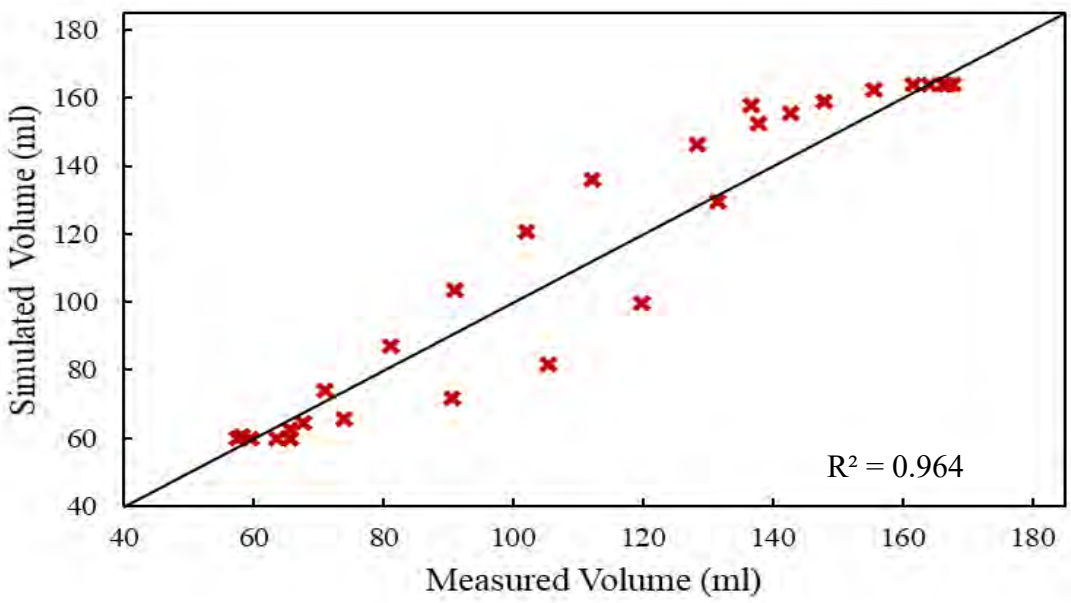

Figure 4. 5: Scatter plot of simulated (y-axis) LV Volume from the model and measured (x-axis) LV Volume from the clinical data for HFpEF case. The R-squared or co-efficient of determination value is 0.964.

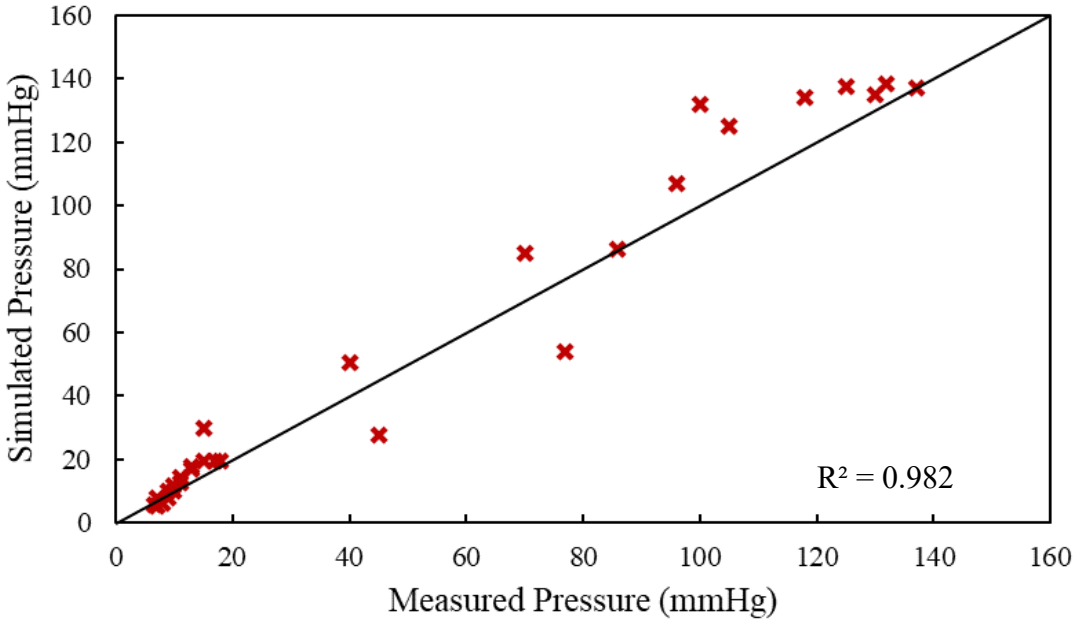

Figure 4. 6: Scatter plot of simulated (y-axis) LV Pressure from the model and measured (x-axis) LV Pressure from the clinical data for HFpEF case. The best linear fit for the pressure points had a R-squared or co-efficient of determination value of 0.982.

4.3 Comparison of Strain between the Normal and HFpEF Case

The longitudinal and circumferential strain profiles have been created for the normal and baseline HFpEF cases (Figure 4.7 and 4.8). Clinically, longitudinal and circumferential strains in LV are generally measured using 2D-Doppler and speckle tracking echocardiography (STE) [96-98]. Typical strain profiles for normal humans measured in clinics are also shown in the figure (Figure 4.7 and 4.8). For the circumferential strain, the model predicted profile was consistent with measurements found in humans. The simulated circumferential strain peaks about 350 ms during systole which falls in the range of 300 - 400 ms for the clinical measurements. Also, similar to the clinical measurements, a rapid change in the circumferential strain occurs at late diastole at around 600 ms for the normal case arising from the contraction of

left atrium. On the other hand, although the shape of the simulated longitudinal strain profile is largely similar to the measurements, but the rate of relaxation during the isovolumic relaxation phase is much slower compared to the clinical measurements (Figure 4.7). For normal case, the peak circumferential and longitudinal strain values of 0.20 and 0.32, respectively falls within the clinical measurements [75]. For the baseline HFpEF case, the peak circumferential is significantly reduced (by 0.6 absolute) compared to the normal (0.26 in baseline HFpEF vs. 0.32 in normal). Whereas the peak longitudinal strain slightly increased (by 0.01 absolute) for the baseline HFpEF case compared to the normal. It has been found the longitudinal strain becomes impaired due to HFpEF [99]. A clinical trial including 219 HFpEF patients demonstrated that LV peak longitudinal and peak circumferential strains are significantly lower in HFpEF patients when compared with normal cases [75]. However, studies have also suggested that reduction in peak longitudinal strain in HFpEF patients are related to the presence of some previously unrecognized myocardial systolic dysfunction associated with this disease [100] and correlates to the reduction in EF during the progression of this disease [75]. The baseline HFpEF patient considered in this study has a relatively high EF of 63.3%, which can be a possibility for the model prediction of 21% peak longitudinal strain similar to the normal subject. As the disease progresses, the peak longitudinal strain of this HFpEF patient will eventually decrease significantly compared the normal.

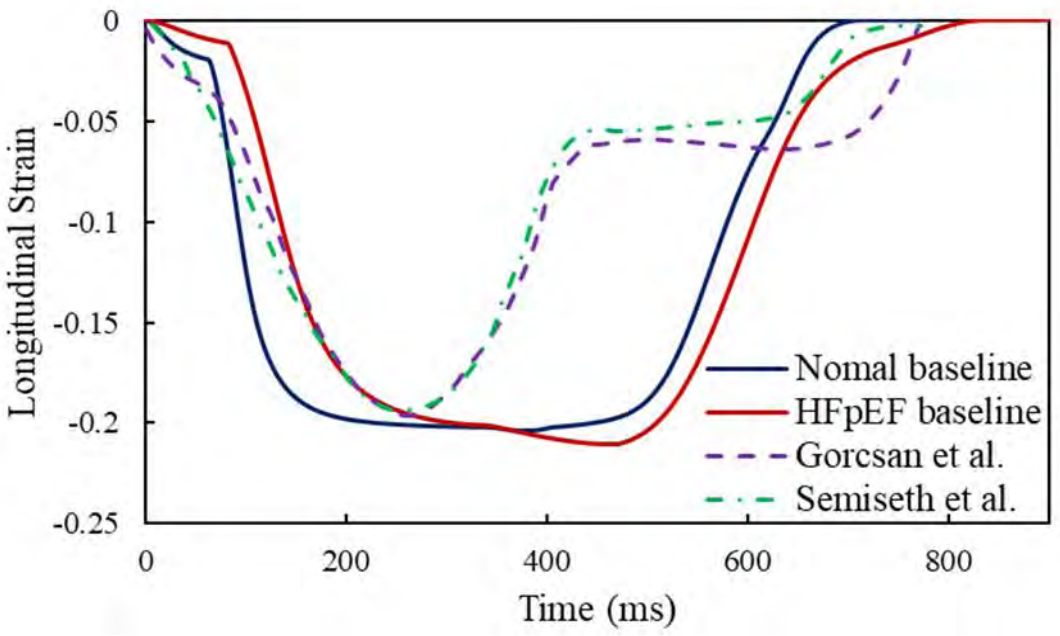

Figure 4. 7: Longitudinal strain waveform calculated by the model for normal and HFpEF cases compared with echo measurements (dotted [99] and dashed [97] lines).

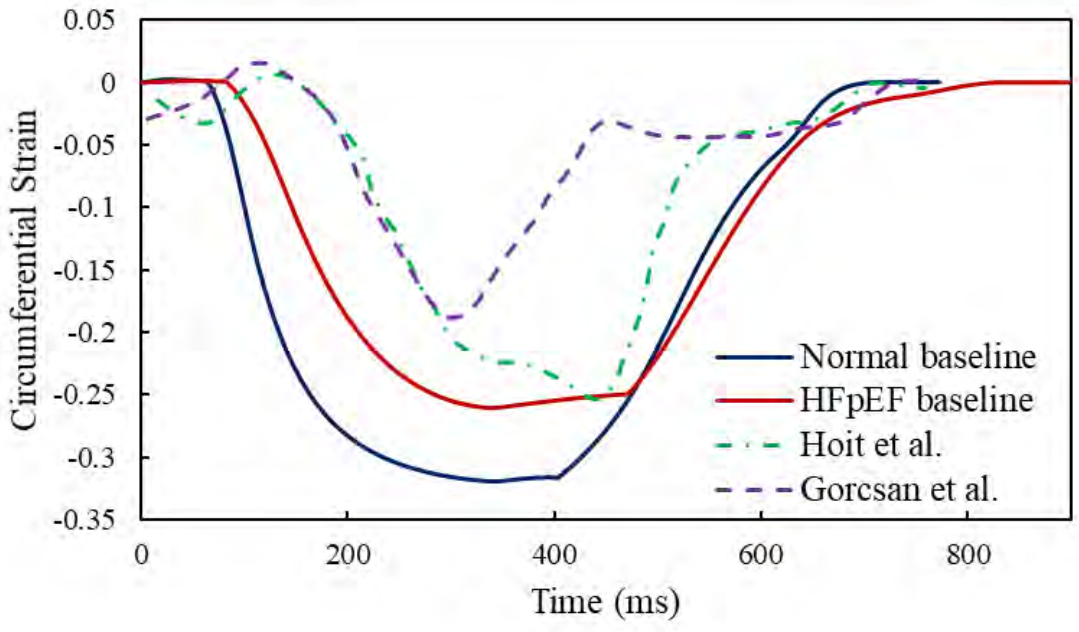

Figure 4. 8: Circumferential strain waveform calculated by the model for normal and HFpEF cases compared with echo measurements (dotted [98] and dashed [97] lines)

4.4 Comparison of Stress between the Normal and HFpEF case

The myofiber stress is associated with the ventricular remodeling [101]. Although the myofiber stress cannot be measured in-vivo or, clinically, computational models can be used to calculate the myofiber stress which can provide important insights on ventricular mechanics and remodeling. The myofiber stress distribution for entire LV at end-systole for normal and baseline HFpEF cases are shown in Figure 4.9 and Figure 4.10. We have considered the end-systolic point as the myofiber stress becomes the maximum at this point for a cardiac cycle. The peak stress for baseline HFpEF case is higher compared to the normal case. Elevated myofiber stress is a feature that is associated with ventricular remodeling [101]. So, the stress distribution found in the HFpEF patient's LV is reasonable. The range of stress values for normal and HFpEF cases (85 to 110 kPa) are within the range found in previously reported studies [102, 103]. The location of peak stress is mostly in the endocardium wall for both normal subject and HFpEF case as it can be seen from the colormaps.

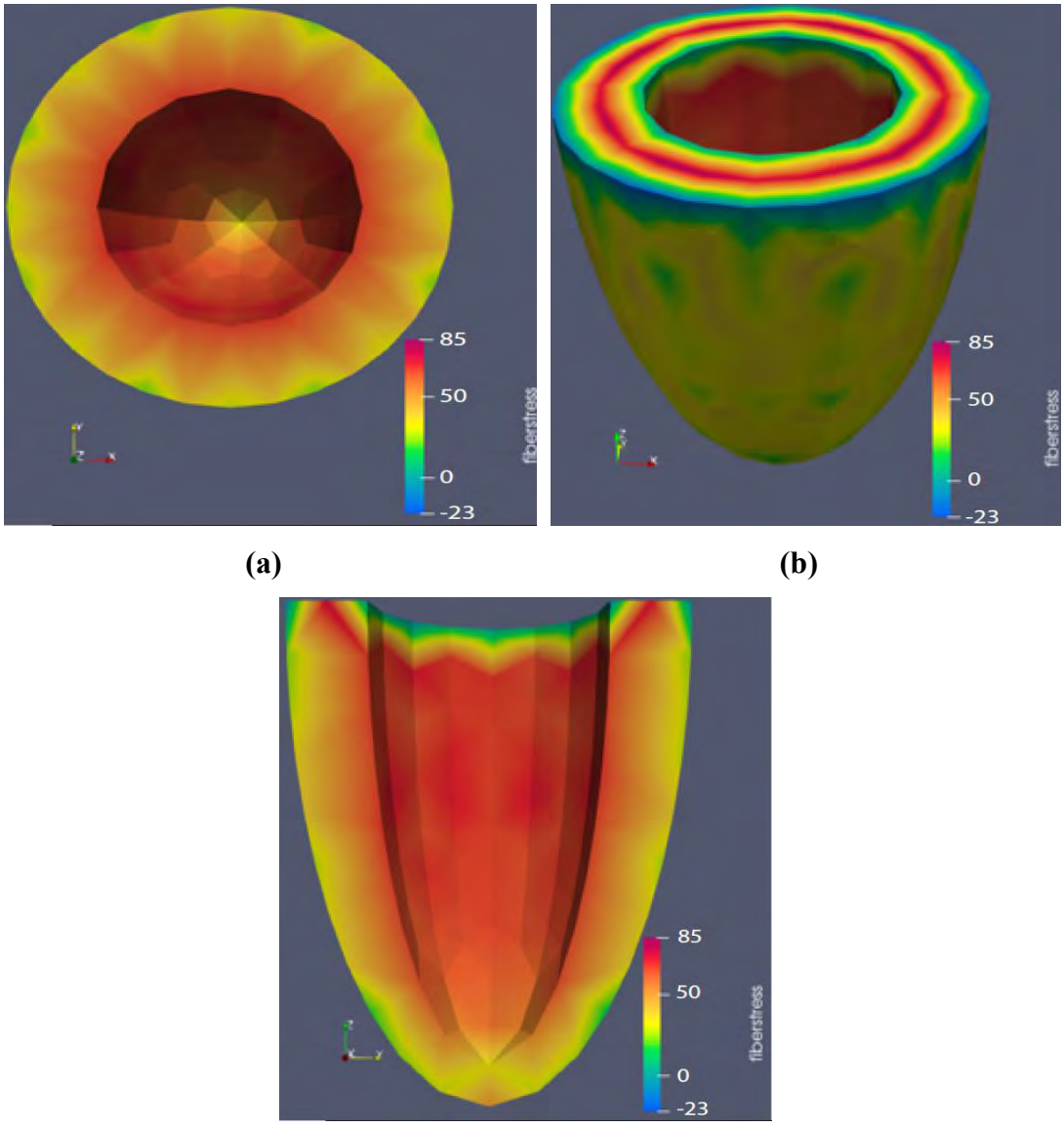

(a) **(b)**

(c)

Figure 4. 9: Snapshot at (a) transverse cross section at midplane, (b) vertical cross section along central axis, (c) isometric orientation of myofiber stress at end systole for normal case. Color-map shows the stress values in kPa.

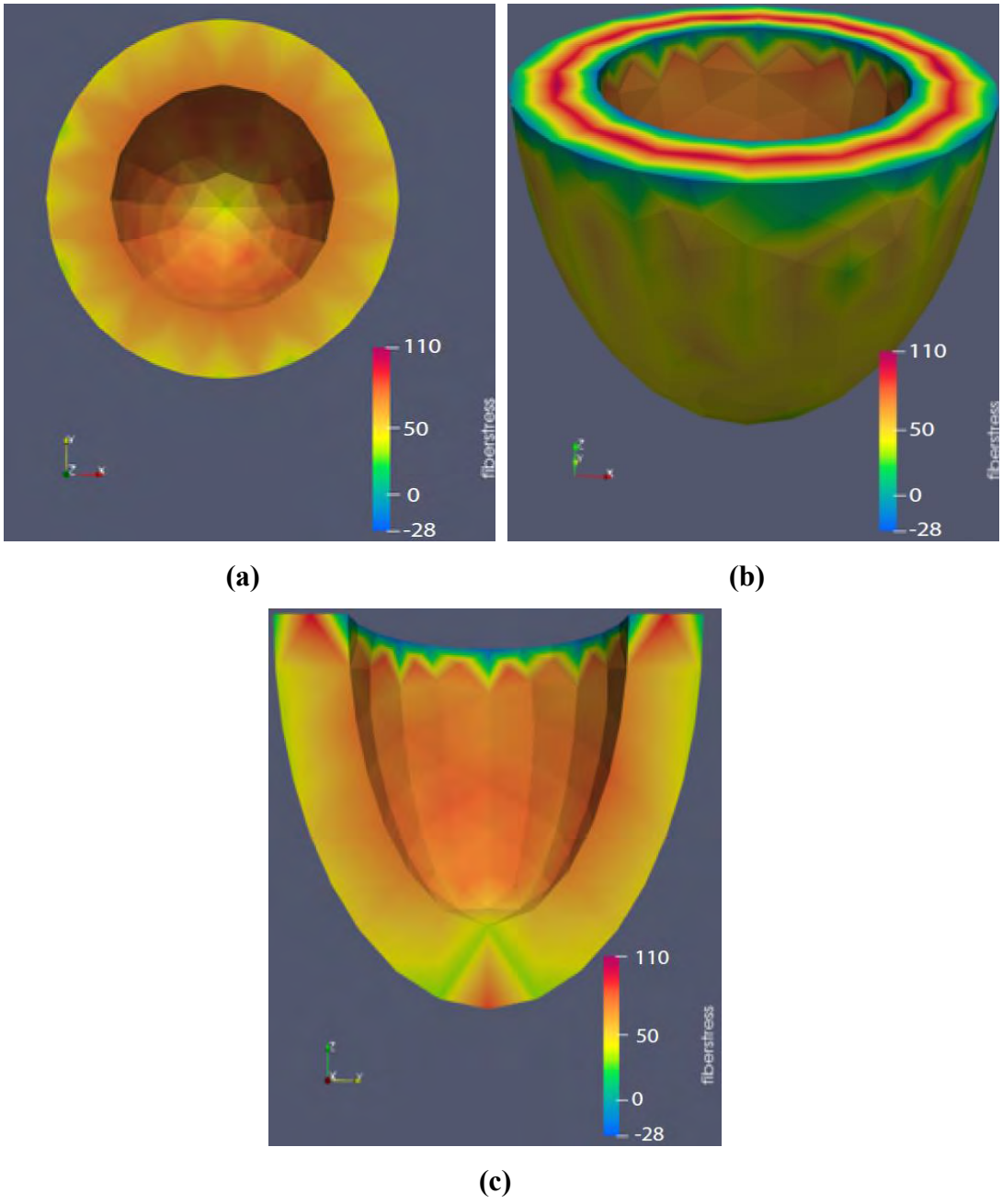

Figure 4. 10: Snapshot at (a) transverse cross section at midplane, (b) vertical cross section along central axis, (c) isometric orientation of fiber stress at end-systole for HFpEF case, Color-map shows the stress values in kPa.

4.5 Summary

Table 4.1 shows the different hemodynamic and functional indices predicted by the model for normal and baseline HFpEF. We can see though the ejection fraction is within normal range for both normal and HFpEF cases, but the HFpEF patient has increased EDV that shows the symptoms of remodeling and increased systolic blood pressure which is the symptom of hypertension. HFpEF patient has higher end-diastolic pressure (EDP) (19.3 mmHg in HFpEF vs. 7.5 mmHg in normal) than normal which suggests HFpEF patient's LV is stiffer than the normal LV. Clinically, EDP higher than 15 mmHg is considered as sign of diastolic dysfunction which is a common feature in HFpEF. In addition, the peak circumferential strain significantly decreased in HFpEF patient compared to the normal whereas the peak longitudinal strain almost remained same. The peak LV myofiber stress is higher in HFpEF than normal which is associated with LV remodeling.

Table 4. 3: Model predicted hemodynamic and functional indices for normal and HFpEF cases.

Parameters	Normal case	HFpEF case
Cycle time (ms)	773	900
End Diastolic Volume (ml)	94.0	163.7
Ejection fraction (%)	68.7 (Clinical 71.3)	63.3 (Clinical 65.2)
End Diastolic Pressure (mmHg)	7.5	19.3
Systolic Blood Pressure (mmHg)	125	137.8
Diastolic Blood Pressure (mmHg)	77	85.4
Peak Circumferential Strain	0.32	0.26
Peak Longitudinal Strain	0.20	0.21
Peak Myofiber Stress (kPa)	85.0	110.0

4.6 Effect of LV Wall Thickness Change in HFpEF Patient

The preserved LV EF in HFpEF patients is not well understood. To compensate for the applied hemodynamic burden or load, the heart might choose one or, multiple compensatory mechanisms such as, change crossbridge formation, augment muscle mass to bear the extra load, recruit mechanisms to increase contractility or, change volume to meet the required load etc. In response to pressure overload in conditions such as hypertension, the parallel addition of sarcomeres causes an increase in myocyte width, which in turn increases wall thickness. This remodeling results in concentric hypertrophy which is, increase in ratio of wall thickness to chamber dimension. We have used our baseline HFpEF model and changed the wall thickness of the LV to simulate the progression of concentric hypertrophy commonly found in many HFpEF patients. The parameters varied and kept constant in this experiment are tabulated in Table 4.4.

Table 4. 4: Design of experiment to find the effect of wall thickness change in HFpEF patient.

Parameter varied		Other parameters	
Wall thickness (cm)	1, 1.45, 1.9.	Preload/EDV (ml)	168.6
		Afterload (Pa ms ml^{-1})	110000
		Fiber Orientation (degree)	-60°/60°

4.6.1 Effect on PV Loop

PV loop, volume waveforms and pressure waveforms for the variation of LV wall thickness are shown in Figure 4.11. It can be observed from PV loops that both EDV and ESV of LV decreased with the increased LV wall thickness. As a result, the EF decreases with increased LV wall thickness. In addition, the LV can generate less pressure; the systolic pressure decreases as the LV wall gets thicker. With increased thickness, the LV wall becomes stiffer and inflate less during filling phase indicated by the higher filling pressures. These results are consistent with the clinical observations such as an alteration of lusitropy which shows similar changes in LV PV loop [104, 105].

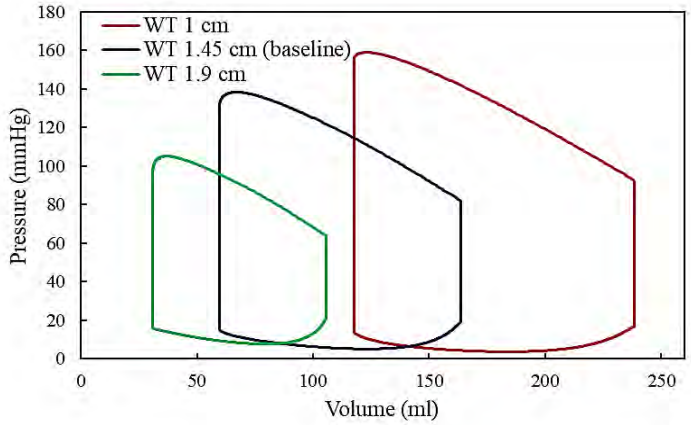

(a)

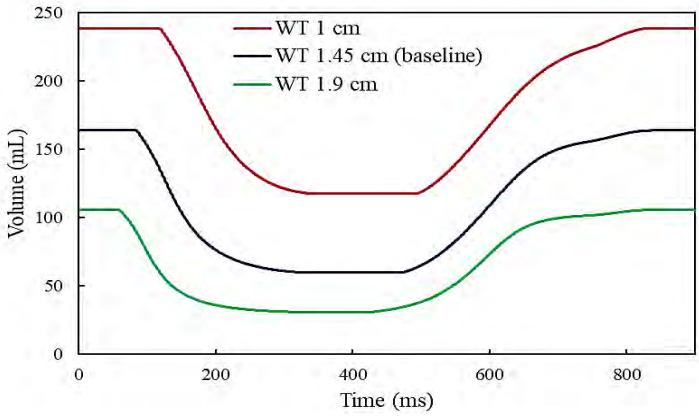

(b)

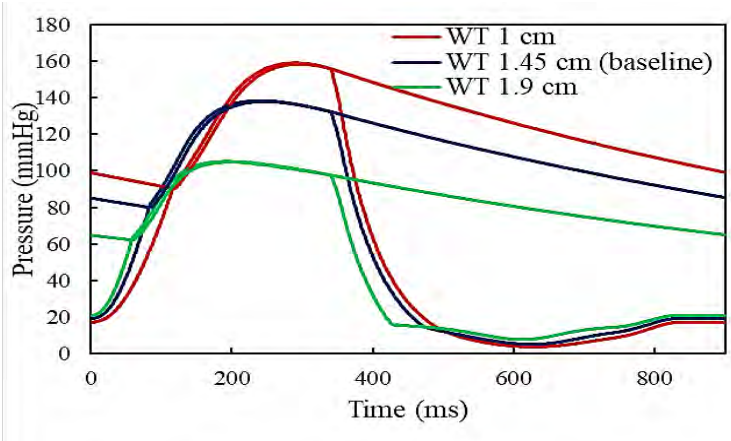

(c)

Figure 4. 11 Comparison among (A) LV PV loop, (B) LV volume waveforms, (C) LV and aortic pressure waveforms for remodeling via wall thickness (WT) change for the HFpEF patient.

4.6.2 Effect on Strain

The major observation from the strain waveforms of circumferential (Figure 4.12) and longitudinal (Figure 4.13) strains is the peak circumferential strain increases, but the peak longitudinal strain decreases with the increased LV wall thickness. The decrement of longitudinal strain is intuitive as the LV stiffness is increased due to the increased of wall thickness which in turn decrease the longitudinal strain. The increased wall thickness oppositely affects the circumferential strain as then there are more fibers to strain more circumferentially. Longitudinal strain has a major effect on blood ejection. So decreased longitudinal strain is the major concern in the progression of HFpEF.

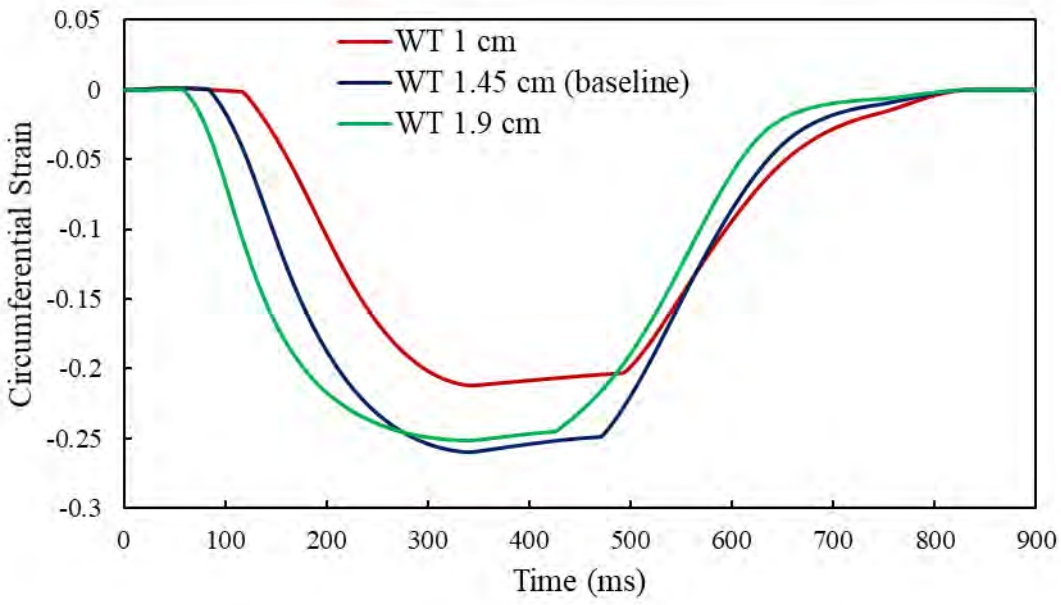

Figure 4. 12: Circumferential strain for the variations of LV wall thickness (WT) change in HFpEF patient.

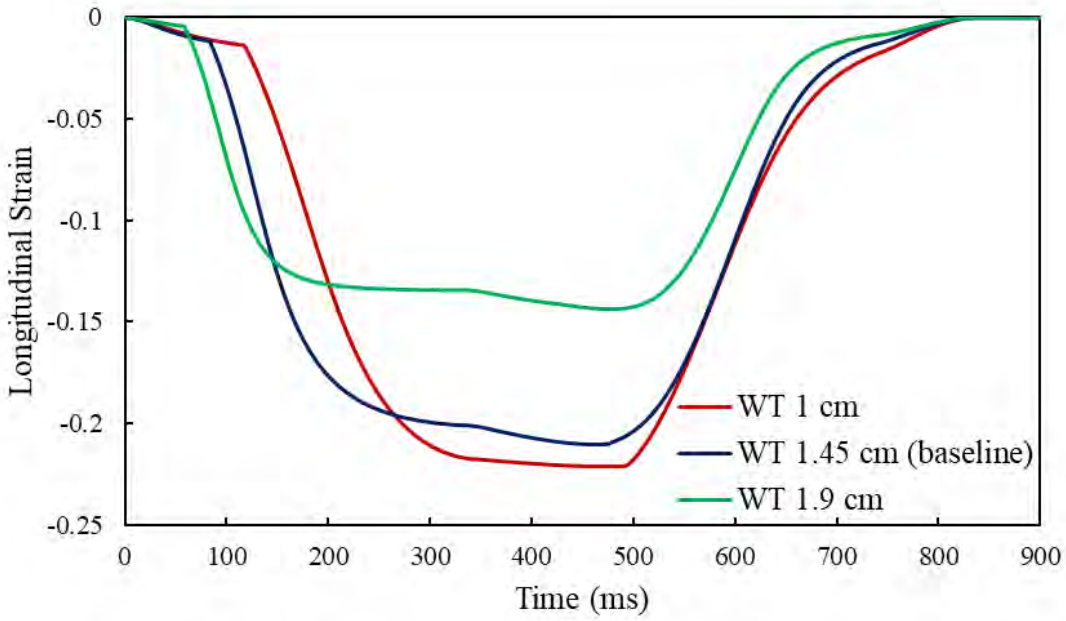

Figure 4. 13: Longitudinal strain for the variations of LV wall thickness in HFpEF patient.

4.6.3 Effect on Stress

As it can be seen from the colormap (Figure 4.14) the myofiber stress is decreased while wall thickness is increased. With the increase of wall thickness, the LV systolic pressure decreases. As the reduced pressure is acting against thicker wall, the myofiber stress is decreased with the increased wall thickness.

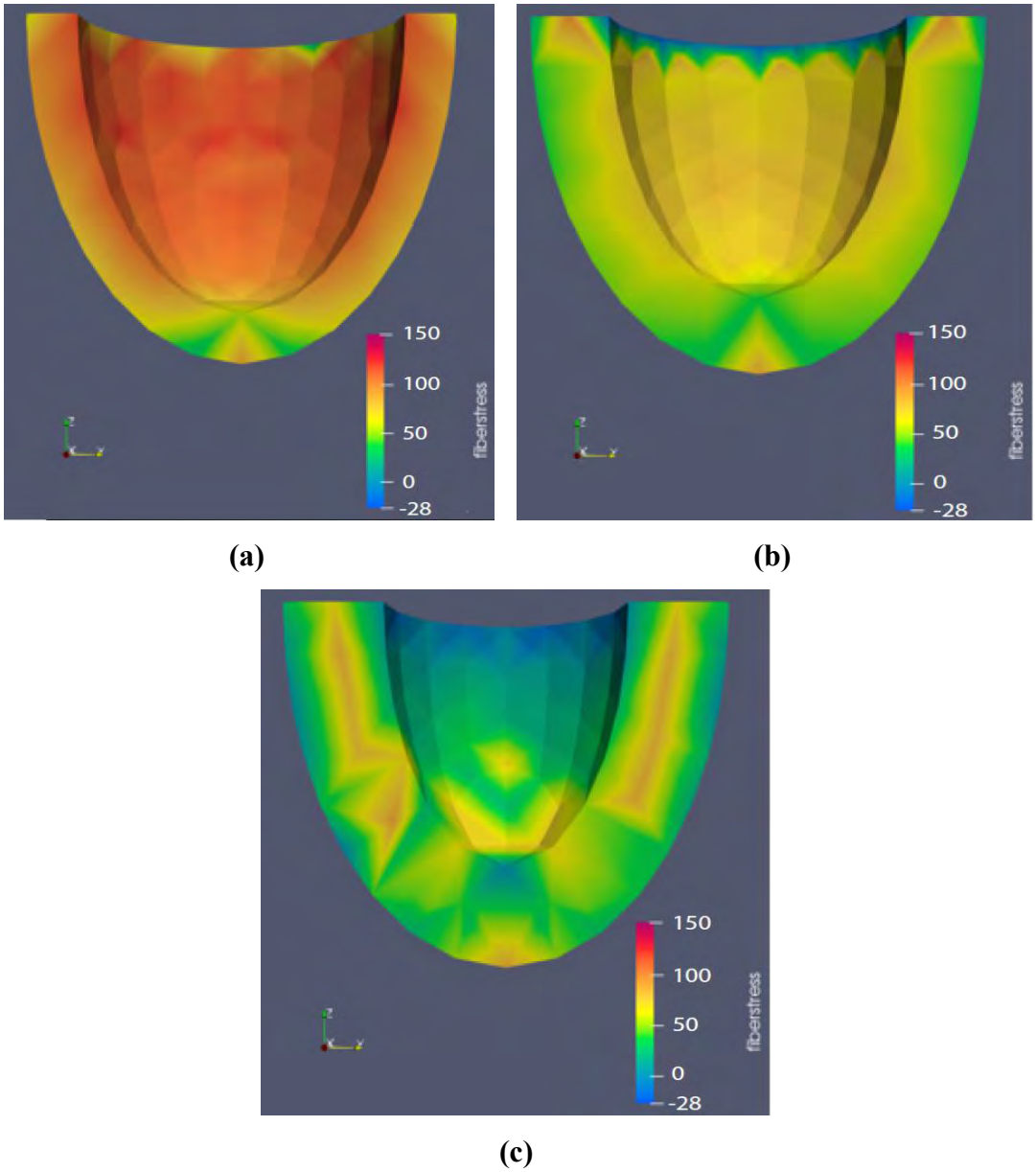

Figure 4. 14: Snapshot at vertical cross section along central axis at end-systole for HFpEF case, having LV wall thickness of (a) 1 cm, (b) 1.45 cm and (c) 1.9 cm; Color-map shows the stress values in kPa.

4.6.4 Summary

In many HFpEF patients as the disease progress, the LV becomes thicker as a result of concentric hypertrophy. This in turn increase the LV passive stiffness which increase the filling pressure and leads to diastolic heart failure. Recalling that, the key

pathophysiological features of the HFpEF are preserved EF, hypertension (elevated systolic pressure), reduced peak longitudinal and circumferential strains. With isolated increase of LV wall thickness the model reproduced all the features except the peak circumferential strain (which increased with the increased LV wall thickness). Thus, the model predicts that only increase of LV wall thickness cannot reproduce the progression of HFpEF. Some other mechanism(s) must be combined with the increased LV wall thickness to reproduce all the key features found in HFpEF.

4.7 Effect of Preload Change in HFpEF Patient

As the LV undergoes remodeling in HFpEF patients, the LV mass to cavity volume ratio might increase progressively. The LV EDV change can be adapted as preload change in the model. The present section shows the effect of change of preload (LV EDV) in HFpEF with our model. The parameters varied and kept constant in this experiment are tabulated in Table 4.5.

Table 4. 5: Design of experiment to find the effect of preload change in HFpEF patient.

Parameter varied		Other parameters	
Preload/EDV (ml)	144.6, 168.6, 194.9.	Wall thickness (cm)	1.45
		Afterload (Pa ms ml^{-1})	110000
		Fiber Orientation (degree)	$-60^{o}/60^{o}$

4.7.1 Effect on PV Loop

The PV loops, LV volume and pressure waveforms and aortic pressure waveforms are shown in Figure 4.15 for the variations of preload. It can be observed from PV loop plots that with increased preload the EF of the LV increases. In addition, the peak systolic pressure which is indicates hypertension is increased with the increased preload. The end-diastolic pressure (EDP) is slightly increased with the increased preload which indicates higher LV stiffness and diastolic dysfunction.

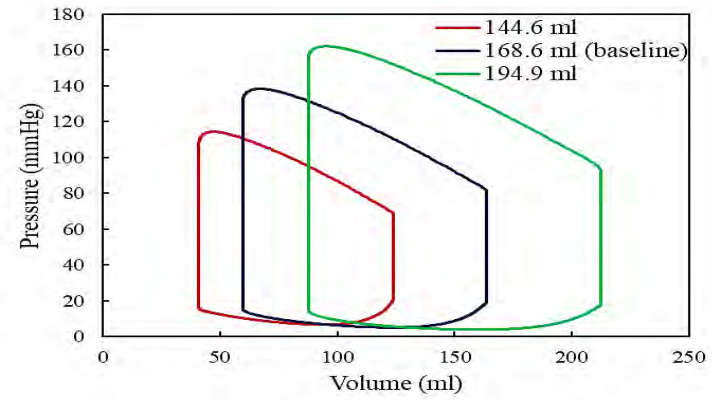

(a)

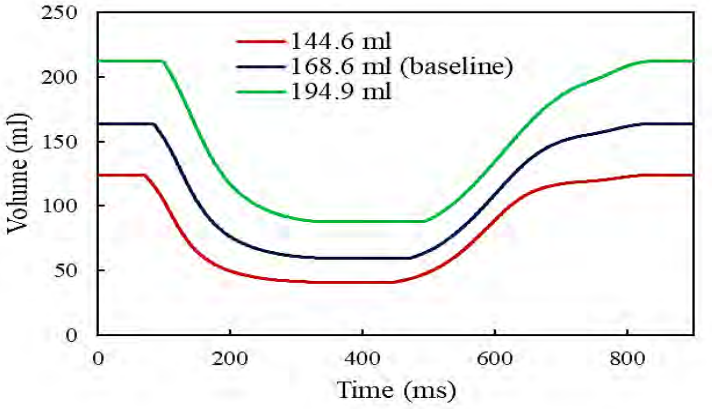

(b)

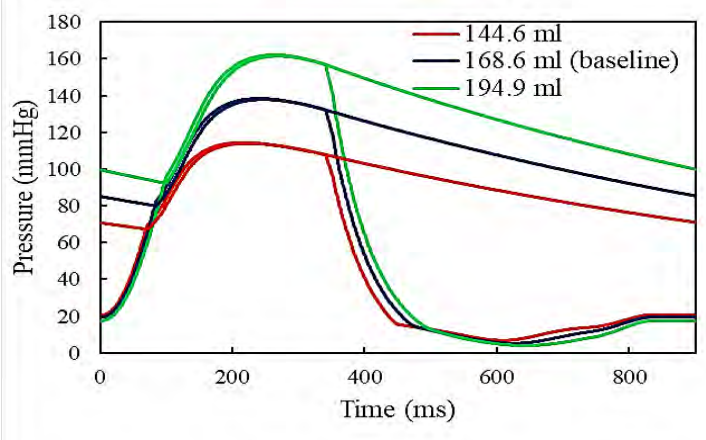

(c)

Figure 4. 15: Comparison among (a) LV PV loop, (b) LV volume waveforms, (c) LV and aortic pressure waveforms for different preloads in the HFpEF patient.

4.7.2 Effect on Strain

From circumferential (Figure 4.16) and longitudinal (Figure 4.17) strain waveforms, it can be seen that the peak circumferential strain is increased, and the peak longitudinal strain is reduced when preload is decreased. The impaired longitudinal strain is an indication towards progression of HFpEF.

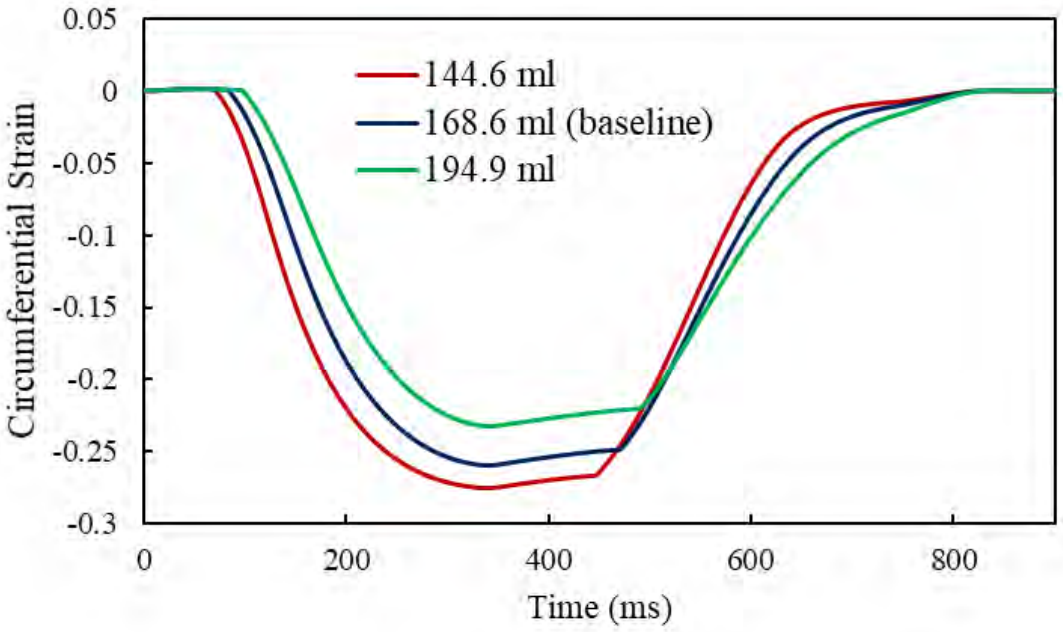

Figure 4. 16: Circumferential strain for the variations of LV preload in HFpEF patient.

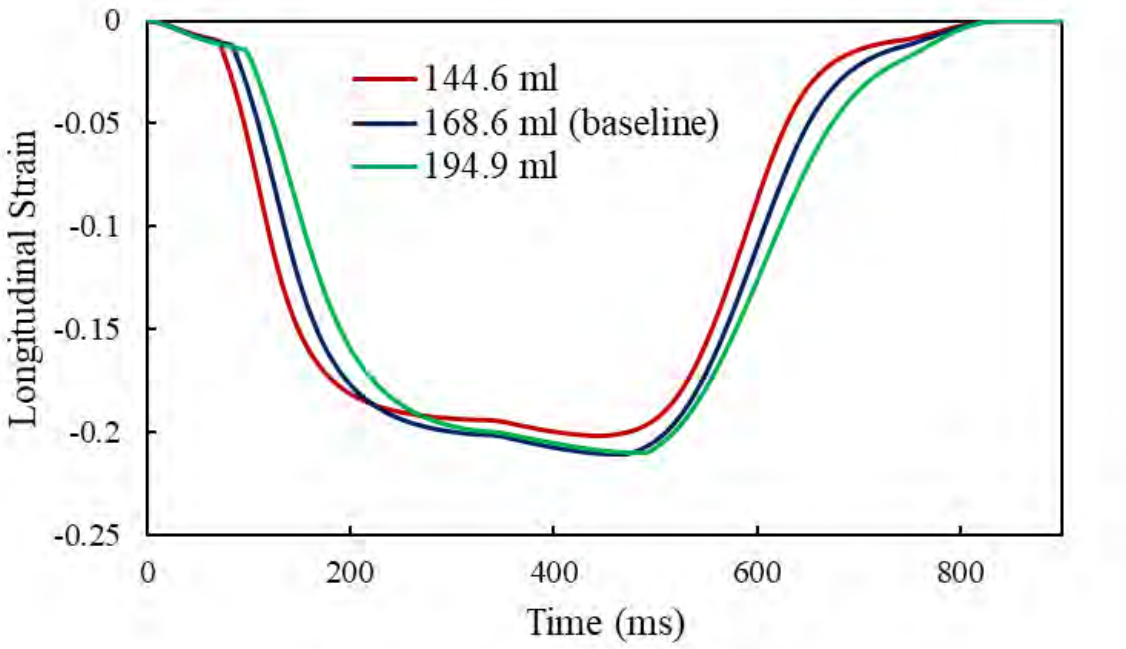

Figure 4. 17: Longitudinal strain for the variations of LV preload in HFpEF patient.

4.7.3 Effect on Stress

Figure 4.18 shows the myofiber stress is increased with the increase of the preload. The increase of preload increases the LV stiffness and pressure attributed from the increased myofiber stress.

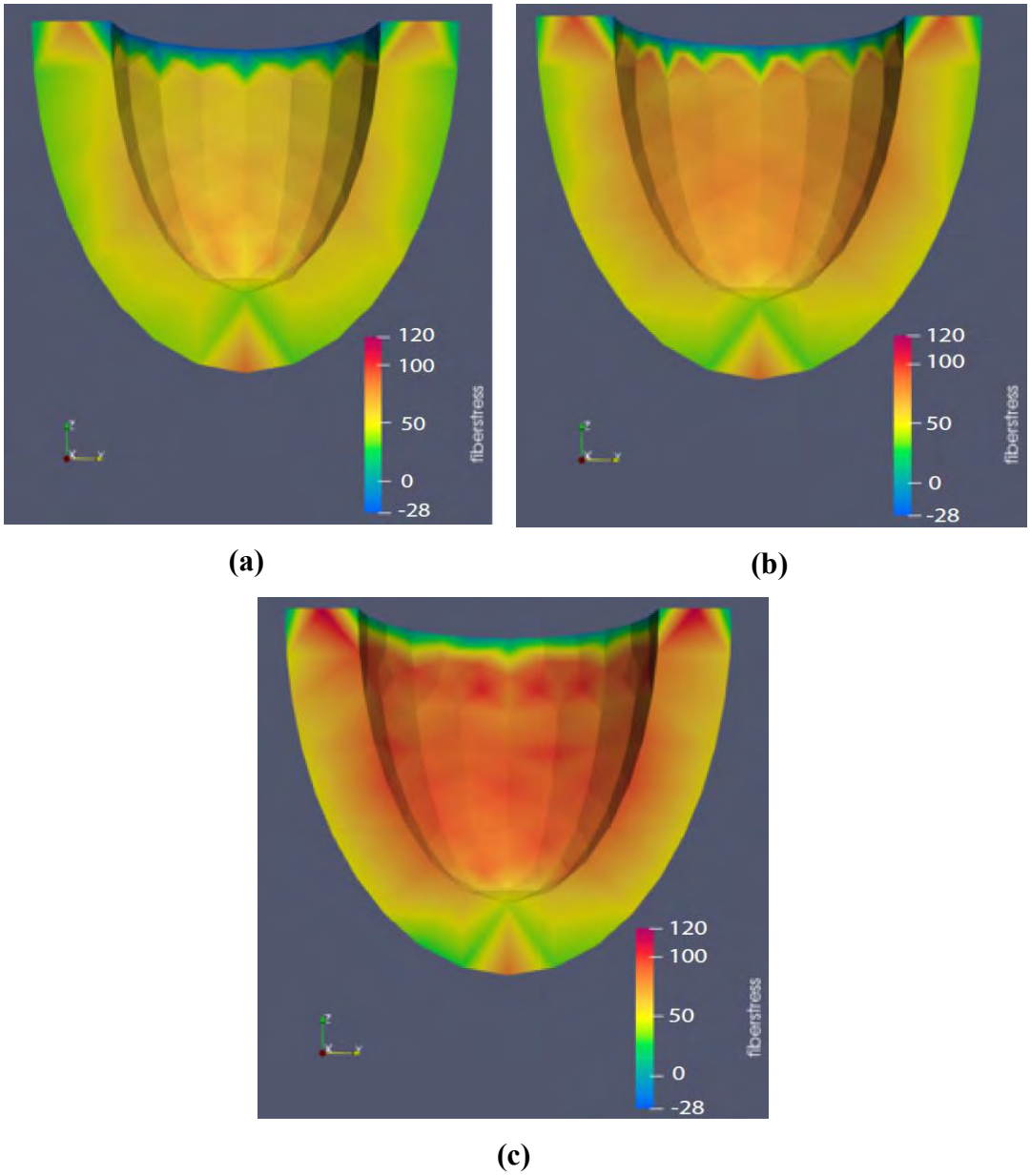

Figure 4. 18: Snapshot at vertical cross section along central axis at end-systole for HFpEF case, having preload of (a) 144.6 ml, (b) 168.6 ml and (c) 194.9 ml; Color-map shows the stress values in kPa.

4.7.4 Summary

Reduced preload can reproduce the reduced peak circumferential and longitudinal strains; however, the EF and peak systolic pressure decreases. During the progression of HFpEF, the LV often undergoes concentric remodeling with increased LV wall thickness and decreased LV cavity diameter which in turn decrease the preload. The progressive concentric remodeling reduces the EF. The results suggest that decreased preload accompanied by increase in wall thickness might be possible path of progression in HFpEF.

4.8 Effect of Afterload Change in HFpEF Patient

Increased afterload increase the LV peak systolic pressure which indicates hypertension, a common feature in many HFpEF patients. Afterload can be altered by changing the peripheral resistance, *Rper* in the model. The parameters varied and kept constant in this experiment are tabulated in Table 4.6.

Table 4. 6: Design of experiment to find the effect of afterload change in HFpEF patient.

Parameter varied		Other parameters	
Afterload (Pa ms ml^{-1})	110000, 137500, 165000, 192500.	Wall thickness (cm)	1.45
		Preload/EDV (ml)	168.6
		Fiber Orientation (degree)	-60º/60º

4.8.1 Effect on PV Loop

For the variation of afterload PV loop, LV volume and pressure waveforms and aortic pressure waveforms are shown in Figure 4.19. It can be observed from the PV loops that the ESV increases keeping EDV approximately same, slightly decreasing the EF with increased afterload. The increased SBP and DBP indicates the increment of blood pressure due increased afterload which causes hypertension.

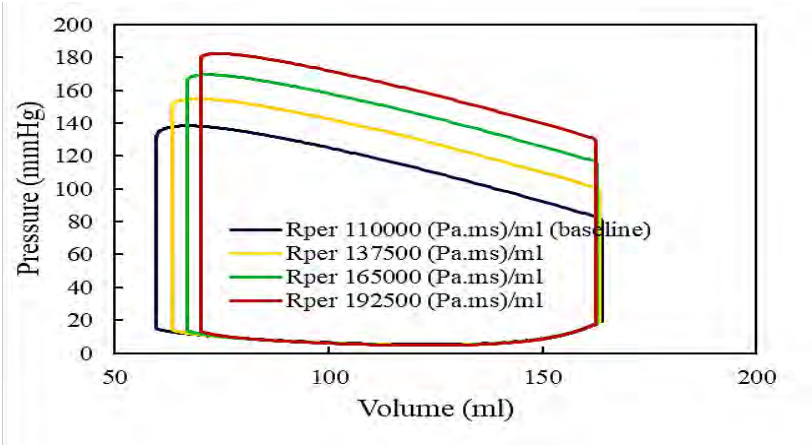

(a)

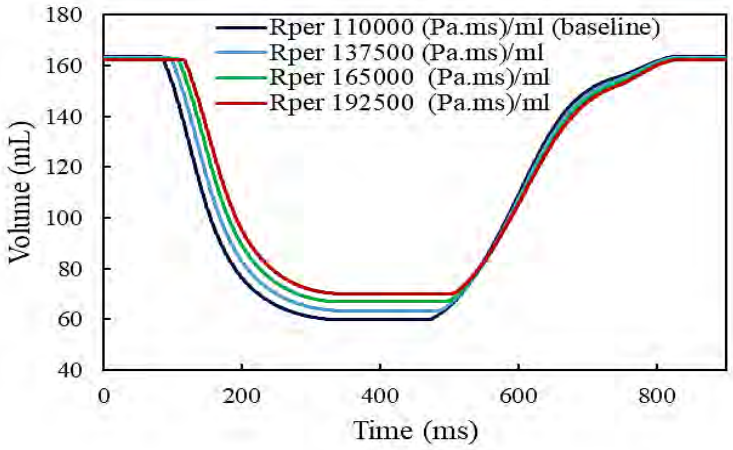

(b)

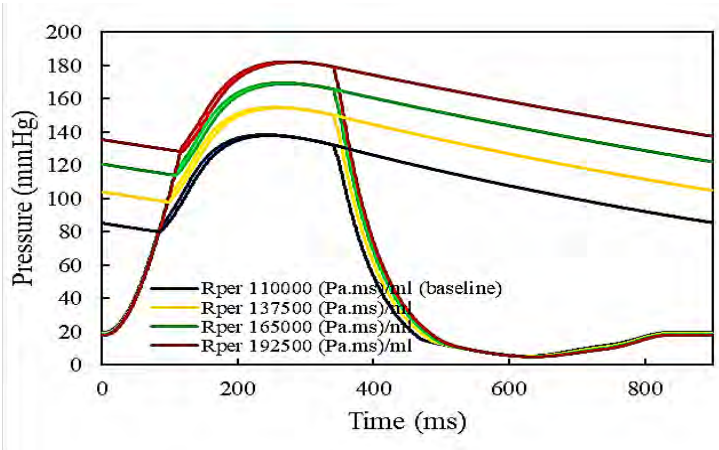

(c)

Figure 4. 19: Comparison among (a) LV PV loop, (b) LV volume waveforms, (c) LV and aortic pressure waveforms for afterload change (Rper, unit Pa ms ml^{-1}) for the HFpEF patient.

4.8.2 Effect on Strain

The major observation from the strain waveforms of circumferential (Figure 4.20) and longitudinal (Figure 4.21) strains is both peak circumferential strain and longitudinal strain decreases while afterload is increased. As strain values are more akin to the stroke volume or, EF, increased afterload reduces the peak circumferential and longitudinal strain despite the increase of the LV peak systolic pressure.

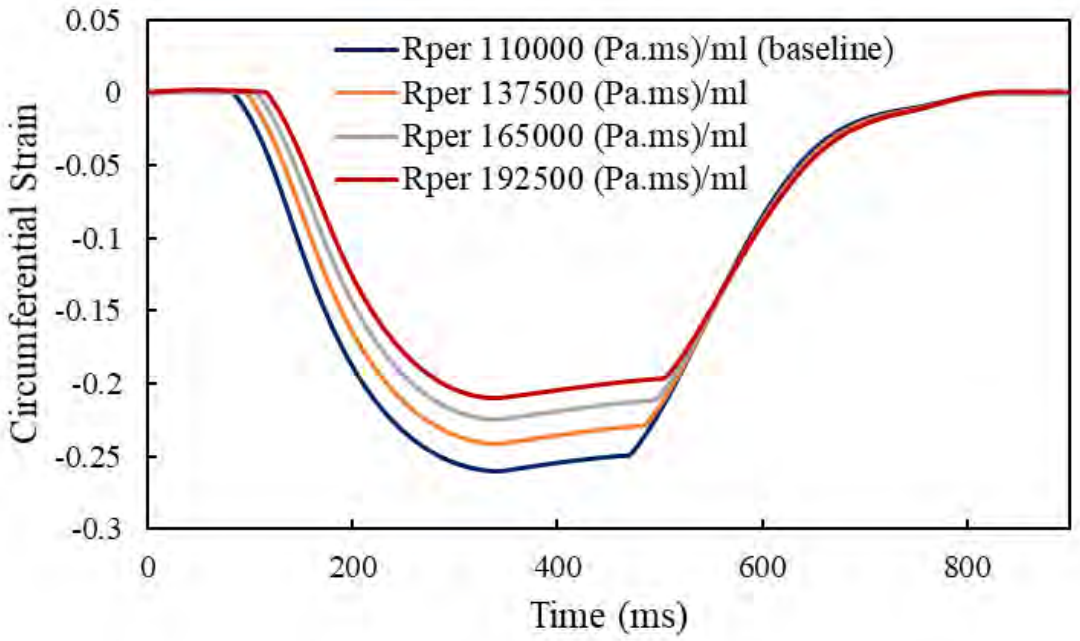

Figure 4. 20: Circumferential strain for the variations of LV afterload in HFpEF patient.

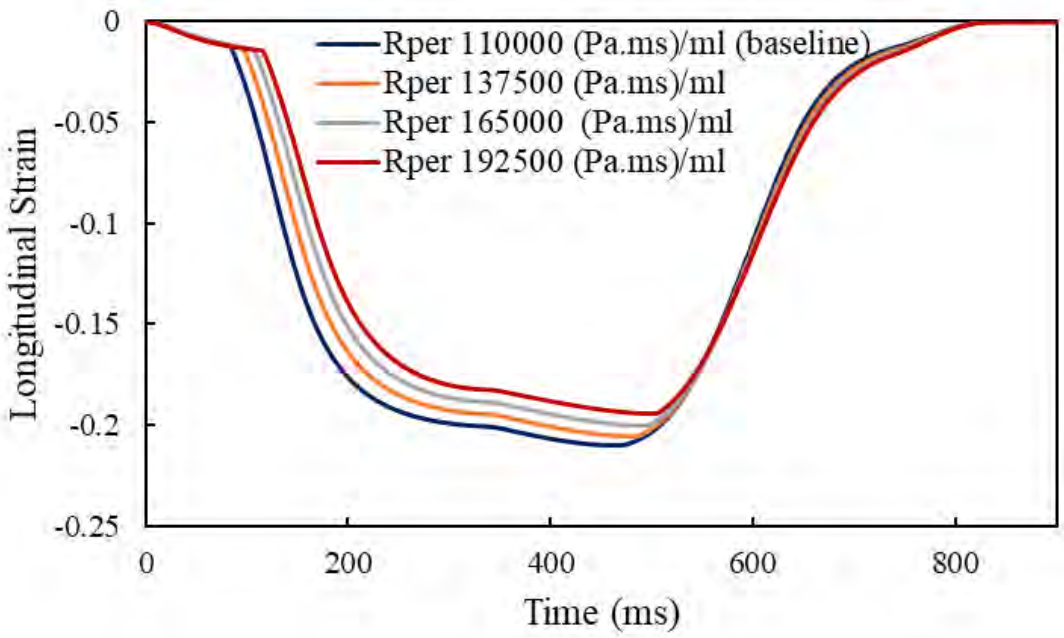

Figure 4. 21: Longitudinal strain for the variations of LV afterload in HFpEF patient.

4.8.3 Effect on Stress

As it can be seen on the colormap (Figure 4.22), the myofiber stress is increased while afterload is increased. This is due to the requirement of higher blood pressure because of increased afterload. So, the increased fiber stress prompts to increase blood pressure though it reduces ejection fraction.

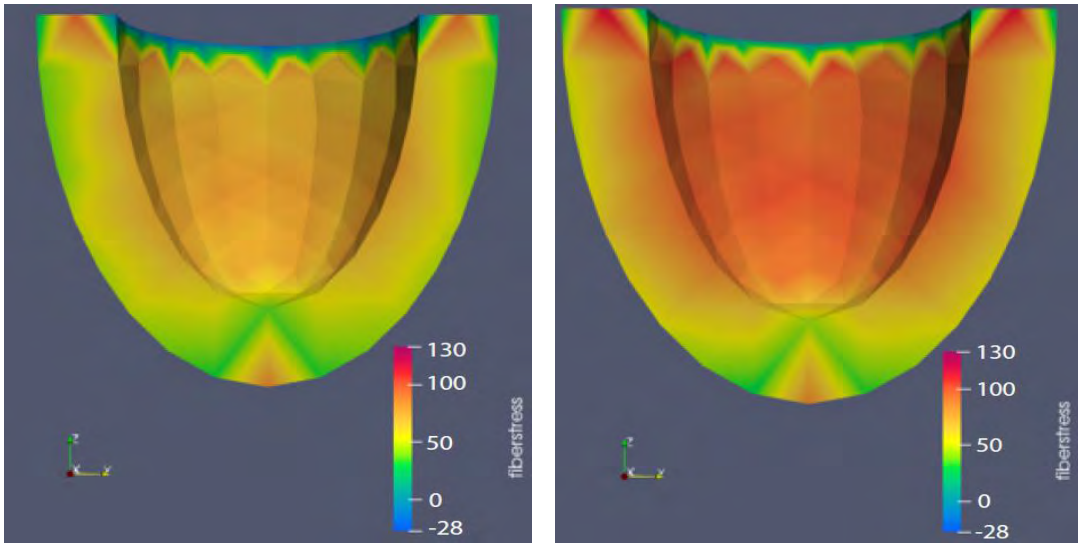

(a) **(b)**

Figure 4. 22: Snapshot at vertical cross section along central axis at end-systole for HFpEF case, having afterload (Rper, unit Pa ms ml−1) (a) 110000, (b) 192500; Color-map shows the stress values in kPa.

4.8.4 Summary

Increase in afterload in HFpEF patient decrease both the peak circumferential and longitudinal strains, however, to significantly reduce the peak strains (in the order of decrease of peak circumferential and longitudinal strain by 0.03-0.05 absolute value found in the reported clinical studies), the model shows that the peak systolic pressure will be very high which is unphysiological. Therefore, a sole increase in afterload cannot reproduce all the features found in progression in HFpEF. But, increase in afterload could be one of the mechanisms as a significant number of HFpEF are hypertensive, but, it surely has to be combined with other mechanisms such as increased LV wall thickness.

4.9 Effect of Fiber Orientation Change in HFpEF Patient

For the baseline HFpEF case, the myofiber orientation was varied from endocardium to epicardium by 60º/-60º. We have changed the fiber orientation by changing the fiber angles and investigated the effect of change of fiber orientation in HFpEF patient. The parameters varied and kept constant in this experiment are tabulated in Table 4.7.

Table 4. 7: Design of experiment to find the effect of fiber orientation change in HFpEF patient.

Parameter varied		Other parameters	
Fiber Orientation (degree)	-50º/50º, -55º/55º, -60º/60º, -65º/65º, -70º/70º.	Wall thickness (cm)	1.45
		Preload/EDV (ml)	168.6
		Afterload (Pa ms ml^{-1})	110000

4.9.1 Effect on PV Loop

PV loop, LV volume and pressure waveforms and aortic pressure waveforms are shown in Figure 4.23 for variations of LV myocardial fiber angle. The change of the fiber angle has a small effect on both LV volume and pressure.

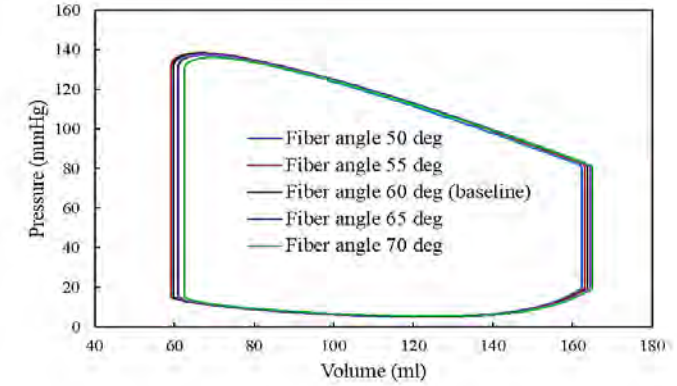

(a)

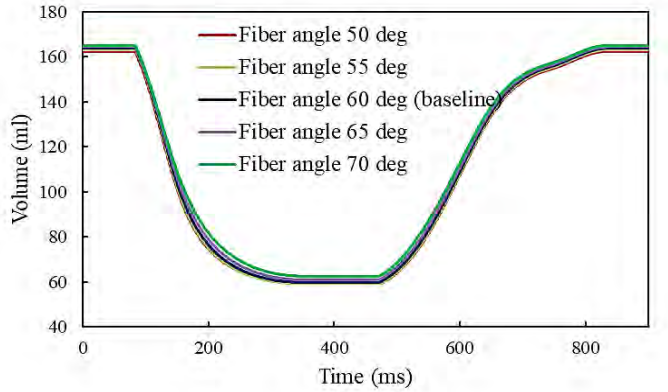

(b)

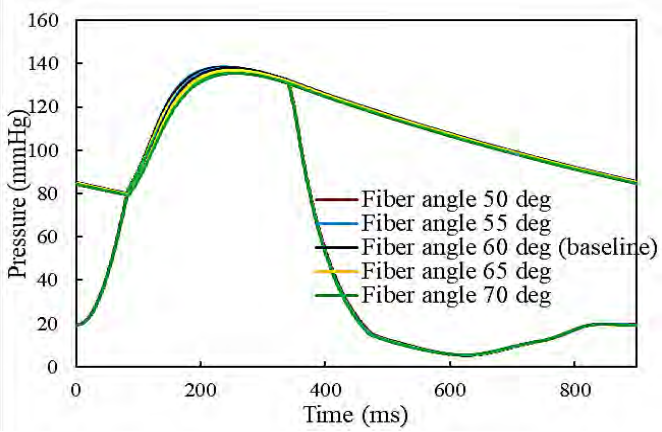

(c)

Figure 4. 23: Comparison among (a) LV PV loop, (b) LV volume waveforms, (c) LV and aortic pressure waveforms for fiber angle change for the HFpEF patient.

4.9.2 Effect on Strain

Interestingly, the change of the fiber orientation has a large effect on the circumferential and longitudinal strain. From circumferential (Figure 4.24) and Longitudinal (Figure 4.25) strain waveforms, it can be seen peak circumferential strain is increased and longitudinal strain is reduced when fiber angle is decreased. When the fiber angle is reduced the myofibers are arranged more circumferentially. A decrease of 10^{o} fiber angle increase the circumferential strain by 0.05 absolute and decrease the longitudinal strain by 0.06 absolute.

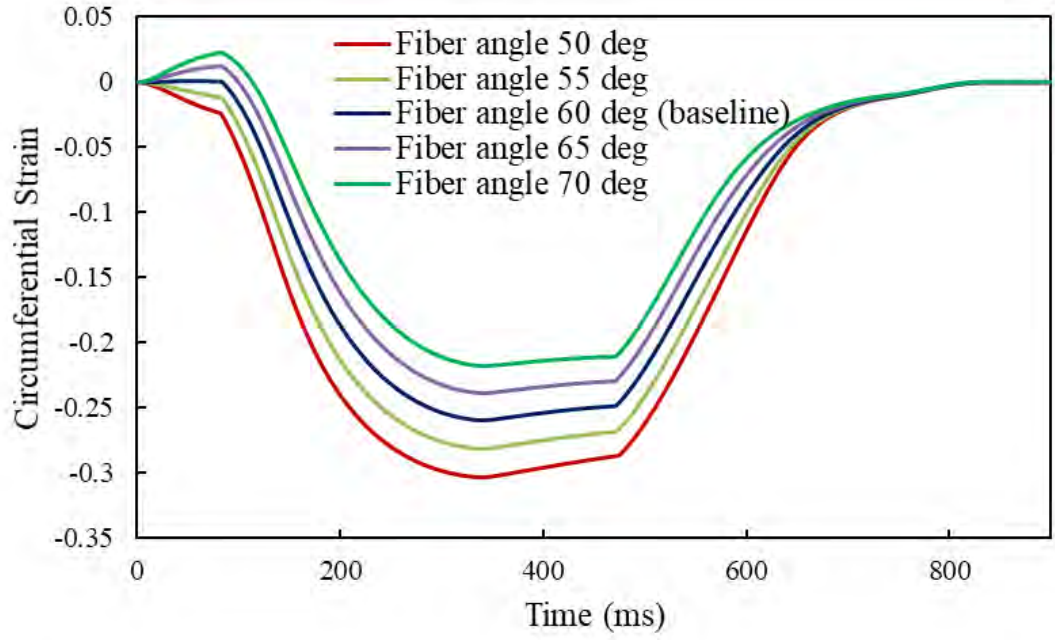

Figure 4. 24: Circumferential strain for the variations of LV fiber orientation in HFpEF patient.

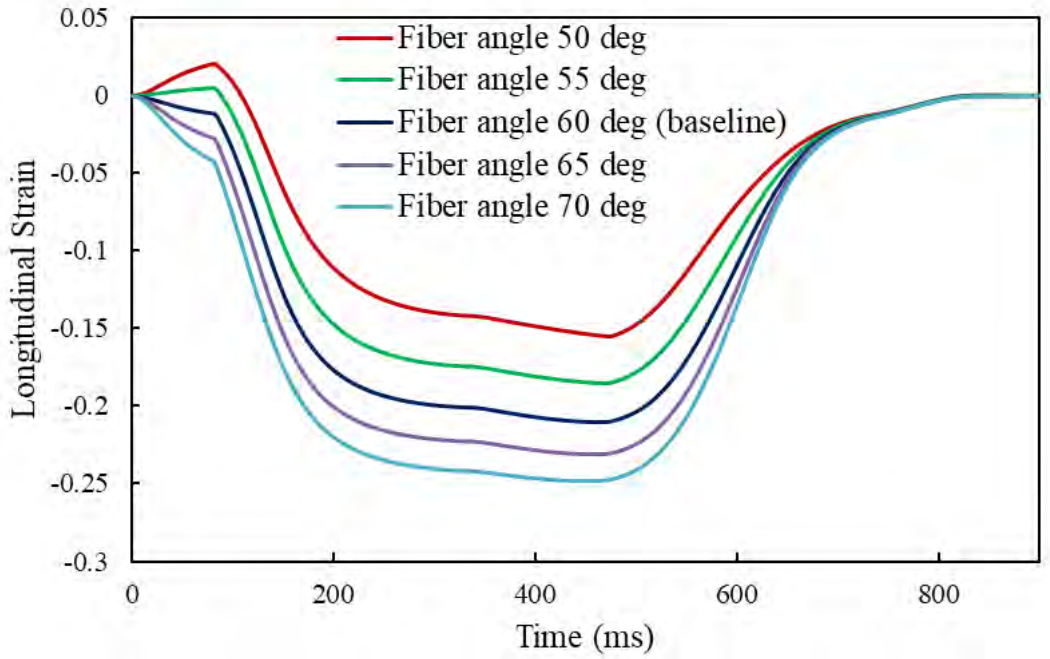

Figure 4. 25: Longitudinal strain for the variations of LV fiber orientation in HFpEF patient.

4.9.3 Effect on Stress

Figure 4.26 shows the fiber stress remains nearly same while LV myocardial fiber angle is changed. This is largely due to having same LV wall thickness and left ventricular cavity volume.

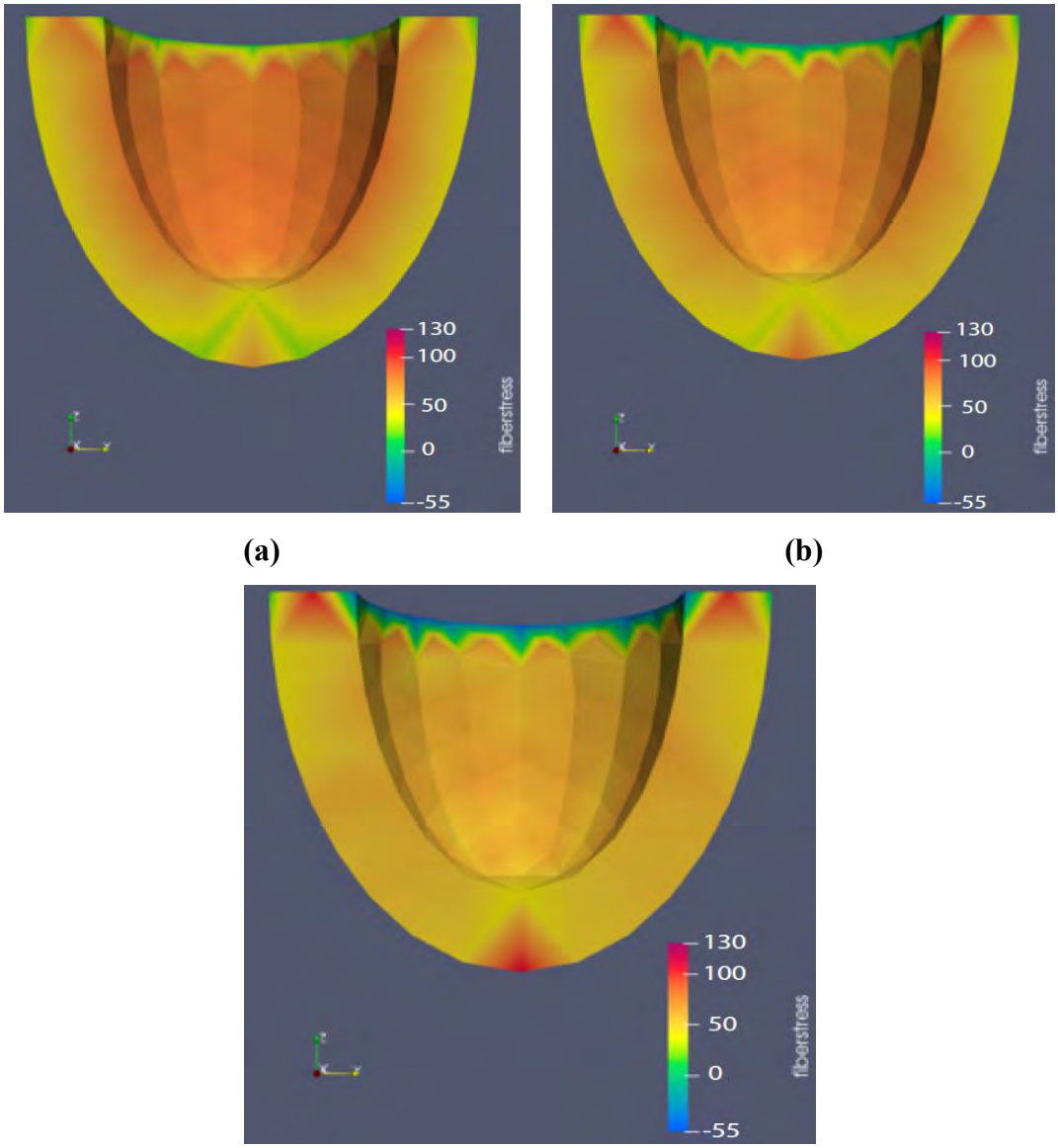

Figure 4. 26: Snapshot at vertical cross section along central axis at end-systole for HFpEF case, having fiber orientation of (a) -50º/50º, (b) -60º/60º and (c) -70º/ 70º; colormap shows the stress values in kPa.

4.9.4 Summary

Isolated LV fiber angle change doesn't have any apparent effect of on LV functioning though it has significant effect on myofiber strain. It has found in many studies that the fiber orientation becomes more circumferential in the diseased hearts [81]. Our model predicts as the fibers becomes more circumferential; the longitudinal strain decreases while increasing circumferential strain. So, Myofiber orientation change could be one of the mechanisms as a significant number of HFpEF patients show reduced longitudinal strain, but it has to be combined with other mechanisms such as increased LV wall thickness to get further insight in HFpEF progression. Therefore, an isolated change in the fiber angle cannot reproduce all the features found during progression of HFpEF.

CHAPTER 5

CONCLUSION

5.1 Conclusions

In this thesis, A coupled LV FE-lumped parameter circulatory modeling framework has been successfully developed and calibrated our model with the measurements of a normal subject and a HFpEF patient. Then the results from these two models were compared to observe important physiological difference between normal and HFpEF cases. After that, the HFpEF model parameters such as, geometry, afterload, and fiber orientation were varied to physiologically reproduce the effects of these parameters on progression of HFpEF due to remodeling, diastolic dysfunction, hypertension, hypertrophy etc. which are the causes and effects of HFpEF progression. The conclusions of this study are summarized below:

- The models for normal and HFpEF cases reproduced the clinical datasets within acceptable limits, where R-squared values were greater than 0.90 for both the models.
- From the model it has been found, the ejection fraction is within normal range for both normal and HFpEF cases, but the HFpEF patient has increased EDV that shows the symptoms of remodeling and increased systolic blood pressure which is the symptom of hypertension. HFpEF patient has higher end-diastolic pressure (EDP) (19.3 mmHg in HFpEF vs. 7.5 mmHg in normal) than normal which suggests HFpEF patient's LV is stiffer than the normal LV. Clinically, EDP higher than 15 mmHg is considered as sign of diastolic dysfunction which is a common feature in HFpEF. In addition, the peak circumferential strain significantly decreased in HFpEF patient compared to the normal whereas the peak longitudinal strain almost remained same. The peak LV myofiber stress is higher in HFpEF than normal which is associated with LV remodeling.
- Increasing wall thickness recreates effects during left ventricular remodeling which progress HFpEF. According to literature, the LV becomes thicker because of concentric hypertrophy. This in turn increase the LV passive stiffness which increase the filling pressure, and leads to diastolic heart failure.

With isolated increase of LV wall thickness the model reproduced all the features except the peak circumferential strain (which increased with the increased LV wall thickness). Thus, the model predicts that only increase of LV wall thickness cannot reproduce the progression of HFpEF. Some other mechanism(s) must be combined with the increased LV wall thickness to reproduce all the key features found in HFpEF.

- Decreasing preload (LV cavity volume) can predicts the reduction in peak circumferential and longitudinal strains. The EF and peak systolic pressure decrease due to reduced preload. During the progression of HFpEF, the LV often undergoes concentric remodeling with increased LV wall thickness and decreased LV cavity diameter which in turn decrease the preload. The progressive concentric remodeling reduces the EF. The results suggest that decreased preload accompanied by increase in wall thickness might be possible path of progression in HFpEF.
- Increase in afterload in HFpEF patient decrease both the peak circumferential and longitudinal strains. However, to significantly reduce the peak strains (in the order of decrease of peak circumferential and longitudinal strain by 0.03-0.05 absolute value found in the reported clinical studies), the model shows that the peak systolic pressure will be very high which is unphysiological. Therefore, a sole increase in afterload cannot reproduce all the features found in progression in HFpEF. But increase in afterload could be one of the mechanisms as a significant number of HFpEF are hypertensive.
- Though, Isolated LV fiber angle change does not have any apparent effect of on LV functioning, it has significant effect on myofiber strain. Our model predicts as the fibers becomes more circumferential; the longitudinal strain decreases while increasing circumferential strain. So, Myofiber orientation change could be one of the mechanisms as a significant number of HFpEF patients show reduced longitudinal strain, but it must be combined with other mechanisms such as increased LV wall thickness to reproduce all the features found during progression of HFpEF.

5.2 Limitations of the Work

Though it was shown that the models fairly reproduce the clinical results, however this model has some limitations. These are discussed below:

- LV was modeled using idealized geometry. The approximated half-prolate geometry of LV neglected asymmetrical geometrical features.
- Only Finite element model of Left ventricle was used in this study. Finite element model of other compartments such as, aorta, left atrium, veins could be incorporated to produce more accurate result.
- In this study one parameter was varied while other parameters were kept constant. There can be a coupled effect among the parameters which cannot be evaluated if more than one parameter is not varied simultaneously.
- The model assumes that the LV contracts homogeneously and neglects any regional activation patterns
- A rule-based myofiber orientation was prescribed in this model, in which the myofiber helix angle varied linearly in the transmural direction from endocardium to epicardium. The myofiber orientation, in reality, may be more complex
- The mechanical effects associated with the right ventricle (RV) and pulmonary circulation was neglected. Although cavity pressure in the RV is substantially lower than the LV, its presence may, nevertheless, affects the LV mechanics through the septum.
- In the mathematical formulation the dynamical behavior of fluid and its interaction with the vessel wall were neglected, so this study did not consider the spatial variation of pressure waveform along the regions of left ventricle.
- Lastly, as the pathophysiology of HFpEF itself, is an incompletely identified field till now, the proper bridging between physiological change with the progression of HFpEF is loosely defined. It requires more clinical study to discover the proper HFpEF progression mechanism.

5.3 Recommendation for Future Works

As discussed, the present model has some limitations. The present model can be developed, and the investigation can be carried out for further improvement. These are:

- More realistic model acquired from MRI scan of human heart and modeling it via CAD can be used to make the results more exactly fit with measured clinical data.
- Finite elements models of other storage compartments like aorta, left atrium can be coupled with current left ventricle model rather than using only the electrical analog. This will surely produce more accurate results.
- This model can be coupled with the fluid dynamics of blood flow to investigate the variation of pressure and velocity of the blood while flowing through various compartments.
- This model has to be updated time to time to incorporate new findings as, mechanism of HFpEF is still an active research area. Researchers are exploring new frontiers in this field with the advancement of time.

REFERENCES

[1] Virani, S. S., Alonso, A., Benjamin, E. J., Bittencourt, M. S., "Heart Disease and Stroke Statistics—2020 Update: A Report from the American Heart Association." *Circul.*, vol. 141(9), pp. e139-e596, 2020.

[2] Owan, T. E., Hodge, D. O., Herges, R. M., Jacobsen, S. J., Roger, V. L., Redfield, M. M., "Trends in prevalence and outcome of heart failure with preserved ejection fraction." *N. Engl. J. Med.*, vol 355, pp. 251–259, 2006.

[3] Jean-Louis, G., Zizi, F., Clark, L.T., Brown, C.D., McFarlane, S.I., "Obstructive sleep apnea and cardiovascular disease: role of the metabolic syndrome and its components." *J. Clin. Sleep Med.,* vol 4(3), pp. 261-272. 2008.

[4] Redfield, M. M., "Heart Failure with Preserved Ejection Fraction." *N. Engl. J. Med.*, vol 375, pp. 1868-1877, 2016.

[5] Glass, L., McCulloch, A., Hunter, P. (1991) *Theory of Heart: Biomechanics, Biophysics, and Nonlinear Dynamics of Cardiac Function.* Springer-Verlag New York, Inc., New York, USA.

[6] Broomé, M., Maksuti, E., Bjällmark, A., Frenckner, B., Janerot-Sjöberg, B., "Closed-loop real-time simulation model of hemodynamics and oxygen transport in the cardiovascular system." *Biomed. Eng. Online.,* vol. 12(69), pp. 1-20, 2013.

[7] Sundnes, J., Wall, S., Osnes, H., Thorvaldsen, T., McCulloch, A.D., "Improved discretisation and linearisation of active tension in strongly coupled cardiac electro-mechanics simulations." *Comput. Methods Biomech. Biomed. Engin.,* vol. 17(6), pp. 604-15, 2014.

[8] Gurev, V., Pathmanathan, P., Fattebert, J.L., Wen, H.F., Magerlein, J., Gray, R.A., Richards, D.F., Rice, J.J., "A high-resolution computational model of the deforming human heart." *Biomech. Model Mechanobiol.,* vol. 14(4), pp. 829-49, 2015.

[9] Maas, S.A., Ellis, B.J., Rawlins, D.S., Weiss, J.A., "Finite element simulation of articular contact mechanics with quadratic tetrahedral elements." *J. Biomech.,* vol. 49(5), pp. 659-667, 2016.

[10] Maurer, M.S., Burkhoff, D., Fried, L.P., Gottdiener, J., King, D.L., Kitzman, D.W., "Ventricular structure and function in hypertensive participants with heart failure and a normal ejection fraction: The Cardiovascular Health Study." *J. Am. Coll. Cardiol.*, vol 49(9), pp. 972-81, 2007.

[11] Russo, C., Jin, C., Tao, L., Desai, K., Goshorn, A., Donovan, M., Ptaszynska, A., "Prognostic significance of left ventricular diastolic dysfunction progression in patients with heart failure with preserved ejection fraction: the I-preserve trial." *J. Am. Coll. Cardiol.*, vol 69, pp. 885-885, 2017.

[12] Upadhya, B., Kitzman, D.W., "Heart failure with preserved ejection fraction: New approaches to diagnosis and management." *Clin. Cardiol.,* vol. 43(2), pp. 145-155, 2020.

[13] Guyton, A. C., Hall, J. E. (1996) *Textbook of medical physiology. 9th ed.* Philadelphia: W.B. Saunders., USA.

[14] Shah, S., Gnanasegaran, G., Sundberg-Cohon, J., Buscombe, J. R., "The Heart: Anatomy, Physiology and Exercise Physiology." in Movahed, A., Gnanasegaran, G., Buscombe, J., Hall, M. (eds.). *Integrating Cardiology for Nuclear Medicine Physicians: A Guide to Nuclear Medicine Physicians,* chap 1, pp. 3-22, Springer Berlin Heidelberg, Berlin, Heidelberg, 2009.

[15] Burkhoff, D., "Mechanical Properties of the Heart and Its Interaction with the Vascular System." *Card. Physio.*, vol. 84, pp. 1-23, 2002.

[16] Saleh, M., Ambrose, J.A., "Understanding myocardial infarction." *Fac. Rev.,* vol. 1378, pp. 7, 2018

[17] Sisakian, H., "Cardiomyopathies: Evolution of pathogenesis concepts and potential for new therapies." *World J. Cardiol.*, vol. 6(6), pp. 478-494, 2014.

[18] Chen, Y.T., Wong, L.L., Liew, O.W., Richards, A.M., "Heart Failure with Reduced Ejection Fraction (HFrEF) and Preserved Ejection Fraction (HFpEF): The Diagnostic Value of Circulating MicroRNAs." *Cells,* vol. 8(12), pp. 1651, 2019.

[19] Antonini-Canterin, F., Poli, S., Vriz, O., Pavan, D., Bello, V. D., Nicolosi, G. L. "The ventricular-arterial coupling: from basic pathophysiology to clinical application in the echocardiography laboratory." *J. Cardiovasc. Echography*, vol. 23, pp. 91-95, 2013.

[20] Yip, G., Wang, M., Zhang, Y., Fung, J. W. H., Ho, P. Y., Sanderson, J. E. "Left ventricular long axis function in diastolic heart failure is reduced in both diastole and systole: time for a redefinition?" *Heart*, vol. 87, pp. 121–125, 2002.

[21] Yu, C. M., Lin, H., Yang, H., Kong, S. L., Zhang, Q., Lee, S. W. L. "Progression of systolic abnormalities in patients with "isolated" diastolic heart failure and diastolic dysfunction." *Circul.*, vol. 105, pp. 1195–1201, 2002.

[22] Kawaguchi, M., Hay, I., Fetics, B., Kass, D. A., "Combined ventricular systolic and arterial stiffening in patients with heart failure and preserved ejection fraction: Implications for systolic and diastolic reserve limitations." *Circul.*, vol. 107, pp. 714–720, 2003.

[23] Borlaug, B. A., Kass, D. A., "Ventricular-Vascular Interaction in Heart Failure." *Cardiol. Clin.*, vol. 29, pp. 447–459, 2011.

[24] Shah, A.M., "Ventricular remodeling in heart failure with preserved ejection fraction." *Curr. Heart Fail. Rep.*, vol. 10(4), pp. 341-349, 2013.

[25] Louridas, G.E., Lourida, K.G., "Heart Failure in Patients with Preserved Ejection Fraction: Questions Concerning Clinical Progression." *J. Cardiovasc. Dev. Dis.,* vol. 3(3), pp. 27, 2016.

[26] Roh, J., Houstis, N., Rosenzweig, A. "Why Don't We Have Proven Treatments for HFpEF?" *Circ. Res*., vol. 120(8), pp. 1243-1245, 2017.

[27] Butler , J. , Hamo , C. E. , Udelson , J. E., Pitt, B., Yancy, C., Shah, S. J., Desvigne-Nickens, P., Bernstein, H. S., Clark, R. L., Depre, C., Dinh, W., Hamer, A., Kay-Mugford, P., Kramer, F., Lefkowitz, M., Lewis, K., Maya, J., Maybaum, S., Patel, M. J., Pollack, P. S., Roessig, L., Rotman, S., Salsali, A., Sims, J. J., Senni, M., Rosano, G., Dunnmon, P., Stockbridge, N., Anker, S. D., Zile, M. R., Gheorghiade, M.. "Exploring New Endpoints for Patients with Heart Failure with Preserved Ejection Fraction." *Circ. Heart Fail.*, vol. 9(11), pp. e003358, 2016.

[28] Lopez-Perez, A., Sebastian, R., Ferrero, J.M., "Three-dimensional cardiac computational modelling: methods, features and applications." *BioMed. Eng. OnLine,* vol. 14, pp. 35, 2015.

[29] Trayanova, N.A., Rice, J.J., “Cardiac electromechanical models: from cell to organ.” *Front. Physiol.,* vol. 2, pp. 43, 2011.

[30] Azevedo, P.S., Polegato, B.F., Minicucci, M.F., Paiva, S.A., Zornoff, L.A., “Cardiac Remodeling: Concepts, Clinical Impact, Pathophysiological Mechanisms and Pharmacologic Treatment.” *Arq. Bras. Cardiol.,* vol. 106(1), pp. 62-69, 2016.

[31] Liang, F., Liu, H., “A Closed-Loop Lumped Parameter Computational Model for Human Cardiovascular System.” *JSME Intl. J. Series C. Mech. Sys., Mach. Elem. and Mfg.,* vol. 48(4), pp. 484-493, 2006.

[32] Capelli, C., Sauvage, E., Giusti, G., Bosi, G.M., Ntsinjana, H., Carminati, M., Derrick, G., Marek, J., Khambadkone, S., Taylor, A. M., Schievano, S., “Patient-specific simulations for planning treatment in congenital heart disease.” *Royl. Socie*. vol. 8(1), pp. 242 ,2017.

[33] Lee, L. C., Sundnes, J., Genet, M., Wenk, J. F., Wall, S. T. "An integrated electromechanical-growth heart model for simulating cardiac therapies." *Biomech. Model Mechanobiol.*, vol. 15, pp. 791–803, 2016.

[34] Shavik, S. M., Wall, S. T., Sundnes, J., Burkhoff, D., Lee, L. C. "Organ-level validation of a cross-bridge cycling descriptor in a left ventricular finite element model: Effects of ventricular loading on myocardial strains." *Physiol. Rep.*, vol. 5, pp. 1-14, 2017.

[35] Kerckhoffs, R. C. P., Neal, M. L., Gu, Q., Bassingthwaighte, J. B., Omens, J. H., McCulloch, A. D. "Coupling of a 3D finite element model of cardiac ventricular mechanics to lumped systems models of the systemic and pulmonic circulation." *Ann. Biomed. Eng.*, vol. 35, pp.1–18, 2007.

[36] Gurev, V., Lee, T., Constantino, J. *et al.,* “Models of cardiac electromechanics based on individual hearts imaging data.” *Biomech. Model Mechanobiol.,* vol. 10, pp. 295–306, 2011.

[37] Kerckhoffs, R.C.P., Omens, J.H., McCulloch, A.D., Mulligan, L.J., “Ventricular dilation and electrical dyssynchrony synergistically increase regional mechanical nonuniformity but not mechanical dyssynchrony: a computational model.” *Circ. Heart Fail.,* vol. 3(4), pp. 528-536, 2010.

[38] Sundnes, J., Wall, S., Osnes, H., Thorvaldsen, T., McCulloch, A. D., "Improved discretisation and linearisation of active tension in strongly coupled cardiac electro-mechanics simulations." *Comput. Methods Biomech. Biomed. Engin.*, pp. 37-41, 2013.

[39] Göktepe, S., Abilez, O.J., Parker, K.K., Kuhl, E., "A multiscale model for eccentric and concentric cardiac growth through sarcomerogenesis." *J. Theor. Biol.*, vol. 265(3), pp. 433-442, 2010.

[40] Kerckhoffs, R.C.P., Omens, J., McCulloch, A.D., "A single strain-based growth law predicts concentric and eccentric cardiac growth during pressure and volume overload." *Mech. Res. Commun*. vol. 42, pp. 40-50, 2012.

[41] Lee, L.C., Genet, M., Acevedo-Bolton, G., et al., "A computational model that predicts reverse growth in response to mechanical unloading." *Biomech Model Mechanobiol*., vol. 14(2), pp. 217-229, 2015.

[42] Lee, L.C., Sundnes, J., Genet, M., Wenk, J.F., Wall, S.T., "An integrated electromechanical-growth heart model for simulating cardiac therapies." *Biomech. Model Mechanobiol.*, vol. 15(4), pp. 791-803, 2016.

[43] Hu, Y., Gurev, V., Constantino, J., Trayanova, N., "Optimizing cardiac resynchronization therapy to minimize ATP consumption heterogeneity throughout the left ventricle: A simulation analysis using a canine heart failure model." *Hear Rhythm*., vol. 11, pp. 1063-1069, 2014.

[44] Kerckhoffs, R.C.P., McCulloch, A.D., Omens, J.H., Mulligan, L.J., "Effects of biventricular pacing and scar size in a computational model of the failing heart with left bundle branch block." *Med. Image Anal*., vol. 13(2), pp. 362-369, 2009.

[45] Lee, L.C., Wenk, J.F., Zhong, L., et al., "Analysis of patient-specific surgical ventricular restoration: importance of an ellipsoidal left ventricular geometry for diastolic and systolic function." *J. Appl. Physiol*., vol. 115(1), pp. 136-144, 2013.

[46] Bassingthwaighte, J.B., Chizeck, H.J., Atlas, L.E., "Strategies and tactics in multiscale modeling of cell-to-organ systems." in *Proceeding IEEE*, Vol. 94(4), 2006, pp. 819-830.

[47] Kerckhoffs, R.C.P., Narayan, S.M., Omens, J.H., Mulligan, L.J., McCulloch, A.D., "Computational Modeling for Bedside Application." *Heart Fail. Clin*., vol. 4(3), pp. 371-378, 2008.

[48] Wenk, J. F., Sun, K., Zhang, Z., Soleimani, M., Ge, L., Saloner, D., et al., "Regional left ventricular myocardial contractility and stress in a finite element model of posterobasal myocardial infarction." *J. Biomech. Eng*., vol. 133, pp. 44501, 2011.

[49] Gao, H., Wang, H., Berry, C., Luo, X., and Griffith, B. E., "QuasiStatic image-based immersed boundary-finite element model of left ventricle under diastolic loading." *Int. J. Numer. Method. Biomed. Eng.*, vol. 30, pp. 1199–1222, 2014.

[50] Genet, M., Lee, L. C., Nguyen, R., Haraldsson, H., Acevedo-Bolton, G., Zhang, Z., et al., "Distribution of normal human left ventricular myofiber stress at end diastole and end systole: a target for in silico design of heart failure treatments." *J. Appl. Physiol.* vol. 117, pp. 142–152, 2014.

[51] Usyk, T. P., LeGrice, I. J., and McCulloch., A. D., "Computational model of three-dimensional cardiac electromechanics." *Comput. Vis. Sci.*, vol. 4, pp. 249–257, 2002.

[52] Trayanova, N. A., Constantino, J., and Gurev., V., "Electromechanical models of the ventricles." *Am. J. Physiol. Heart Circ. Physiol.*, vol. 301, pp. H279–H286, 2011.

[53] Wall, S. T., Guccione, J. M., Ratcliffe, M. B., and Sundnes., J. S. "Electromechanical feedback with reduced cellular connectivity alters electrical activity in an infarct injured left ventricle: a finite element model study." *Am. J. Physiol. Heart. Circ. Physiol.*, vol. 302, pp. H206–H214, 2012.

[54] Xi, C., Latnie, C., Zhao, X., Tan, J. L., Wall, S. T., Genet, M., et al., "Patientspecific computational analysis of ventricular mechanics in pulmonary arterial hypertension." *J. Biomech. Eng.*, vol. 138, pp. 111001, 2016.

[55] Smith, B. W., Chase, J. G., Nokes, R. I., Shaw, G. M., and Wake., G., "Minimal haemodynamic system model including ventricular interaction and valve dynamics." *Med. Eng. Phys.,* vol. 26, pp. 131–139, 2004.

[56] Arts, T., Delhaas, T., Bovendeerd, P., Verbeek, X., and Prinzen, F., "Adaptation to mechanical load determines shape and properties of heart and

circulation: the circadapt model.” *Am. J. Physiol. Heart Circ. Physiol*., vol. 288, pp. 1943–1954, 2005.

[57] Guccione, J. M., McCulloch, A. D., Waldman, L. K., "Passive material properties of intact ventricular myocardium determined from a cylindrical model." *J. Biomech. Eng.*, vol. 113, pp. 42–55, 1991.

[58] Guccione, J.M., McCulloch, A.D., “Mechanics of active contraction in cardiac muscle: Part I--Constitutive relations for fiber stress that describe deactivation.” *J. Biomech. Eng.*, vol. 115(1), pp. 72-81, 1993.

[59] Guccione, J. M., Waldman, L. K., McCulloch, A. D., "Mechanics of active contraction in cardiac muscle: part II–cylindrical models of the systolic left ventricle." *J. Biomech. Eng*., vol. 115, pp. 82–90, 1993.

[60] Burkhoff, D., Tyberg, J.V., “Why does pulmonary venous pressure rise after onset of LV dysfunction: a theoretical analysis.” *Am. J. Physiol.,* vol. 265(5), pp. H1819-28, 1993.

[61] Bhatia RS, Tu J V, Lee DS, et al., “Outcome of heart failure with preserved ejection fraction in a population-based study.” *N. Engl. J. Med.*, vol. 355(3):260-269, 2006.

[62] Borlaug, B.A., Paulus, W.J., “Heart failure with preserved ejection fraction: pathophysiology, diagnosis, and treatment.” *Eur. Heart J*., vol. 32(6), pp. 670-679, 2011.

[63] Somaratne, J.B., Berry, C., McMurray, J.J.V., Poppe, K.K., Doughty, R.N., Whalley, G.A., “The prognostic significance of heart failure with preserved left ventricular ejection fraction: A literature-based meta-analysis.” *Eur J Heart Fail*., vol. 11(9), pp. 855-862, 2009.

[64] Tribouilloy, C., Rusinaru, D., Mahjoub, H., et al., “Prognosis of heart failure with preserved ejection fraction: A 5-year prospective population-based study.” *Eur. Heart J*., vol. 29(3), pp. 339-347, 2008.

[65] Asif, M., Egan, J., Vasan, S., et al. “An advanced glycation endproduct cross-link breaker can reverse age-related increases in myocardial stiffness.” in *Proceeding of N. Acad. Sci.*, Vol. 96(6), March 2000, pp. 2809-13.

[66] Liu, J., Masurekar, M.R., Vatner, D.E., et al. “Glycation end-product cross-link breaker reduces collagen and improves cardiac function in aging diabetic heart.” *Am. J. Physiol. Heart Circ. Physiol.*, vol. 285(6), pp. H2587-91, 2003.

[67] Solomon, S.D., Zile, M., Pieske, B., et al., “The angiotensin receptor neprilysin inhibitor LCZ696 in heart failure with preserved ejection fraction: A phase 2 double-blind randomised controlled trial.” *Lancet*, vol. 380(9851), pp. 1387-95, 2012.

[68] Van, T. B.W., Arena, R., Biondi-Zoccai, G., et al., “Effects of Interleukin-1 Blockade with Anakinra on Aerobic Exercise Capacity in Patients with Heart Failure and Preserved Ejection Fraction (from the D-HART Pilot Study).” *Am. J. Cardiol*., vol.113(2), pp. 321-327, 2014.

[69] Yamagami, K., Oka, T., Wang, Q., et al., “Pirfenidone Exhibits Cardioprotective Effects by Regulating Myocardial Fibrosis and Vascular Permeability in Pressure Overloaded Hearts.” *Am. J. Physiol. Heart Circ. Physiol.*, vol. 309(3), pp. H512-22, 2015.

[70] Ponikowski, P., Voors, A.A., Anker, S.D., et al., “ESC Guidelines for the diagnosis and treatment of acute and chronic heart failure.” *Eur. Heart J.*, vol. 37(27), pp. 2129-2200m, 2016.

[71] Sengupta, P.P., Marwick, T.H., “The Many Dimensions of Diastolic Function: A Curse or a Blessing?” *JACC Cardiovasc. Imaging.*, vol. 11(3), pp. 409-410, 2018.

[72] Zile, M.R., Baicu, C.F., Gaasch, W.H., “Diastolic Heart Failure — Abnormalities in Active Relaxation and Passive Stiffness of the Left Ventricle.” *N. Engl. J. Med.*, vol. 350(19), pp. 1953-1959, 2004.

[73] Velagaleti, R.S., Gona, P., Pencina, M.J., et al., “Left ventricular hypertrophy patterns and incidence of heart failure with preserved versus reduced ejection fraction.” *Am. J. Cardiol.,* vol. 113(1), pp. 117-122, 2014.

[74] Zile, M.R., Gaasch, W.H., Carroll, J.D., et al., “Heart failure with a normal ejection fraction: is measurement of diastolic function necessary to make the diagnosis of diastolic heart failure?” *Circulation*, vol. 104, pp. 779-782, 2001.

[75] Kraigher-Krainer, E., Shah, A.M., Gupta, D.K., et al., "Impaired systolic function by strain imaging in heart failure with preserved ejection fraction." *J. Am. Coll. Cardiol.*, vol. 63(5), pp. 447-455, 2014.

[76] Morris, D.A., Ma, X.X., Belyavskiy, E., et al., "Left ventricular longitudinal systolic function analysed by 2D speckle-tracking echocardiography in heart failure with preserved ejection fraction: a meta-analysis." *Open Heart*., vol. 4(2), pp. 168, 2017.

[77] Shah, A.M., Claggett, B., Sweitzer, N.K., et al., "Prognostic Importance of Changes in Cardiac Structure and Function in Heart Failure with Preserved Ejection Fraction and the Impact of Spironolactone." *Circ. Hear. Fail.* vol. 8(6), pp. 1052-8, 2015.

[78] Zou, H., Xi, C., Zhao, X., et al., "Quantification of Biventricular Strains in Heart Failure with Preserved Ejection Fraction Patient Using Hyperelastic Warping Method." *Front Physiol*., vol. 9, pp. 1295, 2018.

[79] Borlaug, B.A., Lam, C.S.P., Roger, V.L., Rodeheffer, R.J., Redfield, M.M., "Contractility and ventricular systolic stiffening in hypertensive heart disease insights into the pathogenesis of heart failure with preserved ejection fraction." *J. Am. Coll. Cardiol.*, vol. 54(5), pp. 410-418, 2009.

[80] Adeniran, I., MacIver, D.H., Hancox, J.C., Zhang, H., "Abnormal calcium homeostasis in heart failure with preserved ejection fraction is related to both reduced contractile function and incomplete relaxation: an electromechanically detailed biophysical modeling study." *Front. Physiol.*, vol. 6, pp. 78, 2015.

[81] Dabiri, Y., Sack, K.L., Shaul, S., Sengupta, P.P., Guccione, J.M., "Relationship of transmural variations in myofiber contractility to left ventricular ejection fraction: Implications for modeling heart failure phenotype with preserved ejection fraction." *Front. Physiol*., vol. 9, pp. 1003, 2018.

[82] Genet, M., Lee, L.C., Baillargeon, B., Guccione, J.M., Kuhl, E., "Modeling Pathologies of Diastolic and Systolic Heart Failure." *Ann. Biomed. Eng*., vol. 44(1), pp. 112-127, 2016.

[83] MacIver, D.H., Townsend, M., "A novel mechanism of heart failure with normal ejection fraction." *Hear*t, vol. 94(4), pp. 446-9, 2008.

[84] Shavik, S.M., Jiang, Z., Baek, S., Lee, L.C., “High Spatial Resolution Multi-Organ Finite Element Modeling of Ventricular-Arterial Coupling.” *Front. Physiol.,* vol. 9, pp. 119, 2018.

[85] Teo, L.Y., Chan, L.L., Lam, C.S., “Heart failure with preserved ejection fraction in hypertension.” *Curr. Opin. Cardiol*., vol. 31(4), pp. 410-6, 2016.

[86] Shah, S. J., Borlaug, B. A., Kitzman, D. W., McCulloch, A. D., Blaxall, B. C., Agarwal, R., Chirinos, J. A., Collins, S., Deo, R. C., Gladwin, M. T., Granzier, H., Hummel, S. L., Kass, D. A., Redfield, M. M., Sam, F., Wang, T. J., Desvigne-Nickens, P., Adhikari, B. B., “Research Priorities for Heart Failure with Preserved Ejection Fraction.” *Circulation*, vol. 141(12), pp. 1001-1026, 2020

[87] Upadhya, B., Kitzman, D.W., “Heart failure with preserved ejection fraction: New approaches to diagnosis and management.” *Clin. Cardiol.*, vol. 43(2), pp. 145-155, 2020.

[88] Mann, B., Bhandohal, J.S., Mushiyev, S., “Prognostic Significance of Diastolic Dysfunction with Multiple Comorbidities in Heart Failure Patients.” *Cureus*., vol. 12(5), pp. e8297, 2020.

[89] Loon, T. V., Knackstedt, C. Cornelussen, R., Reesink, K. D., Rocca, H.P.B.L., Tammo Delhaas, Empel, V.V., Lumens, J., “Increased myocardial stiffness more than impaired relaxation function limits cardiac performance during exercise in heart failure with preserved ejection fraction: a virtual patient study.” *Eur. Heart J. – Dig. H.*, vol. 1(1), pp. 40–50, 2020.

[90] Pezzuto, S., Ambrosi, D., “Active contraction of the cardiac ventricle and distortion of the microstructural architecture.” *Int. J. Numer. Method. Biomed. Eng.*, vol. 30, pp. 1578–1596, 2014.

[91] Pezzuto, S., Ambrosi, D., Quarteroni, A., “An orthotropic active-strain model for the myocardium mechanics and its numerical approximation.” *Eur. J. Mech. A Solids*, vol. 48, pp. 83–96, 2014.

[92] Alnæs, M., Blechta, J., Hake, J., Johansson, A., Kehlet, B., Logg, A., Richardson, C., Ring, J., Rognes, M. E., Wells, G. N., "The FEniCS project version 1.5." *Arch. Numer. Softw*., vol. 3, pp. 9–23, 2015.

[93] Streeter, D. D., Spotnitz, H. M., Patel, D. P., Ross, J., Sonnenblick., E. H., "Fiber orientation in the canine left ventricle during diastole and systole." *Circ. Res*., vol. 24, pp. 339–347, 1969.

[94] Triposkiadis, F., Giamouzis, G., Boudoulas, K.D., Karagiannis, G., Skoularigis, J., Boudoulas, H., Parissis, J., "Left ventricular geometry as a major determinant of left ventricular ejection fraction: physiological considerations and clinical implications." *Eur. J. Heart Fail.*, vol. 20(3), pp. 436-444, 2018.

[95] Dang, A. B., Guccione, J. M., Mishell, J. M., Zhang, P., Wallace, A. W., Gorman, R. C., et al. "Akinetic myocardial infarcts must contain contracting myocytes: finite-element model study." *Am. J. Physiol. Heart Circ. Physiol.*, vol. 288, pp. H1844–H1850, 2005.

[96] Gorcsan, J. 3rd, Tanaka, H., "Echocardiographic assessment of myocardial strain." *J. Am. Coll. Cardiol*., vol. 58(14), pp. 1401-13, 2011.

[97] Hoit, B. D., "Strain and Strain Rate Echocardiography and Coronary Artery Disease." *Circ. : Cardiovas. Imag.,* vol. 4(2), pp. 179-180, 2011.

[98] Smiseth, O.A., Torp, H., Opdahl, A., Haugaa, K.H., Urheim, S., "Myocardial strain imaging: how useful is it in clinical decision making?" *Eur. Heart J*., vol. 37(15), pp. 1196-207, 2016.

[99] Borlaug, B.A., "The pathophysiology of heart failure with preserved ejection fraction." *Nat. Rev. Cardiol*., vol. 11(9), pp. 507-15, 2014.

[100] Buggey, J., Alenezi, F., Yoon, H.J., Phelan, M., DeVore, A.D., Khouri, M.G., Schulte, P.J., Velazquez, E.J., "Left ventricular global longitudinal strain in patients with heart failure with preserved ejection fraction: outcomes following an acute heart failure hospitalization." *ESC. Heart. Fail*., vol. 4(4), pp. 432-439, 2017.

[101] Cohn, J. N., Ferrari, R., Sharpe, N., "Cardiac remodeling—concepts and clinical implications: a consensus paper from an international forum on cardiac remodeling." *J. of the Am. College of Cardio*., vol. 35(3), pp. 569-582, 2000.

[102] Carrick, R., Ge, L., Lee, L.C., Zhang, Z., Mishra, R., Axel, L., Guccione, J.M., Grossi, E.A., Ratcliffe, M.B., "Patient-Specific Finite Element–Based Analysis

of Ventricular Myofiber Stress After Coapsys: Importance of Residual Stress." *The Annal. of thor. surg.,* vol. 93(6), pp. 1964-1971, 2012.

[103] Shavik, S.M., Zhong, L., Zhao, X., Lee, L. C., "In-silico assessment of the effects of right ventricular assist device on pulmonary arterial hypertension using an image based biventricular modeling framework." *Mech. Research Comm.,* vol. 97, pp.101-111, 2019.

[104] Katz, A.M., "Influence of altered inotropy and lusitropy on ventricular pressure-volume loops." *J. Am. Coll. Cardiol*., vol. 11(2), pp. 438-45, 1988.

[105] Burkhoff, D., Mirsky, I., Suga, H., "Assessment of systolic and diastolic ventricular properties via pressure-volume analysis: a guide for clinical, translational, and basic researchers." *Am. J. Physiol. Heart Circ. Physiol*., vol. 289(2), pp. H501-12, 2005.